May 2014

Enhancing the Structure and Performance of P3HT/PC70BM Polymer Solar Cells with N-Dodecylthiol

Mahmoud Ismail Algazzar
University of Wisconsin-Milwaukee

ENHANCING THE STRUCTURE AND PERFORMANCE OF P3HT/PC70BM POLYMER SOLAR CELLS WITH N-DODECYLTHIOL

By

Mahmoud Ismail Algazzar

A dissertation Submitted in Partial

Fulfillment of the Requirements for the Degree of

Doctor of Philosophy

in Engineering

at

University of Wisconsin-Milwaukee

May 2014

ABSTRACT
ENHANCING THE STRUCTURE AND PERFORMANCE OF P3HT/PC70BM POLYMER SOLAR CELLS WITH N-DODECYLTHIOL

by

Mahmoud Ismail Algazzar

The University of Wisconsin-Milwaukee, 2014
Under the Supervision of Associate Professor Nidal Abu-Zahra

Polymer solar cells (PSCs) have attracted much attention because of their low cost, high flexibility, lightweight, and large surface area compared to long-established silicon solar cells. In most cases, bulk heterojunction type solar cells (BHJ) use a phase-separated blend of organic electron donor and acceptor components, where a conductive polymer is the donor and a fullerene derivative is the acceptor. To achieve high performance BHJ-type PSCs, the electron-donating conjugated polymer needs to be strong absorbent of a wide range of solar light waves and possess good hole mobility. This results in short-circuit current (J_{sc}) and/or open-circuit voltage (V_{oc}) at their optimum values.

In this research, n-dodecylthiol (0-5% vol.) was added to P3HT/PC70BM polymer solution to improve the crystallinity of P3HT and enhance the P3HT/PC70BM phase separation. Higher P3HT crystallinity reduces the amount of PCBM dissolved in the amorphous regions of P3HT, thus promoting the aggregation of PC70BM, which contributes to PC70BM/P3HT phase separation. Adding 2% n-dodecylthiol to the active layer resulted in forming the smallest polymer crystallites size L, which was nearly 11.2 nm at optimum annealing conditions at (150°C for 30 min in a vacuum atmosphere). The smaller crystallite size suggests a shorter path of the charge carriers between P3HT backbones, which increases

the short circuit current (J_{sc}) and decreases the open circuit voltage (V_{oc}) in the solar cells.

UV-Vis and EQE analysis showed enhancement of self-organization ability, which led to improved P3HT crystallinity and intensified phase separation of P3HT/PC70BM in polymer films. EQE increased due to enhanced hole and electron polaron mobility with n-dodecylthiol. AFM images showed increased surface roughness with adding n-dodecylthiol, yielding more spaces for P3HT crystallites to form, and hence resulting in higher crystallinity. DLS analysis of P3HT:PC70BM:n-dodecylthiol dissolved in chlorobenzene solution showed an increase of aggregate size by adding n-dodecylthiol; which confirms the SEM images. This also shows that n-dodecylthiol does not enhance the dispersion of P3HT:BC70BM in the chlorobenzene solution. Also, it shows that the more n-dodecylthiol is added, the more aggregation will be formed. In addition, increasing mixing time and temperature improves the mixing process and results in smaller aggregates.

Kinetics of cold crystallinity for P3HT:PC70BM using Avrami model showed an overall increase in crystallization rate ($1/t_{0.5}$) with increasing the annealing temperature. The increase in phase separation balancing for exciton dissociation and charge transport and collection resulted in a 33% increase in solar cell efficiency when the volume fraction of n-dodecylthiol is 2%. The enhancement of cell performance after thermal annealing deteriorated at temperatures higher than 150 °C.

To My Parents & My Wife

Contents **Page**

Contents **Page**

LIST OF FIGURES

LIST OF TABLES

NOMENCLATURE

Abbreviations

AAF	Advanced analysis facility
AFM	Atomic force microscope
AM	Air mass
BHJ	Bulk heterojunction
CDs	Compact discs
DC	Drop cast
DSC	Differential scanning calorimetry
DVDs	Digital versatile discs
EM	Electron microscope
EQE	External quantum efficiency
FDTD	Finite-difference time-domain
FF	Fill factors
FIB	Focused ion beam
G	Global
H.T.	Heat treatment
HOMO	Highest occupied molecular orbital
IPCE	Incident photon to current efficiency
ITO	Indium-tin oxide
LiF	Lithium fluoride
LUMO	Lowest unoccupied molecular orbital
OLED	Organic light emitting diode
OPV	Organic photovoltaic
PCE	Power conversion efficiency
PPVs	Poly(phenylenevinyles)
PSCs	Polymer solar cells
PVD	Physical vapor deposition
R2R	Roll to roll

SC	Spin coating
SEM	Scanning electron microscope
SWCNTs	Single walled carbon nanofibers
t	Time
T	Temperature
TE	Thermal evaporation
TEM	Transmission electron microscope
TW	Terawatts
V	Volt
VD	Vapor deposition
VE	Vacuum evaporation
Voc	Open-circuit voltage
VTE	Vacuum thermal evaporation
XRD	X-ray diffraction

Symbols

S_q or R_q	Root mean square roughness
S_{sk} or R_{sk}	Surface skewness
S_{ku} or R_{ku}	Surface kurtosis
Sp	Maximum peak height
Sv	Maximum valley depth
Sz	Peak height
Sa or Ra	Roughness average
K	Crystallization rate constant
$1/t_{0.5}$	Overall crystallization rate
$t_{0.5}$	Half time of crystallization
X(t)	Relative crystallinity
$t_{0.5}$	Half time of crystallization
P3HT	Poly(3-hexylthiophene)
PCBM	1-(3-methoxycarbonyl)-propyl-1-phenyl-(6,6)C61
J	Current density

η	Efficiency
ω	Angular velocity
θ	Angle
J_{opt} or J_{mp}	Current density at maximum power output and
V_{opt} or V_{mp}	Voltage at maximum power output
λ	Wavelength
L	Size of polymer crystallites
Jsc	Short-circuit current
T_m	Melting temperature
X_c	Crystallinity
ΔH	Enthalpy

Acknowledgements

I would like to thank my advisor, Dr Nidal Abu-Zahra for guiding and supporting me over the years. Dr Nidal is an excellent mentor, instructor, and advisor. I would like to thank my thesis committee members for their thesis review. Also, I would like to thank Engineer Kehan Yu, Dr Zhenhai Wen, and Professor Junhong Chen, director of the Laboratory of Nanotechnology for Sustainable Energy and Environment, Mechanical Engineering Department, University of Wisconsin-Milwaukee, for their support through the Laboratory of Nanotechnology for Sustainable Energy and Environment.

Chapter I

Literature Review

1 Introduction

As we know, non-renewable sources of energy are almost exhausted, so all human efforts are directed towardshaving energy from renewable sources like air, water, and the sun. The sun is the most important source of energy for the next 5 billion years [1], so researchers have invented photovoltaic devices which can convert light energy to electrical energy. These devices have many advantages: there is no mechanical movement associated with their function, making them silent, easy to process as well as low manufacturing cost. This can be achieved by the synthesis of materials with suitable electronic properties and high absorption coefficients. Solar cells work under sun light and produce electrical current, which can be used directly or stored by mechanical means such as fly wheels or chemicals like batteries, hydrogen, etc. [2]. But solar cells have some disadvantages. The current conversion of power from sunlight to electrical power is not highly efficient; low efficiency is due to our use of these devices to generate energy when the sun is shining, so energy output from these devices is highly dependent on weather. Also, the electricity generated is hard to store. We can store this energy by converting it into other types of energy, like chemicals such as hydrogen, formic acid, methanol or methane. There is always improvement to be made [4].

Human energy consumption in 2004 was about 15 terawatts (TW) with everything included. Most of this energy (87%) was from non-renewable sources. Human population growth, continuous industrialization of developing countries and human welfare increase are expected to expand our energy demands in the

future. In 2050, the predicted level of energy consumption by humans will be 2835 TW. Thisrepresents a challenge, as we currently cannot produce this amount with the energy sources available on our planet.Additionally,energy derived from non-renewable sources emits carbon dioxide which leads to global warming and pollution as a result of our excessive abuse of fossil fuel resources.There is no doubt that we have to change from fossil fuels to renewable and non–CO_2–emissive sources of energy [1].

The idea of the first photovoltaic device is based on Si PN-junction. Monocrystalline silicon solar cells work better than polycrystalline silicon cells with current efficiencies of less than or equal to 25%. The best reported efficiencies for small-scale laboratory solar cell devices, crystalline silicon (24.7% efficiency), are only achieved by cells made of gallium arsenide (GaAs, 25.1 % efficiency) for single junction devices. Monocrystalline photovoltaic cell materials have high manufacturing costs, while various thin film-technologies offer lower cost both in terms of stock material and thermal budget. Amorphous silicon is the most popular technology due to lower cost, but it suffers from degradation under illumination. The technology offers stable efficiencies of around 5-10%. Finally, solar cells falling broadly under the beginning of third-generation photovoltaics can be divided into organic, dye-sensitized and polymer solar cells [1].

The photovoltaic technology has to be efficient, with low costand stable properties. Polymer photovoltaic holds some promisebecause it is a technology that is complementary to the prototypical silicon-based solar cells. This technology offers low cost, a low thermal budget, solution processing, reel-to-reel

(R2R) manufacturing, flexibility, and very fast methods for fabrication. This technology succeeds while the inorganic photovoltaic (based on semiconductor materials) technologies have failed because of their high manufacturing costs. On the other hand, organic photovoltaic have until recently exhibited low power conversion efficiency and low thermal stability. Power conversion efficiencies of up to 6.5% have been achieved in the laboratory scale. Polymer solar cells offer light weight, high flexibility, low production costs and environmental benefits.

The structure of most polymer solar cells is bulk heterojunction (BHJ), which has been described in 1995 by Yu *et al* [3]. In this solar cell, the donor material, which is a polymer, is mixed with an acceptor (a soluble fullerene) in an organic solvent and then drop cast (DC) or spin coated (SC) on a substrate of indium-tin oxide (ITO) coated glass. During evaporation of the solvent and latter heat treatments, a microphase separation happens with the formation of an interpenetrating network. A hole-blocking layer such as lithium fluoride (LiF) may be added, and in the final step or layer a metal electrode (aluminum) is evaporated on top by using a metal thermal evaporator (see Figure 1).

The bulk heterojunction is a mixture of polymer fullerene, and is important because a large interfacial area between the donor and acceptor materials is created where charge separation can happen.

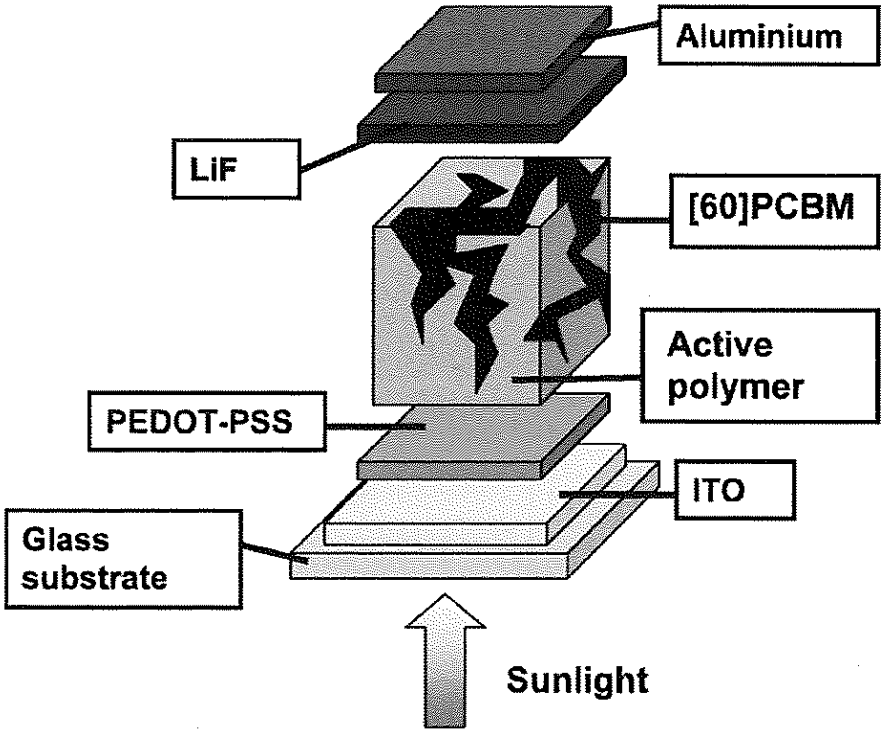

Figure 1: Schematic diagram of polymer solar cell structure [1].

2 The substrate

The preparation of the OPV (organic photovoltaic) device starts with the substrate. The substrate is typically a glass slide with a very thin layer of indium-tin oxide (ITO), which is a transparent electrically conducting material. The ITO represents the anode of the OPV devices and it needs to be patterned to avoid making short circuits inside the cell when contacting the completed device. This is achieved by the structure shown in Figure 2. The conducting side of the glass-ITO slide is determined by measuring the resistance with a simple multimeter. These devices are delicate and we have to use gloves to avoid depositing grease from our fingers. The metal cathode which is usually made from Aluminum is

evaporated by thermal evaporator technique. When making connections to the back electrode, there is a high risk that the device may short circuit. If this occurs, an electrical connection will be created between the front and back electrode and the device will have low voltages [1].

A nanoscale phase separation of donor and acceptor materials in the active layer is required in order to have efficient exciton dissociation and charge transport to the electrodes [39].

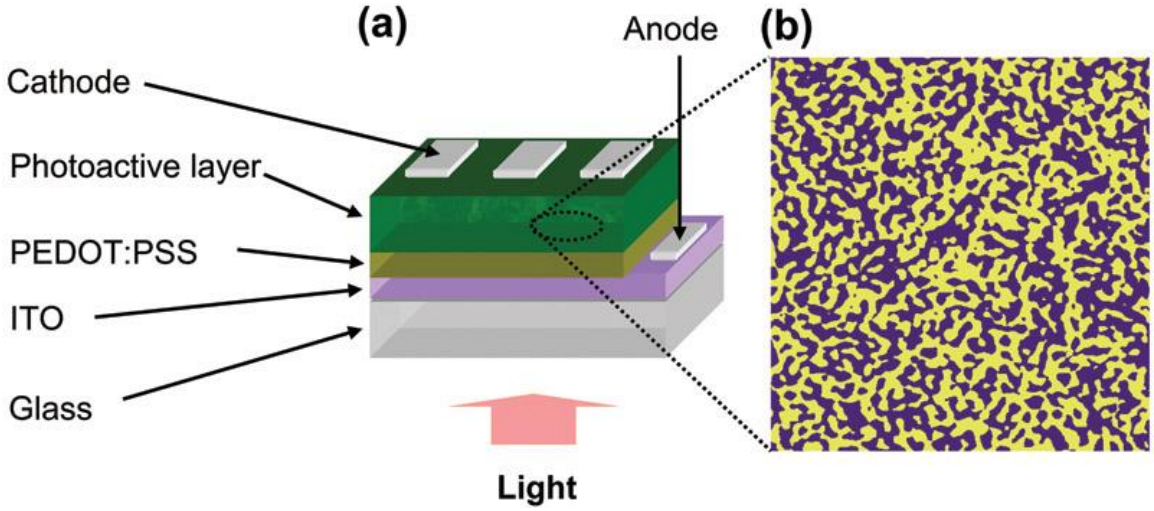

Figure 2: (a) A typical solar cell structure composed of PEDOT:PSS deposited onto a glass/ITO substrate. The photoactive layer is spin coated on the PEDOT:PSS film, then the aluminum cathode electrode evaporates.
(b) SEM image showing phase separation where yellow and purple areas are donor and acceptor phases, respectively [1].

3 The hole conducting PEDOT:PSS layer

The ITO-glass slides should be etched and then cleaned before the application of the PEDOT:PSS layer. Then the slides are then submerged in 2-propanol (also known as isopropanol) in a beaker and cleaned ultrasonically for a 5-10 minutes.

If there is an ozone treater, it is better to use it after the cleaning step. If there is no ultrasonic cleaner available it can be rinsed in distilled water. The most effective method is cleaning the substrates in several solvents, starting with cyclohexane, chloroform, and acetone and finally with 2-propanol or water. Then, apply a hole conducting PEDOT:PSS layer which improves and stabilizes the electrical contact between the transparent anode(ITO) and the polymer active layer. Also, it improves the surface roughness of the substrate. It is possible to synthesize polymer solar devices without PEDOT:PSS if it is not available, but it is not recommended to skip this step during synthesis of the solar cell. We can add the PEDOT:PSS layer using a spin coater. We put the slide on the spin coater with the ITO side facing up. If there is a dust problem, the slide can be rinsed by spinning the slide while washing with millipore water supply. The PEDOT:PSS is then applied while the slide is spinning, or by spinning the slide after dropping the solution. The spin coating must be applied when the slide is dry. The spin coating of the PEDOT:PSS layer must be performed at a high speed of 2000-3000 rpm, which gives a smooth, thin layer. Spinning has to be continued for a few minutes because the PEDOT:PSS dispersion dries slowly, which is why we should wait until the slide is completely dry. Usually a plastic syringe is used to add or disperse the PEDOT:PSS layer, or a pipette through a microfilter can be used if it is available. After adding the PEDOT:PSS layer, the connection area to the ITO electrode is cleaned with a cotton stick soaked in water, since PEDOT:PSS is a water based solution. The coating process must be complete because if the spin coater is stopped before the film is completely

dry, particles may form, resulting in a poor PEDOT:PSS layer or non-uniform layer [1].

4 Active layer

4.1 electron donating material, e.g. a p-type conjugated polymer materials

Many researchers have studied active polymers and discovered that Alkyl and alkoxy polymers such as P3HT, MEH-PPY, and MDMO-PPV are very successful materials in solar cells. They have excellent properties such as easy processing, semicrystallinity and solubility in organic solvents.Film thickness is a factor for the achievement of maximum absorbance and carrier (exciton) lifetime/mobility. Another factor is the semiliquid character of the film that is also given by the side chains. This flexibility allows changes in the structure to happen either with heat treatment or with time. The latter property is discovered in the annealing procedure where the PCBM component of the film will form micro-crystallites [4].

Seok-In Na *et al*[5] modified electrode architecture for air-stable and efficient polymer solar cells ((MAOSCs) with an active layer made of poly(3-hexylthiophene) (P3HT) and 1-(3-methoxycarbonyl)-propyl-1-phenyl-(6,6)C61 (PCBM). Based on the Finite-Difference Time-Domain (FDTD) scheme as a numerical method, improved light trapping within the photoactive layer, resulting from the high reflection rate of incident light at the large area of cathode, could be achieved by conventional organic solar cell structures modification. The improved power conversion efficiency of 4.3% was obtained in the P3HT/PC60BM tested by solar simulator with air mass (AM) 1.5 global (G) condition (see Table 1). In

addition, the stability of the solar cell in air was highly improved due to the limited exposure of their active layers. The stacking or accumulation of layers protects the active layer.

Table 1: Photovoltaic parameters and efficiencies of conventional OSCs and MAOSCs with two different active layer thicknesses (P3HT:PCBM)[5].

	Thickness (nm)	V_{oc} (V)	J_{sc} (mA/cm^2)	FF (%)	η_p (%)
Conventional OSC	~160	0.638	10.1	50.4	3.25
	~90	0.642	9.10	57.0	3.33
MAOSC	~160	0.630	12.01	49.2	3.72
	~90	0.634	12.3	55.1	4.30

Jianyong Ouyang and Yijie Xia [6] studied high-performance polymer photovoltaic cells with P3HT:PCBM film prepared from a polymer solution mixed with 1-dodecanethiol (P3HT and PCBM). Their results showed that an enhancement in the energy conversion efficiency of polymer photovoltaic cells by the addition of 1-dodecanethiol into the polymer solution for the device with a P3HT:PCBM (1:2 w/w) film is more important than for the solar device composed of a P3HT:PCBM (1:1w/w) film. Devices with energy conversion efficiency reached 4% with a thick layer of P3HT:PCBM film prepared using a fast drying process [6].

Seok-Soon Kim *et al*[??] studied the synthesis of more efficient annealing-free P3HT:PCBM polymer solar cells using a simple brush painting. They found that it is considered a promising method for the mass production of organic devices

based on the high-speed roll-to-roll system. They recorded that the highest device efficiency can reach the same level of those devices prepared with the spin coating technique. This is achieved by improved polymer chain organization and the balanced carrier transport induced by the most effective application of shear stress to the polymer chains during the brushing process. In addition, full brush painted polymer solar cells reached a high power conversion efficiency of 3.6% without any annealing treatment and processing additives [7].

Quentin Bricaud *et al*[??] studied Conjugated polymers of hybrid structures containing cyanovinylene linkages and were made by Knoevenagel condensation of diformyl terthienyls with para-dicyanomethylbenzene. UV–vis and cyclic voltammetric results showed that these polymers combined can reduce the value of the band gap and it can improve the low lying HOMO energy level and light absorbance properties. But the low solubility of the polymers did not allow for the fabrication of bulk heterojunction polymer solar cells. Bilayer heterojunction solar cells have been synthesized using thermally evaporated films of fullerene (C60) as an acceptor material. The (J-V) results were as shown in Figure 3, and the best device shows a maximum external quantum efficiency EQE of nearly 20% and a power conversion efficiency (PCE) of 0.40% under simulated AM 1.5 solar illumination [8].

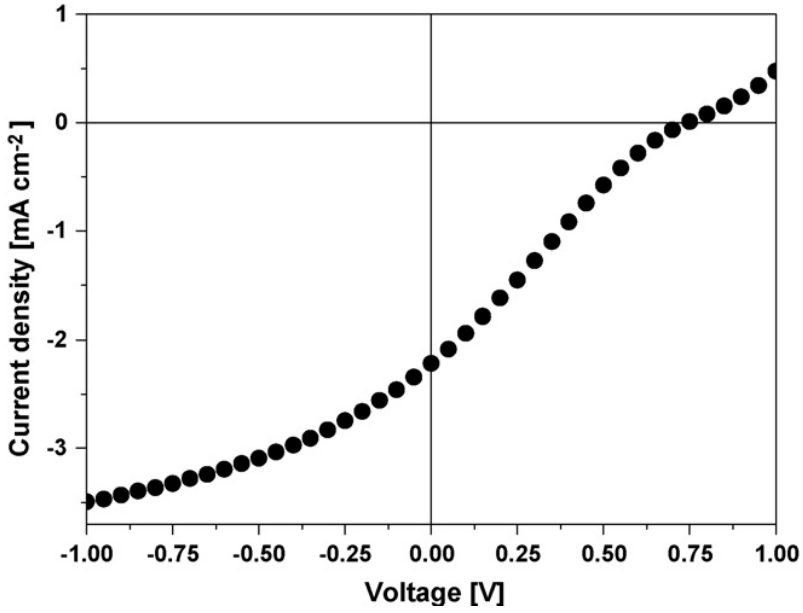

Figure 3: J-V characteristic of a bilayer heterojunction device under simulated AM1.5 illumination (100mWcm^{-2}) [8].

S. Millefiorini *et al* [9] synthesized and tested bulk heterojunction polymer solar cells with high oxidation potential, Poly-(dithieno[3,2-b:2′,3′-d] thiophene)-3-decylthiophene (P1), as electron donor material mixed with [6,6]-phenyl-C61-butyric acid methyl ester (PCBM) as electron acceptor material. They studied the photovoltaic properties of polymer solar cells made with different P1:PCBM mixture-blend compositions. The incident photon-to-current efficiency EQEs reached 40%, evidencing good charge photo-generation. The most power conversion efficiency PCE, η=0.83% under AM1.5 illumination, was found for solar cells containing 67 weight percent of PCBM. They discovered that the polymers with high oxidation potentials, the open circuit voltage (V_{oc}) can get high values of more than or equal to 0.8 V, from the photoactive blend composition, but the fill factors (FF) of the cells was low (FF: 0.3–0.38), which is

an evidence of low, poor charge transport properties. These results suggest that transport properties probably originate from bad polymer hole mobility, which is the main limitation for cell performance.

4.2 Acceptor materials

The poly(phenylenevinyles) (PPVs) and polythiophenes (especially poly 3-hexylthiophene(P3HT)) organic polymers are rich electron materials that can be oxidized fairly readily. These materials have high-energy HOMO levels, and are hole-conducting materials. Organic materials with high electron affinity have been synthesized in the lab or research company for several years. A few of the electron-conducting materials are C_{60} and fullerene derivatives. C_{60} is insoluble material, but a soluble PCBM derivative is now commercially available. The active organic layer in the organic solar cells is a mixture of PCBM and polymer to form bulk heterojunction [1].

In 1995 PCBM was first described by Hummelen *et al* [10], and they stated that the oval egg-shaped C_{70} can replace the symmetrical C_{60}, due to low energy transitions and increased light absorption. Cells with a mixture of PC70BM and MDMO-PPV were able to obtain an efficiency of 3% [11]. PCBM helps to form crystallites in the active layer, and the size and morphology of PCBM has a great effect on the power conversion efficiency of the polymer solar devices. Padinger *et al* [12]found that crystallite size increases by heat treatment (annealing process) of a PCBM/P3HT device, which improves the power conversion efficiency.The PCBM crystallites may grow too large to function well in the solar cell devices because of an optimization of heat treatment or annealing. The

diffusion of PCBM is mainly controlled by the annealing temperature and the glass transition temperature (T_g) of the polymer [12].

5 Spin coating

There are many kinds of coating techniques, as mentioned in several books and books chapters [13–18]. The most important film-forming technique that has been used for the development of polymer solar cells is spin coating. This technique has been subject to many essential studies [19]. In spite of the complex film formation process, it produces highly reproducible films and has several advantages over other coating techniques. During the drying process it allows the formation of the homogenous films over a large area (the diameter of the substrate up to 30 cm). This technique is used in the microelectronics industry for applying polymeric photoresists to silicon wafers and in crucial steps during digital versatile disc (DVD) and compact disc (CD) production. The spincoating operation refers to the addition of a liquid solution to a substrate then acceleration of the substrate to a specific rotational speed (see Figure 4). The liquid solution may be put on while the sample is spinning, or before spinning. The substrate's high angular velocity with the solution results in ejection of most of the applied liquid where only a thin film is left on the substrate. The rest of solution gets off the surface and is considered a disadvantage of the spin coating process, since we do not use most of the solution. The thickness, surface topography and morphology of the final deposited film obtained from a particular material in a solvent at a given concentration is highly reproducible, and this is

considered an advantage of using spin a coating technique. We are limited to only the range of thicknesses that can be obtained, because we depend on the observation of the resulting morphology, thickness and surface topography and the preparation of a film depending on different specifications. These properties depend on viscosity, rotational speed, volatility, concentration and molecular weight. They barely depend on the rate of deposition, the amount of solution deposited and the spinning time during the spinning process. The film thickness obtained from a spin coating technique can be calculated using an empirical formula [18]:

$$d=k\omega^{\alpha} \quad \text{.....(1)}$$

where:

ω = the angular velocity and, k and α are empirical constants referring to the physical properties of the solvent, solute and the substrate. The constant α has a value of nearly -0.5 and the constant k depends on some parameters like the initial viscosity of the processed solution [18].

The main disadvantage that comes with spin coating is that most of the applied solution is ejected during spin-coating due to the high rotational speed. A very small amount is required to complete the operation. Highly experience technicians can successfully spin-coat using only small amounts of solution. When a solution is deposited on the substrate and most of the extra solution has been ejected during spin coater rotation, the wet film is subject to several changes, which include changes in viscosity, evaporation of solvent, radial velocity of the solution, molecular arrangement at the solid–liquid and formation

of aggregates, etc. All these parameters can affect the final properties of polymer solar cells and that is why many scientific reports have dealt with different aspects of the spin coating process related to solar cell device output function [18].

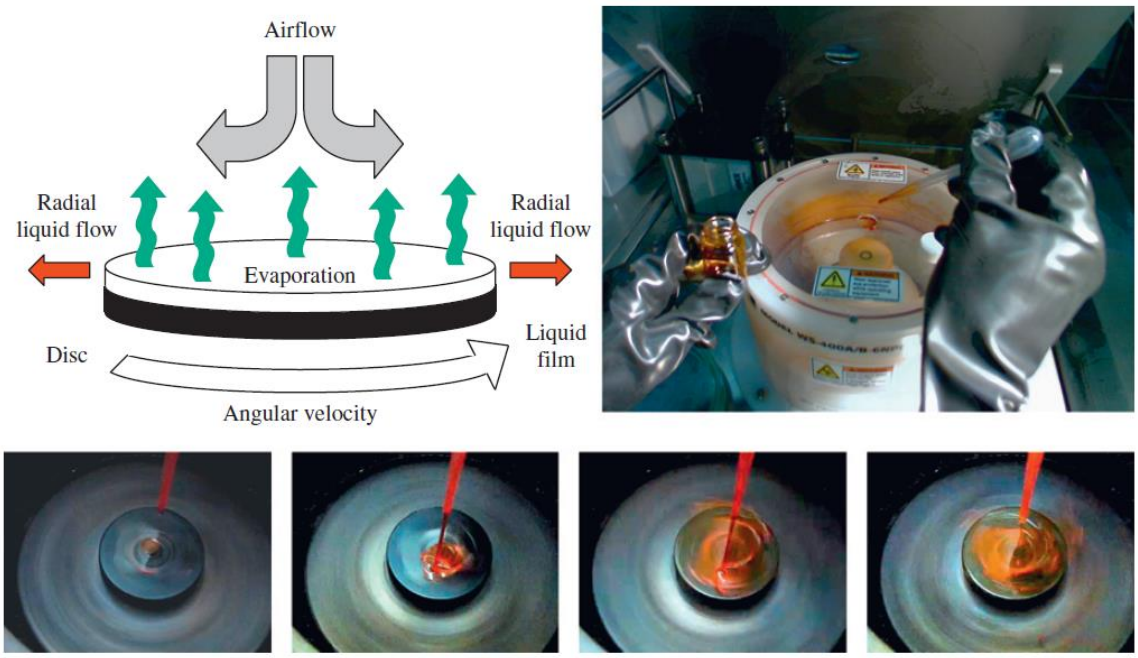

Figure 4: Schematic diagram of spin-coating process (top left) and a photograph of actual spin-coating operation inside a glove-box environment (top right) and high-speed images which show application of a solution of MEHPPV on a substrate and film formation. The images were recorded at camera speed of 300 images s^{-1} (below). The time frame of the images (from left to right) after impact of the first drop is: t = 17,100,137 and 180 ms [18].

Most of the studies of film formation using the spin coating [20-23] technique have been focused on the thickness of the film. It also depends on the viscosity of the solution and the spinning rotational speed [18]. Polymer solar cells film

thickness is important. Film homogeneity and concentration of defect is very important, because pinholes can lead to short circuits. Moreover, the study of the film shape is relevant in the context of polymer solar cells as the proper nanoscale morphology which can improve the performance of the device and the surface topography. The interfacial properties are under control and this technique produces reproducible films. Fixed film thickness and surface topography make us choose spin coating technique for film depositing. An example of this technique is when we spin coat P3HT:PCBM mixtures with 1,2-dichlorobenzene as a solvent [18] and allow for the wet film to dry slowly. Spin-coating technique is very useful on a laboratory scale during device optimization and materials screening, but it is not the optimum method or technique for high production of mass production polymer solar cells. The first reason for this is that the technique does not allow for patterning the formed film or adding a mask. We can apply the solution on a specific area and this is expected to be critical to the successful application of the technology. The second reason is that we handle the substrates individually, which is not compatible with R2R (roll to roll) technology. The third reason is thatthis technique wastes most of the solution, so this technique is not suitable for industry because it is not economic compared to R2R technology. It is too early to dismiss this technique in a production scale context, but this technology needs further improvement. There are other coating techniques such as doctor blading, which allows for the formation of films with a well-defined thickness. Additionally, screen printing is a very multi-purpose printing technique that gives us a full 2-dimensional patterning of the layer printed

on the substrate. It is economical because there is no loss of coating solution during printing [18].

6 Thermal evaporation of electrode

The last layer of a polymer solar cell is usually aluminum because it is a highly conductive material. Vacuum thermal evaporation is used to add this type of layer. Thermal evaporation (TE), also known as vapor deposition (VD), metal evaporation, vacuum evaporation (VE), or vacuum thermal evaporation (VTE), is one of the oldest techniques for thin films deposition. This technique has been used for depositing metals or metal alloys onto substrates. However, because of the growing semiconductor industry, demand for the depositing of organic thin films is growing. The principle of TE is very simple, as shown in Figure 5. A selection of experimental parameters that are based on understanding the details of the physical processes allows us to control the morphology of the resulting thin film.

The process of TE involves these steps:

(1) A material that is supposed to sublimate is placed in a boat in a vacuum and the boat is heated.

(2) By increasing the current through the filament, the temperature will go up and the material will start to boil or sublime (transform from solid directly into a gas).

(3) The evaporated material then travels from the heated boat in all directions in straight lines until an obstacle is reached, for example, the substrate or any

other surface inside the vacuum chamber.

(4) If a substrate is placed behind a mask, then the material condenses on the substrate surface on an area controlled by the mask [1].

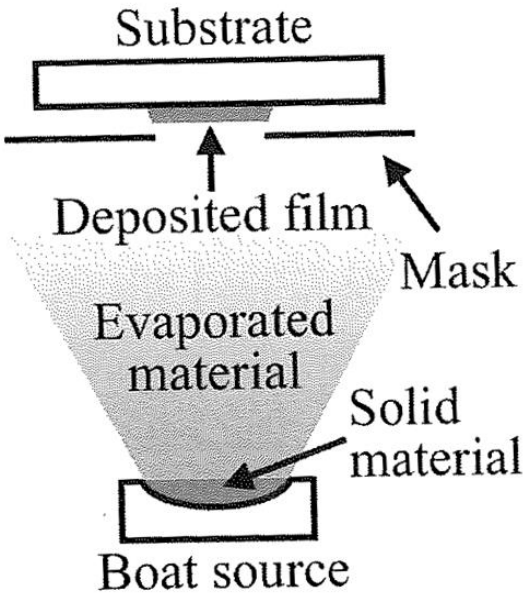

Figure 5: Schematic diagram of thermal evaporation [1].

7 Characterization of polymer solar cells

7.1 J-V characteristics and efficiency

Before talking about efficiency of polymer solar cells, we should understand some basic information about how much energy reaches the surface of earth. Air mass (AM) is the amount of atmosphere that light has to pass through before reaching the surface of the earth. The spectrum obtained after passage through a specific air mass is usually described by the abbreviation (AM) followed by a number that indicates how much air mass the sunlight has been transmitted through. In the space just outside the earth's atmosphere, the solar constant is 1366.1 $W.m^{-2}$ and the spectrum is called AM0 according to the ASTM E490-00 Standard. At the equator, the sun's spectrum is called AM1.0. At higher latitudes in northern Europe and the United States, the sunlight has to travel longer distances through the atmosphere to reach the earth’s surface, and the air mass there is called AM1.5, which corresponds to a receiving surface tilted by 37 degrees toward the equator, as shown in Figure 6 [1].

When the solar simulator is switched on, we should wait until the output stabilizes, and thus calibrates. Then we can connect the solar cell to the measuring device. The most common laboratory method of measuring solar cells involves recording the electrical response of the organic photovoltaic device in the dark and under illumination. The electrical response is measured by using a source meter. The source meter has the capacity to apply a voltage to the two terminals under test, such as a solar cell, and measure the current, so the voltage is the input and the measured current density is the output.

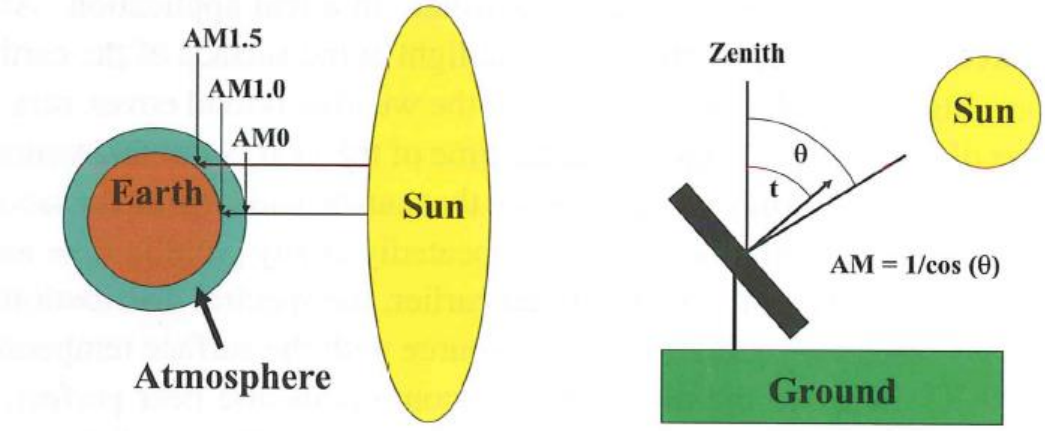

Figure6: Illustration of the air masses AM 0, AM 1.0 and AM 1.5. Schematic diagram of the receiving surface for the solar cell along with a calculation of the air mass AM. The normal of the receiving surface is inclined by an angle, t, towards the equator. The angle between the ground normal and the sun at zenith, θ, is used to calculate the air mass by the equation using the inverse of cos(θ). For AM 1.5 the tilt angle t = 37 degree and the zenith [1].

Alternatively, we can apply a current through the device and measure the voltage. Most researchers apply the voltage and then measure the current. The reason for this is based on the fundamental nature of the OPV device, which is a thin film. Furthermore, it is unpredictable what current range a given device will respond in, and the passage of a particular current set by the experimenter may require unrealistic voltages, leading to breakdown and destruction of the device due to short circuit. Most commonly, voltage ranges for single devices range between -1 V to +1 V. There are many commercially available Source meters, but the most commonly used source meter is the Keithley 2400 SourceMeter. It has a reasonable size and is accurate and reliable. Furthermore, it has many

different means of interfacing to computers such as a serial interface, IEEE-488 interface, and an Ethernet port (IP address). It is possible to perform two-contact and four-contact measurements, but for most OPVs we use two-contact measurements [1].

Minas M *et al* [30]studied the incorporation of modified single walled carbon nanofibers which contain pendant thiophene rings into organic solar cells. The chemical modification of the single walled carbon nanofibers (SWCNTs) increased both the device current (as shown in Figure 7) fill factor and the efficiency by 26% compared to the cells with the as-prepared SWCNTs. This improvement in performance of the cell is due to an extension of the excitons dissociation area and a faster electron transfer through the nanotubes, resulting in a more efficient dispersion of the nanotubes within the photoactive layer.

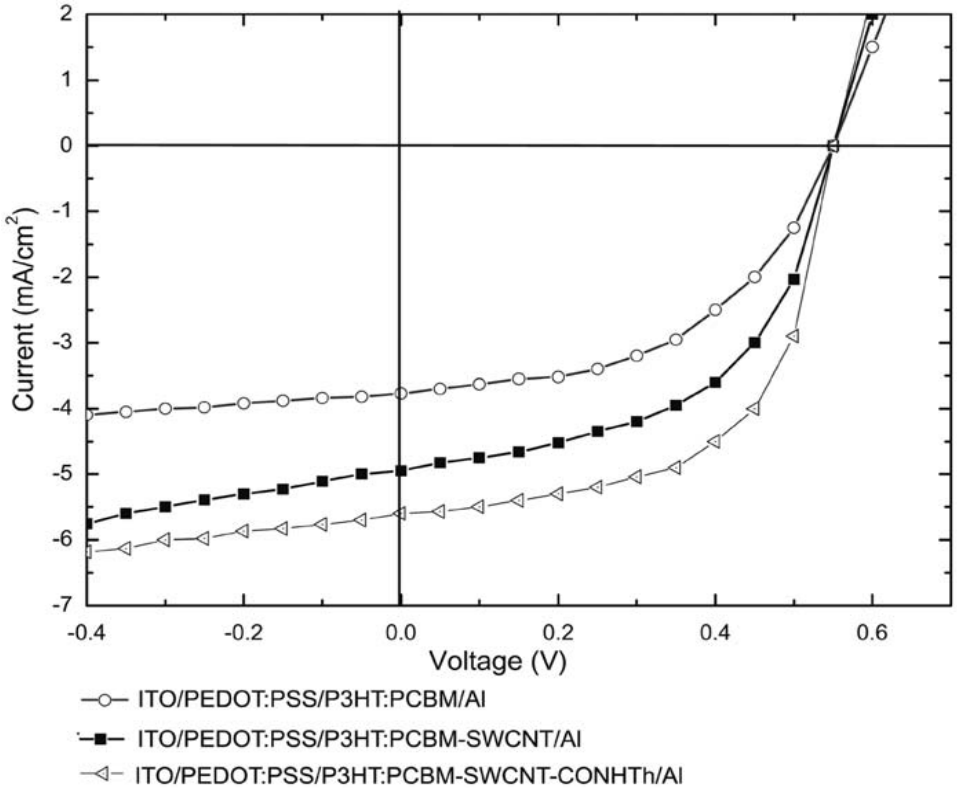

Figure 7: (J–V) curves of the polymer solar cells under 100mW/cm^2 AM1.5 solar simulator illumination [30].

Zhihui Feng *et al* [31] studied the effect of three small-molecule materials BCP, CuPc and pentacene as EBLs (electrode buffer layers) for polymer solar devices.They found that the insertion of EBLs can enhance the photovoltaic properties of the PV devices, especially the power conversion efficiency (PCE). The device with 1 nm BCP cathode buffer layer shows the highest PCE (3.06%), a 1.6X increase in efficiency compared to the cells without the buffer layer. The devices with 3 nm anode buffer layer (CuPc or pentacene) also exhibit enhanced improvement of photovoltaic performance, which results in a nearly 67% increase in the PCE over that of the typical device [31].

Fill factor is defined as the ratio (given as percent) of the actual maximum obtainable power, (V_{opt} x J_{opt}) to the theoretical (not actually obtainable) power, (J_{sc} x V_{oc}). This is a key parameter in evaluating the performance of solar cells

The fill factor is calculated by [32]:

$FF=J_{mp}.V_{mp}/(J_{sc}.V_{oc})$…… ……(2)

where :

J_{opt} or $J_{mp:}$ The current density at maximum power output and

V_{opt} or $V_{mp:}$ The voltage at maximum power output

V_{oc} : Open-circuit voltage

J_{sc} : Short-circuit current

Graphically, the ff is a measure of the "squareness" of the solar cell and is also the area of the largest rectangle which will fit in the current-volt curve as shown in Figure 8.

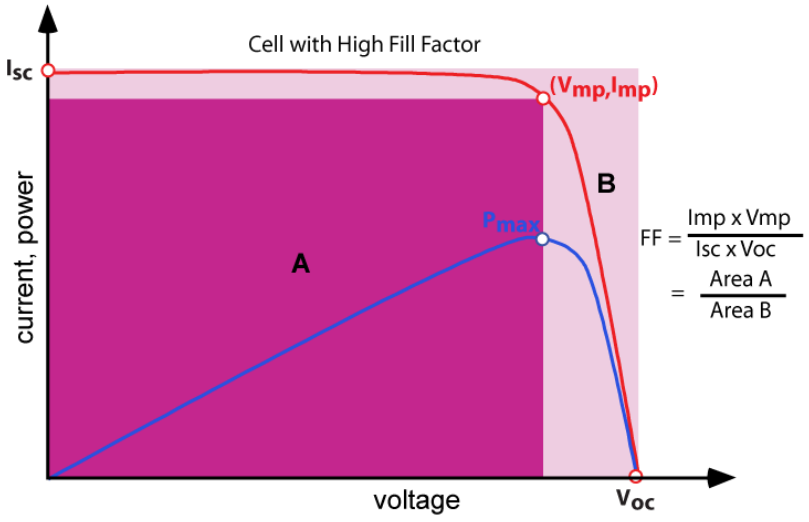

Figure 8: Illustration of cell output current (red line) and power (blue line) as function of voltage. Also shown are the cell short-circuit current (I_{sc}) and open-circuit voltage (V_{oc}) points, and the maximum power point (V_{mp}, I_{mp}) [40].

The power conversion efficiency (PCE),η, is calculated by [32]:

$$\eta = \frac{\text{output power}}{\text{input power}} = \frac{\text{Jsc.Voc.ff}}{\text{Total incident power density}} \quad \text{.....(3)}$$

External quantum efficiency (EQE) is the number of generated photons which escaped from a substance or a device divided by the number of electrons flowing through it. EQE is also defined as the ratio of the number of charge carriers collected by the solar cell to the number of photons of a given energy shining on the solar cell from outside. Incident photon to current efficiency (IPCE) is a "monochromatic version" of EQE, and it determines the ratio of generated electrons by the photons in the external circuit to incident photons of monochromatic light. In contrast to EQE, IPCE can be determined from the measuring of monochromatic light power density and calculated as a function of short circuit current density (Jsc), incident light power density, and wavelength (λ). Incident photon to current efficiency (IPCE) can be determined using some devices like (PEC-S10, Peccell Technologies, Inc.)

$$IPCE(\%) = \frac{I}{e \times photons} \times 100 \quad \text{.....(4)}$$

Where:

I : is the current density in amper per unit area,

e : is the elementary charge or 1.602 X 10^{-19} C $electron^{-1}$,

photons: is the number of photons from the lamp in unit area per second. Mi Sun *et al* found that annealing at 130 ºC gives the highest EQE as shown in Figure 9 shows the effect of thermal annealing on the prepared polymer solar cell [34].

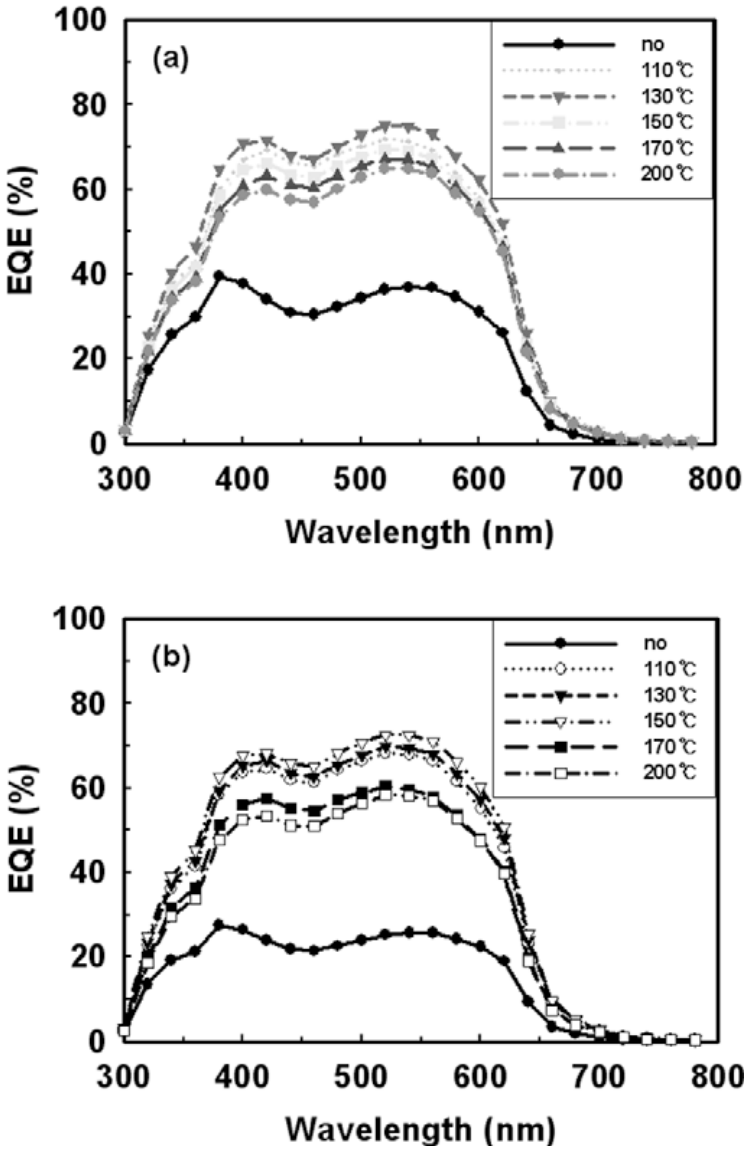

Figure 9. EQE of the devices (a) with and (b) without TiOx layer as a function of annealing temperature. [34]

7.2 Morphology

The most common characterization techniques used for monitoring morphology in organic solar cells are SEM (scanning electron microscope), TEM (transmission electron microscope), AFM (atomic force microscope), and XRD (x-ray diffraction).

7.2.1 Electron microscopy: SEM and TEM

An electron microscope is the microscope that produces an electronically-magnified image of a specimen for detailed study observation. The electron microscope (EM) uses a particle beam of electrons to create a magnified image of it. The microscope has a greater magnification than a light-powered optical microscope because it uses electrons that have wavelengths about 100,000 times shorter than visible light (photons), so we can achieve magnifications of up to 1,000,000X, compared to light microscopes which are limited to 1,000x magnification. The basic principle of SEM analysis consists of bombarding a highly-focused primary electron beam on the surface. Secondary electrons are consequently emitted from the sample surface and detected using a special detector. While generating the primary electron beam over the sample surface, a secondary electron image, the SEM image, is obtained. SEM has become a standard tool for visualizing material morphology. The advantage of the electron microscope is its superior lateral resolution and its capability of analyzing a broad range of scales from the nanometer range to the millimeter range. The disadvantage is the lack of a depth scale. [35]

SEM has a superior lateral resolution which can be used to visualize the bulk morphology by imaging a cross section of any material. Figure 10 shows the structure and thicknesses of each layer, together with two cross sections of the device using both SEM and transmission electron microscopy (TEM). The TEM is on a sample prepared by focused ion beam (FIB) lift-out technique. To protect the specimen during the FIB wedge milling, a layer of CVD glass and a sputtered gold layer are deposited on the sample. From the SEM image we can observe that the top Ag NP contact is not a fully sintered bulk Ag film, but is characterized by a merging of NPs into domains which allow a higher cell conductivity compared to non treated NPs. ZnO layer is also an aggregation of NPs and not a uniform, continuous layer. [36]

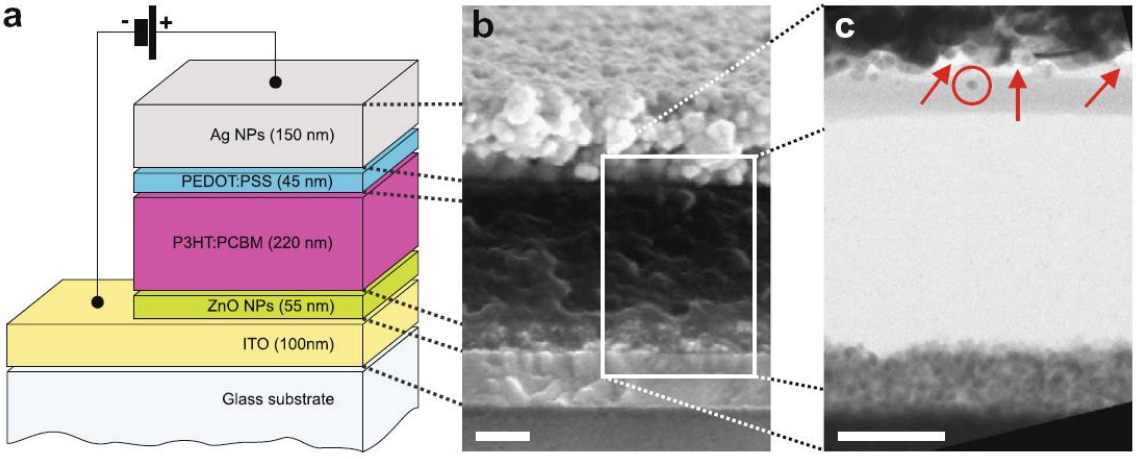

Figure 10. Morphology of PSC (a) Structure, (b) SEM and (c) FIB/TEM cross sections of the inverted polymer solar cell synthesis using a spray coated Ag top contact. The white scale bars represent 100 nm, the arrows indicate voids between PEDOT:PSS and the Ag NPs, and the circle highlights a NP embedded within the PEDOT:PSS layer. [37]

7.2.2 Atomic force microscope (AFM)

Atomic force microscopes produce a topographic image by using a scanning needle across the surface using contact or non-contact mode. The main weakness of AFM technique is the small analyzing area (nearly100x100µm2), and this, as well as the long acquisition time, makes it not suitable for screening purposes. One advantage of AFM is its excellent height resolution and lateral resolution in the angstrom range. Figure 11 is a good example of the usefulness of AFM as a characterization tool, where the morphology of the layers was characterized by AFM after thermal annealing (5min at 100 ºC). This Figure shows the 3D bilayer topography of PEDOT:PSS on ITO and P3HT/PCBM. The average surface roughnesses of the sample are1.1 nm and 1.2 nm for PEDOT:PSS and P3HT/PCBM layers, respectively, which are about the same roughness as the ITO layer (1nm). This morphology is relatively coarse compared to layers made by spin coating. [37]

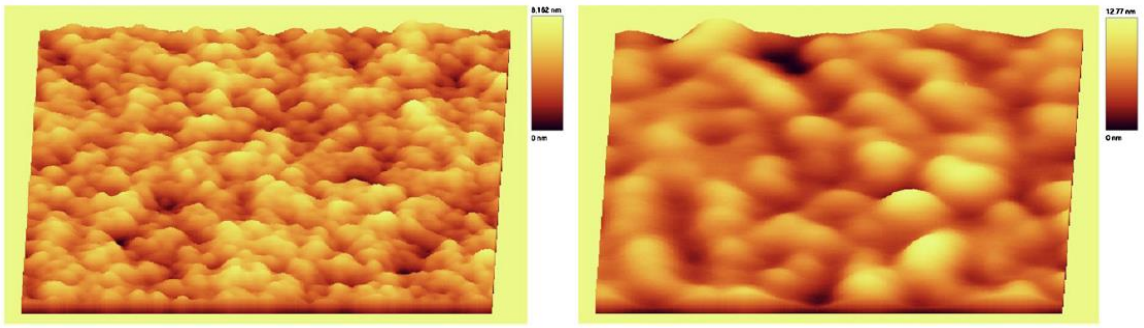

Figure 11. AFM topographic 3D images (left) :PEDOT:PSS (made by R2R ,1m/min); (right) :P3HT/ PCBM (made by R2R,1m/min on PEDOT:PSS made by R2R,1m/min); and scan range of 2×2 µm^2 .[37]

7.3 X-ray diffraction (XRD)

The X-ray diffraction pattern of the sample is obtained by illuminating the sample with X-rays. When the X-rays hit the material surface of the sample, the electrons interact with the X-rays and are diffracted by their interactions with the electrons. The diffraction pattern is recorded by special detectors. There are two main methods of X-ray diffraction: powder diffraction and single-crystal diffraction. The data collected from the diffraction pattern is a reciprocal space representation of the crystal lattice. X-ray diffraction is useful to monitor the structural molecular ordering of materials, which is highly relevant for applications regarding optimization of the charge transport properties in materials used for organic solar cells. [61]

Figure 12 shows how XRD can be used to monitor the effect of annealing at 150 °C on the crystallinity of regioregular P3HT:PCBM blended films drop casted onto a PEDOTPSS/ITO substrate. Furthermore, it shows that the annealing process increases the polymer crystallinity. The inset shows the crystal structure of P3HT (polymer active layer). The increased intensity due to the annealing process observed at diffraction angle equal nearly 5º corresponds to the interchain spacing in P3HT. The increased intensity at nearly 23º corresponds to the interchain spacing associated with face-to-face packing of the P3HT thiophene rings. [38]

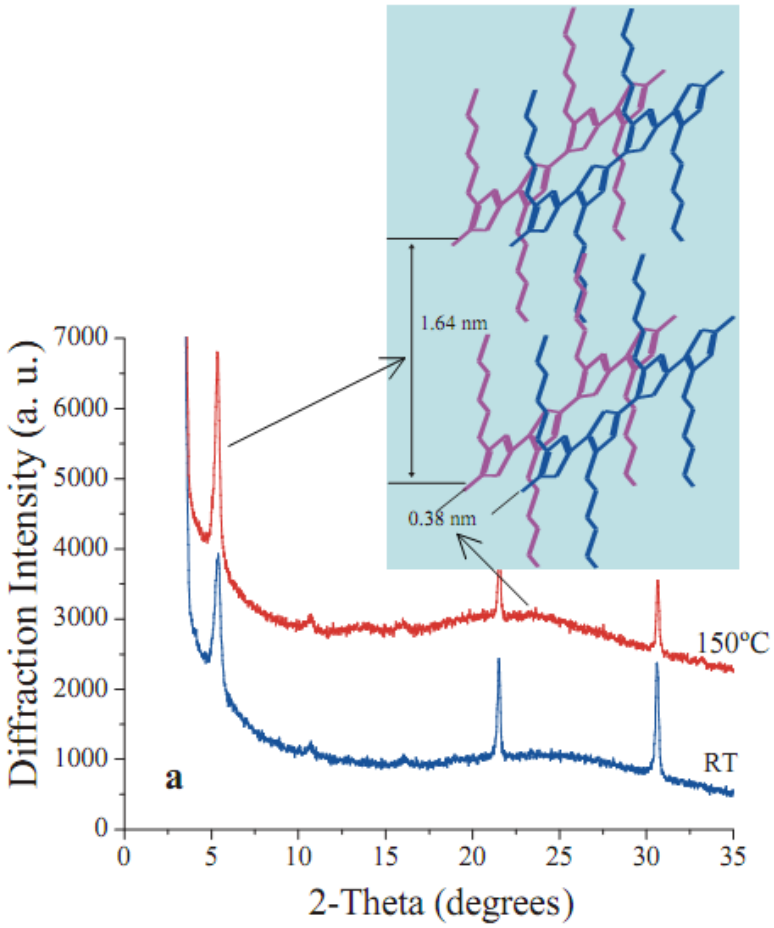

Figure 12: XRD spectra of a P3HT:PC60BM film drop spin casted onto a PEDOT:PSS/ITO substrate with and without annealing at 150°C for 30 min, and the inset shows the crystal structure of P3HT[38].

8. Organic Electronics Forecasts

Organic electronics include thin film transistors and electronic products, where the key component is organic and all parts are expected to be made from organic material. Today we have organic lasers, batteries, photo-detectors, fuel cells, and much more. Every product that organic material will be deposited in uses similar inks, or roll-to-roll at high speeds on similar or identical equipment. That means lower cost electronics and electric devices, with greater reliability, fewer

interconnects and improved tolerance of damage. But another big challenge is the replacement of traditional lighting with slimmer, flexible organic alternatives with lower costs and better environmental properties. The predicted global sales of each type of conductive polymer by 2020 are shown in Figure 13.[33]

IDTechEx finds that the organic electronics market will be nearly a $30 billion business in 2015 mainly used in logic, displays and lighting. They also expect that it will be a $250 billion business by 2025, with at least $10 billion from organic light emitting diode (OLED) like logic/ memory, organic displays for electronic products, OLED billboards, non-emissive organic displays, OLED lighting, batteries and photovoltaics with sensors. Most of these products will be printed, flexible, laminar products using the same or similar processes as printing techniques. Important other products such as laminar organic fuel cells, RF protection and organic electrostatic are also predicted. [33]

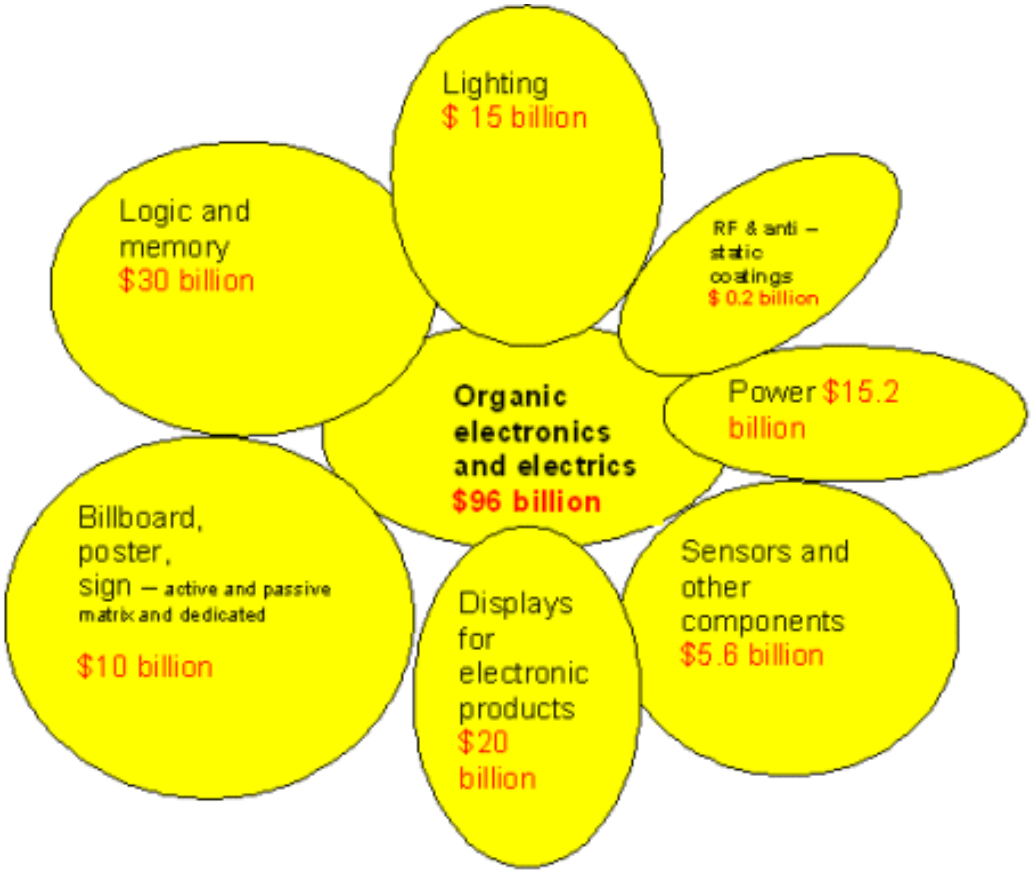

Figure 13: The expected annual global sales of each organic type by 2020. [33]

Chapter II

Objective and background

1 Research objectives

- To synthesize polymer solar cells made of P3HT/PC70BM with n-dodecylthiol for better performance.
- To study the effect of adding n-dodecylthiol and thermal annealing on the structure and performance of P3HT:PC70BM polymer solar cells, measured by PCE and EQE.
- To study the crystallinity kinetics of P3HT:PC70BM under various annealing conditions.

2 Research Hypotheses

- It is expected that adding n-dodecylthiol to P3HT will improve crystallinity. Crystallinity improvement will enhance charge mobility due to an increase in intermolecular interactions between polymer chains [41].
- Heat treatment (annealing) of P3HT:PC70BM will improve crystallinity. Literature search [78] shows that highly ordered structures involve higher absorbance of photons.
- Annealing usually reduces crystallite size which is associated with large PCBM clusters [83]. Larger PCBM clusters form better pathways for electron transport, which result in improving of short circuit current (Jsc) and hence improving power conversion efficiency (PCE) [84]. The research hypothesis are summarized in figure 14.

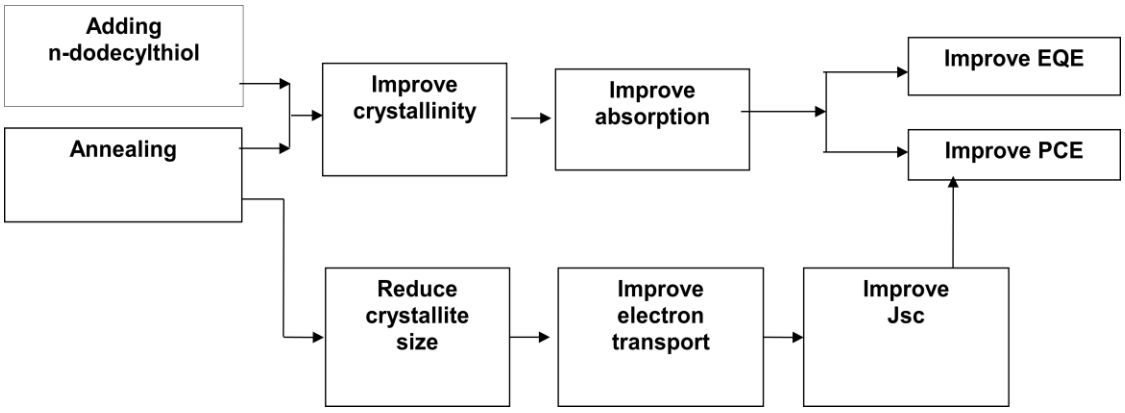

Figure 14: Schematic diagram showing the effect of annealing and n-dodecylthiol on polymer solar cell performance.

3 Novelty in the proposed work

- There is no published research on the effect of annealing on the physical and electrical properties of P3HT:PC70BM:n-dodecylthiol PSCs.
- Using XRD in conjunction with DSC to study the crystallinity and crystallinity kinetics of P3HT:PC70BM solar cells.

4 Significance of this research

Understanding the relationship between structure (e.g., crystallinity) and performance (e.g. QE, PCE) will help us push the envelope on the practical levels of energy conversion efficiency for polymer solar cells.

Chapter III

Experimental Work

1 Materials

Regioregular P3HT Rieke ‘‘E’’ was purchased from Rieke Metals, Inc. and used as received. PC70BM (synonyms 71BFA, [70]PCBM, PC71BM) was purchased from SES Research Incorporation. Poly(3,4-ethylenedioxythiophene) poly(styrenesulfonate) (PEDOT:PSS) 1.3 wt % dispersion in H_2O, conductive grade, was purchased from Sigma-Aldrich. Chlorobenzene was purchased from Sigma-Aldrich. ITO coated glass slides (1.1 mm, 25 slides Resistance, 10 Ohm/sq, Size 1"x3" and ITO thickness is 20-100 nm) were purchased from the website (nanocs.com).

2 Fabrication of solar cells

The solar cell devices used here were prepared on glass/ITO substrates. The substrates were cleaned by an ultrasonic sonicator in detergent and distilled water, then dried at 110 °C for 30 min. A 30-50 nm thick poly (ethylenedioxythiophene): poly(styrenesulfonate) (PEDOT:PSS) layer was spin-coated on the ITO glass and dried at 110-160 °C for 30 min using a Laurell Spin Coater (WS-400 BZ 6 NPP/LITE). A 100nm-150nm thick active layer (P3HT/ PC70BM:n-dodecylthiol blends) was then deposited by spin-coating it under a nitrogen atmosphere. Finally, the samples were transferred into an evaporator; a 100nm thick of Al electrode was deposited by using a metal evaporator. The active surface area of a typical device is 0.25 cm^2. Figure 15(a) shows a schematic diagram of the synthesized polymer solar cell.

3 Characterizations

The crystallinity of the films was studied by X-ray diffraction (XRD) (Cu K-α source) under 40 kV and 40 mA tube current. The X-ray profile was recorded from 4° to 7° with a rate of 0.2°/minute. Differential scanning calorimetry (DSC) measurements were collected using TA instruments Q2000 with heating rate of 5 °C/min and sample weight of 5-10 mg. The current density–voltage (J–V) curves of the photovoltaic devices under white light illumination were measured using a solar simulator (Newport, 94021A) at one sun (AM 1.5G, 100 mW/cm^2) by a Keithley 2420 source meter equipped with a calibrated Si-reference cell (Oriel, P/N 91150V). Quantum Efficiency was measured using NewPort 200. Sample preparation is described in Appendix A.Dynamic Light Scattering (DLS) (Brookhaven instruments-Plas Zeta potential analyzer) was used to study the aggregation of P3HT:PC70BM:n-dodecylthiol dissolved in chlorobenzene solution.

4 How polymer solar cell works

The active layer of organic solar cells is composed of donor (polymer) and acceptor (fullerene) materials for charge separation and transportation. The mechanism of an organic solar cell is shown in figure 15(b). The active layer usually made of fullerene and polymers. The cell is made of an aluminum electrode and conductive ITO glass with the active layer between the two materials with a buffering material such as PEDOT:PSS to improve charge transportation. Photons are generally absorbed in the donor material to produce

excitons (holes and electron). These excitons migrate towards the acceptor material and separate into electrons and holes at the interface. The electrons and holes diffuse across the acceptor and donor materials respectively until they reach the aluminum and ITO electrodes.

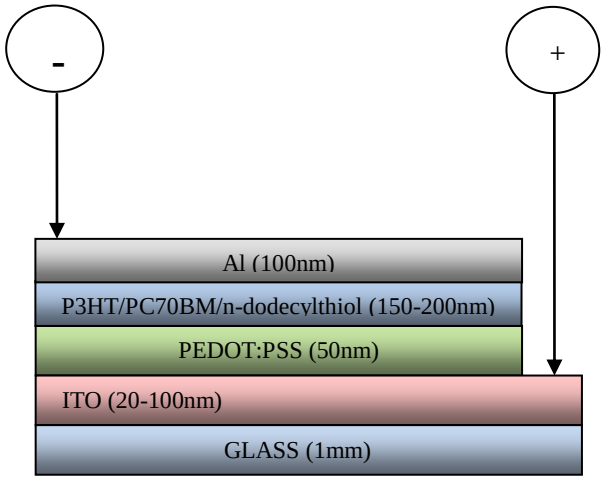

a)

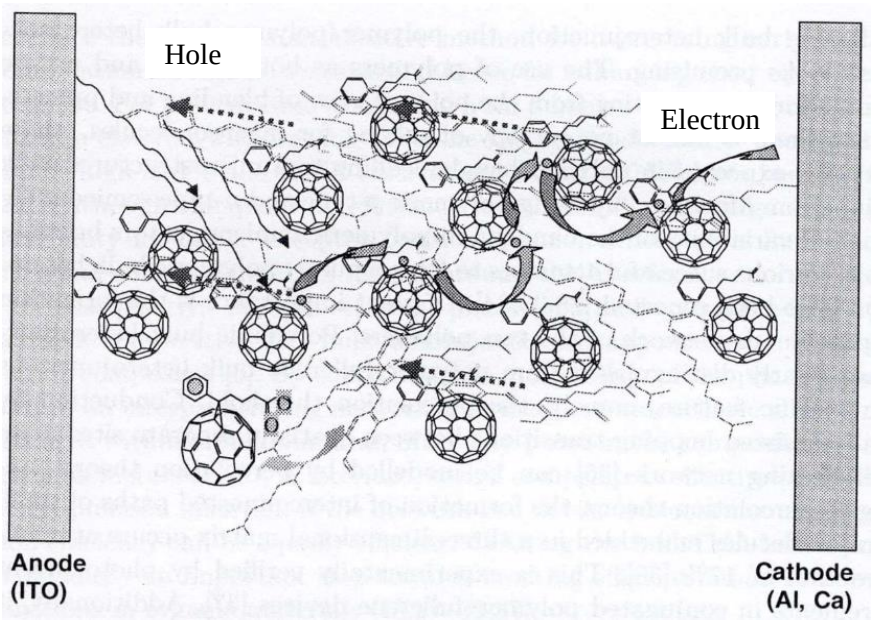

b)

Figure 15: (a) Schematic diagram of the synthesized polymer solar cell.

(b) Schematic diagram showing how organic solar cell works.

Chapter IV

Results

1 UV–vis absorption and External Quantum Efficiency (EQE)

Solid-state UV–Vis absorption spectra were recorded using a UV–Vis spectrometer (Perkin Elmer, Lamda 650) for P3HT/PC70BM blend films with different volume fraction of n-dodecylthiol (0% - 5%), as shown in Fig. 16. Absorption intensities increased by increasing the amount of n-dodecylthiol in the film composites with peaks at 470-500 nm and two shoulders at 595 nm and 645 nm. The peak and the vibronic shoulder correspond to P3HT only [48,49]. The peaks shift slightly to a higher wave length as we increase the %n-dodecylthiol added to the composite, and this shift is beneficial because it is shifted toward the peak of photon flux as shown in figure 16(b) [1]. This can lead to enhancement of the overall PCE. The shoulder was not distinguishably observed for P3HT:PCBM (without any n-dodecylthiol additive in the solution), and after adding n-dodecylthiol, the vibronic shoulders absorption became more visible. Previous research shows that the shoulders at wavelengths higher than 500 nm correspond to the absorption of extended conjugation of P3HT in the film solid-state [41, 45] and the second one at 650 nm results from the inter chain stacking of P3HT [41, 46]. The peak shifting associated with π-π stacking transition indicates that the chains of P3HT have a strong interaction. It has been previously demonstrated by S. Rughooputh *et al.* [44] and Jiangang Liu *et al.* [41] that adding n-dodecylthiol to P3HT:PCBM improves the crystallization of the polymer film and its self-organization ability. Our results are in line with previous

research, which shows that adding n-dodecylthiol enhances absorbance of P3HT/PCBM [41].

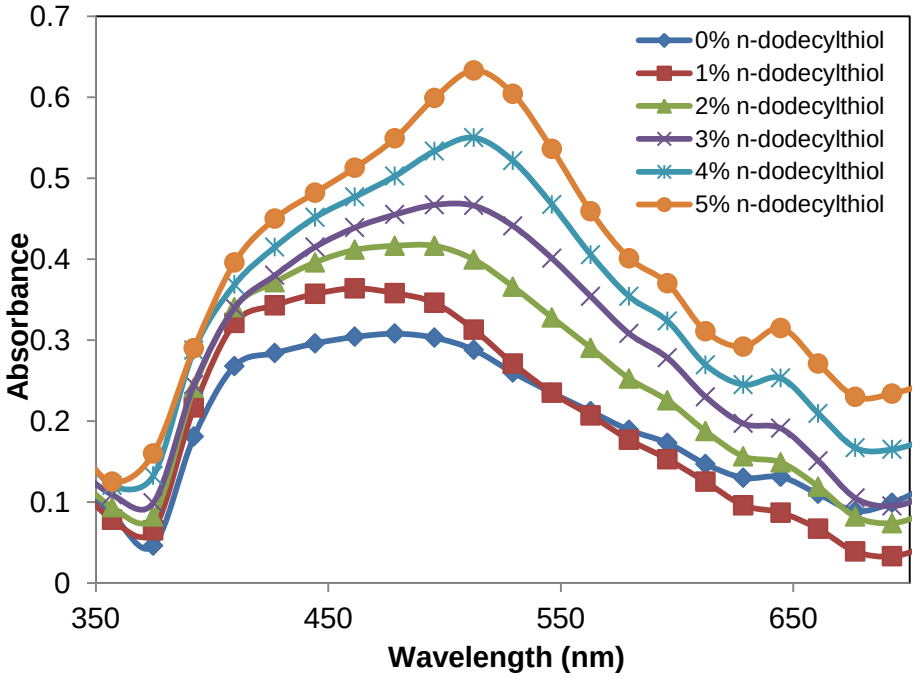

a)

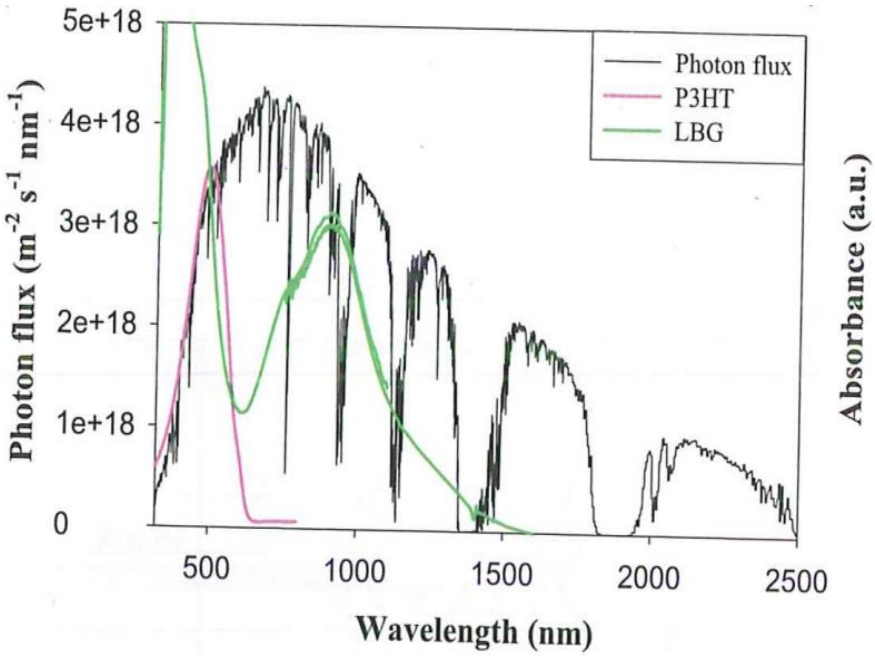

b)

Figure 16:a) Absorption spectra for P3HT/PC70BM blend films with different volume fraction (0%, 1%, 2%, 3%, 4% and 5%) of n-dodecylthiol. b) Absorption spectra of P3HT, a low bandgap polymer and solar spectrum [1].

External quantum efficiency (EQE) is the number of generated photons which escaped from a substance or a device divided by the number of electrons flowing through it. Also, EQE is defined as the ratio of the number of charge carriers collected by the solar cell to the number of photons of a given energy shining on the solar cell from outside. Figure 17 shows the EQE values of the P3HT:PC70BM:(0-5 % n-dodecylthiol).The graph shows that the P3HT:PC70BM EQE increases by increasing the percentage of n-dodecylthiol. Unannealed devices with 5% n-dodecylthiol exhibit the highest EQE value of 70.4% compared to 60.1% for the device without n-dodecylthiol additives. The EQE value corresponds to a wavelength ranging from 450 to 570 nm. From this graph, we conclude that the EQE values are related to the crystallinity and the surface morphology of the active layer [41]. The improvement of EQE leads to an increased hole and electron polaron mobilities. Results from EQE are compatible with the results obtained from UV-vis absorption, which indicates that the higher the percentage of n-dodecylthiol, the more absorption and EQE obtained from the cell, i.e. higher electron mobility and better J-V characteristics as presented earlier by Jiangang Liu *et al*[41].

In order to explain the improvement in UV-Vis absorption and EQE with the addition of n-dodecylthiol, a series of tests were performed to characterize the structure of P3HT:PC70BM:n-dodecylthiol using XRD and DSC analysis.

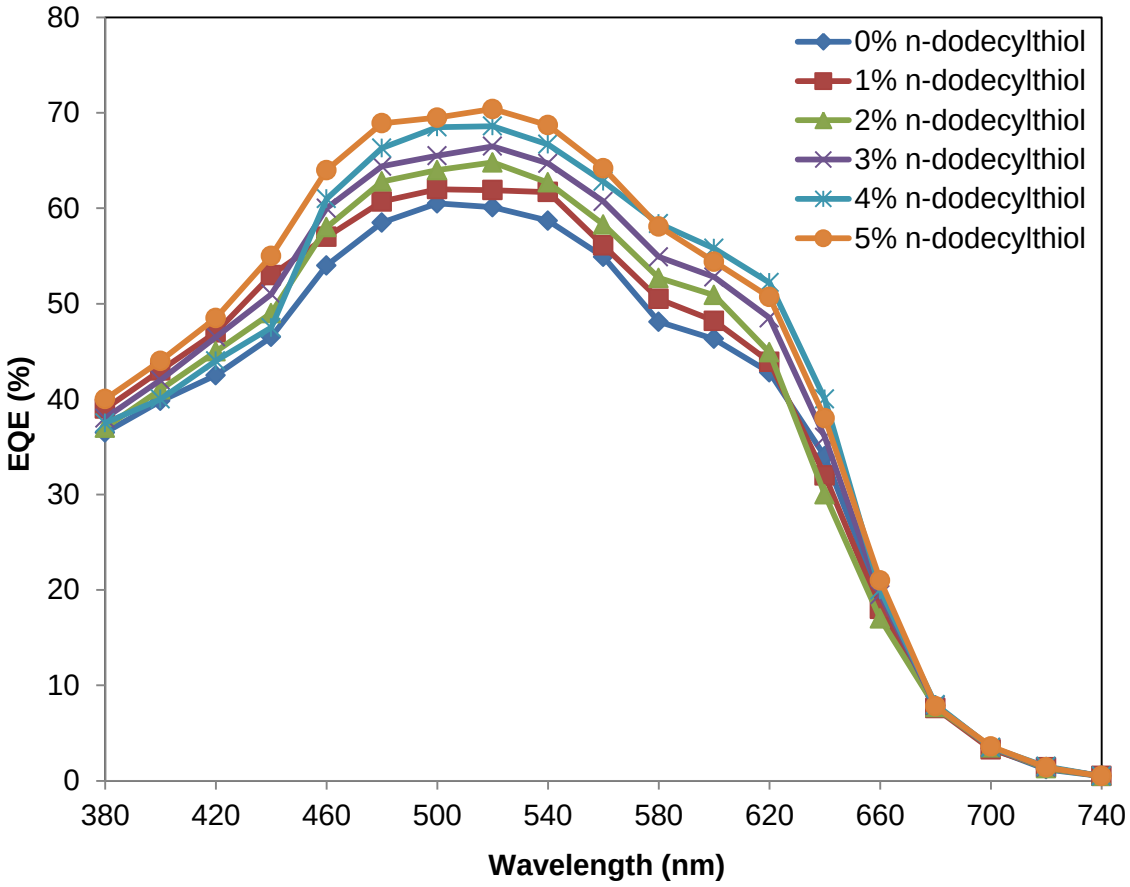

Figure 17: EQE for P3HT/PC70BM blend films with different volume fraction (0%, 1%, 2%, 3%, 4% and 5%) of n-dodecylthiol.

2 Crystallinity Analysis (XRD)

The structural properties of the films were studied by X-ray diffraction (XRD) using Cu K-α source under 40 kV and 40 mA tube current. The X-ray spectrum was recorded from 4° to 7° with a rate of 0.2°/minute using automatic slits. The improvement of P3HT self-organization ability with the addition of n-dodecylthiol was reflected in the XRD results shown in Figure 18 (a, b, c and d). All P3HT:PC70BM:n-dodecylthiol films showed an intense diffraction peak at 2θ = 5.4°, corresponding to the ordered structure of P3HT main chains. This indicates that some of the P3HT chains escaped from the amorphous region and then rearranged as single molecules in the solution. Also, it is evident in Figure 18(a) that there is a small increase in the peaks of the polymer with 0-5 % n-dodecylthiol before annealing, which confirms claims made by other researches [50,51]. The intensity of the peaks at 2θ = 5.4° shows that increasing the crystallinity of the films is directly proportional to the addition of n-dodecylthiol, and this is in line with other researchers such as Jiangang Liu *et al.* [41].

Figure 18(b, c and d) shows XRD spectra for PSC samples which were annealed for 10, 20 and 30 minutes at 150 °C in vacuum, respectively. Annealing temperature and time were selected in line with previous research work showing that P3HT:PCBM exhibited optimum electrical properties after annealing at 150 °C [21]. Annealing shows an increase in the peak intensity with increase the amount of n-dodecylthiol, which increases crystallinity of P3HT due to the enhanced self-organization ability in the presence of n-dodecylthiol. Diffraction peaks caused by PC70BM were barely noticeable in the XRD spectra of

P3HT:PC70BM films, both with and without n-dodecylthiol. Therefore, it is safe to assume that the addition of n-dodecylthiol only affects the crystallization of P3HT with little or no influence on the crystallization of PC70BM. Previous research [49] showed that PCBM is not a crystalline material.

Up to now, there is no research on the effect of annealing on P3HT:PC70BM: n-dodecylthiol PSCs. Our research shows that annealing has a big effect on physical and electrical properties of P3HT:PC70BM: n-dodecylthiol. Figure 18(b) shows that the peaks at 2θ = 5.4° are getting higher compared to the samples without annealing, showing a slight increase in crystallinity after annealing for 10 minutes at 150 °C. The peaks are getting higher by increasing the annealing times. Annealing for 20 and 30 minutes are very close in peak intensities, showing that annealing for 20 and 30 minutes have closer crystallinity values,as shown in Figure 18(c and d). Figure 18(d) shows that the highest crystallinity among the heat treated samples occurred with 2% n-dodecylthiol concentration. Increasing n-dodecylthiol content above 2% led to a decline in crystallinity due to uncontrolled phase separation, interruption in P3HT crystallization, and/or aggregation and insufficient dissolving of particles, as described by Soo et al [71].

Crystallite size has been calculated using Scherrer's equation [72].

Size of polymer crystallites (L) is calculated as follows:

$$\mathbf{L\ (nm) = 0.9\ \lambda / (\Delta_{2\theta} * \cos\theta)} \quad \text{..... (5)}$$

Where:

λ= Cu K-α wave length= 0.154 nm

Δ2θ= is the full width half maximum of the peak

θ= is half the angle at peak

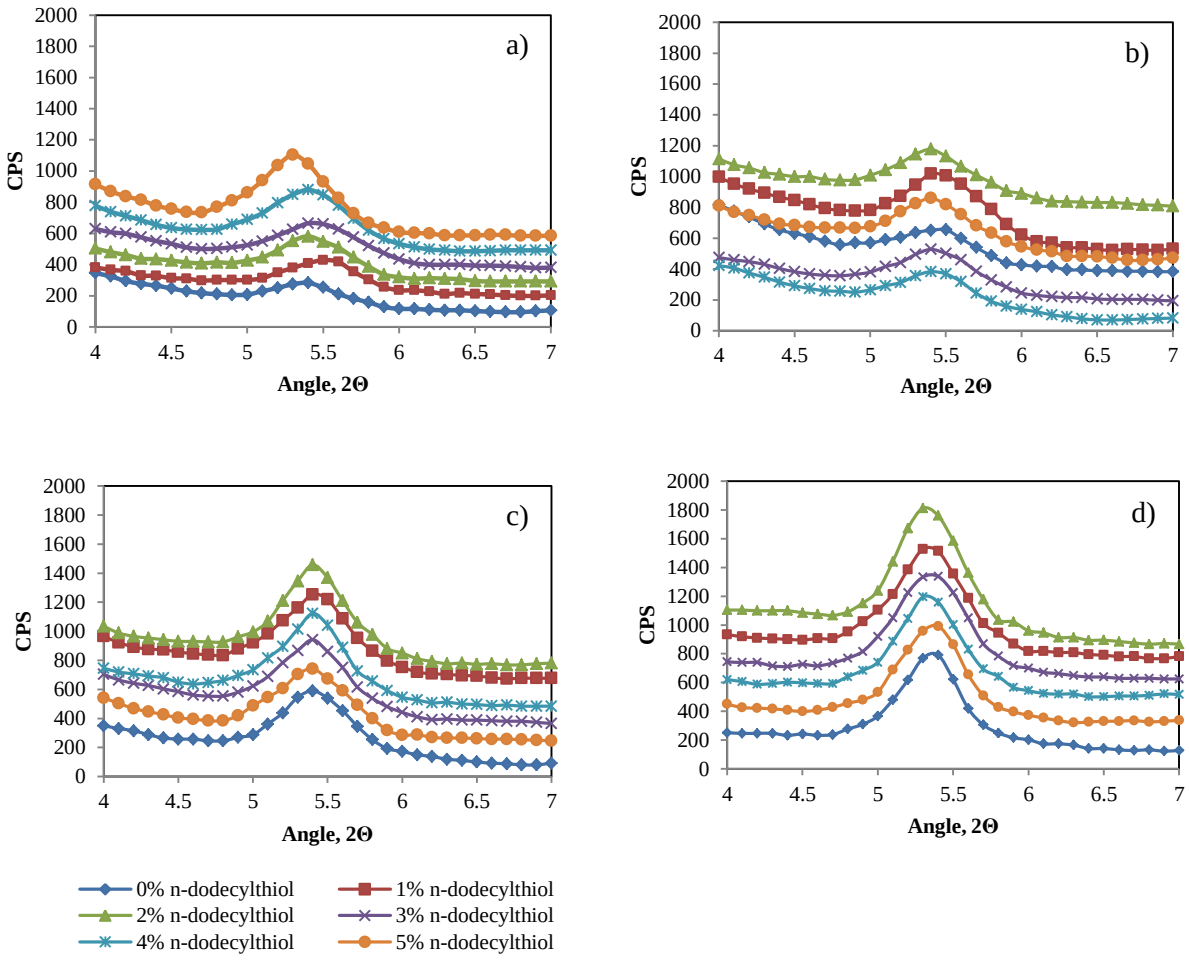

Figure 18: XRD spectra for P3HT : PC70BM : (0-5%) n-dodecylthiol: a) Before annealing, b) After annealing at 150 °C for 10 min, c) After annealing at 150 °C for 20 min, d) After annealing at 150 °C for 30 min.

The higher XRD peaks indicate that more P3HT crystallites have been formed; i.e. higher crystallinity. However, these crystallites are higher in number but shorter in size as depicted in Figure 19. Table 2 summarizes the calculations for

the crystallite size after annealing for 30 minutes at 150 ºC. Crystallite size calculations for annealed samples show that 2% n-dodecylthiol samples exhibit the smallest crystallite size of 11.19 nm. A smaller crystallite size suggests a shorter path of the charge carriers between P3HT backbones, which is beneficial for getting a higher short circuit current (J_{sc}) of the devices [51]. Therefore, the reduced crystallite size and the increased number of P3HT single chains after the addition of n-dodecylthiol in the polymer solution contribute to enhancing the crystallinity of P3HT.

Table 2: Calculation of polymer crystallites size after annealing at 150 ºC for 30 min.

% n-dodecylthiol	**$\Delta_{2\theta}$ (degree)**	**$\Delta_{2\theta}$ (radian)**	**Size of polymer crystallites at 150 ºC for 30 min L (nm)= 0.9 $\lambda/(\Delta_{2\theta}*\cos\theta)$**
0	0.45	0.0078	17.7
1	0.65	0.0113	12.2
2	0.71	0.0124	11.2
3	0.6	0.0105	13.2
4	0.54	0.0094	14.7
5	0.5	0.0087	15.9

Table 2 (continued):

L(nm) Sample group 1	L(nm) Sample group 2	L(nm) Sample group 3	Average	Max - Min	Error
17.65	18.47	16.91	17.68	1.56	0.044
12.22	12.04	11.68	11.98	0.54	0.023
11.19	10.88	10.59	10.89	0.60	0.027
13.24	12.81	13.24	13.10	0.43	0.016
14.71	15.28	14.19	14.73	1.09	0.037
15.89	16.21	15.58	15.89	0.63	0.020

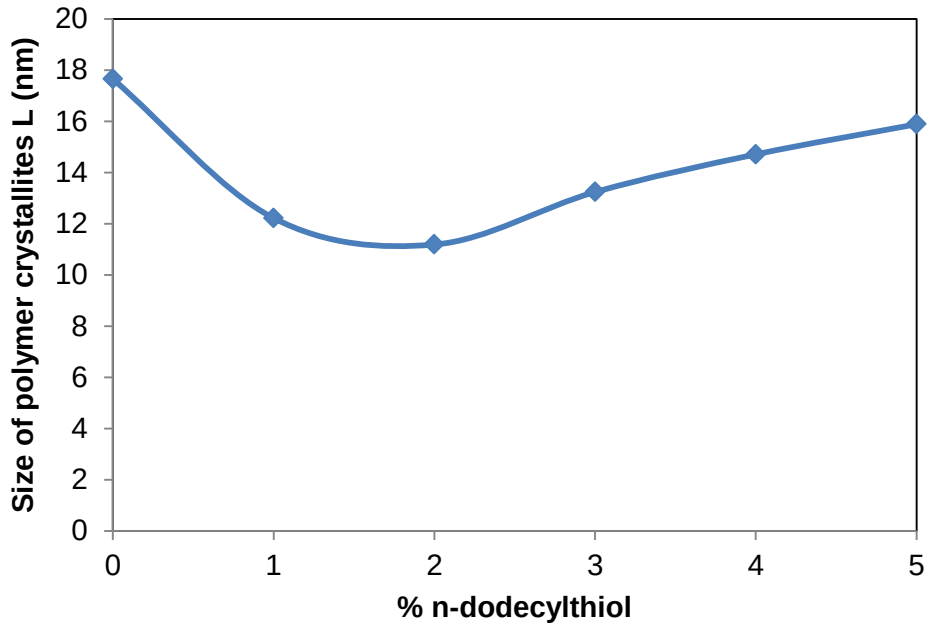

Figure 19: Effect of % n-dodecylthiol on crystallite size of P3HT.

3 DSC for Study of Crystallinity

To further investigate the effect of adding n-dodecylthiol on crystallinity of polymer nanocomposite, differential scanning calorimetry (DSC analysis was used similar to previous published research [52-54]. Melting temperature (Tm) and enthalpy changes of melting were measured under thermal pre-treatment conditions (5°C/min for heating scan, and under nitrogen atmosphere of 50 ml/min). Figure 20(a) shows DSC thermograms for heat flow of P3HT:PC70BM:0-5%n-dodecylthiol obtained by heating of samples prepared without heat treatment. The melting temperature of P3HT:PC70BM:0-5%n-dodecylthiol was observed at a temperature range of 180-220 °C, which fits in the range of previous researchers [70], corresponding to the ordered structure of P3HT main chains. This indicates that some of the P3HT chains escaped from the amorphous region and then rearranged as single molecules in the solution. Also, it is evident in Figure 20(a) that there is a small increase in the melting heat flow of the polymer with 0-5 % n-dodecylthiol before annealing, which confirms the results obtained by XRD. The intensity of melting heat flow shows that increasing the crystallinity of the films is directly proportional to the addition of n-dodecylthiol.

Figure 20(b) shows DSC heat flow for PSC samples which were annealed for 30 minutes at 150 °C in vacuum. Annealing temperature and time were selected in line with previous research work showing that P3HT:PCBM exhibited optimum electrical properties after annealing at 150 °C [21].Annealing shows an increase in the melting heat flow with increasing the amount of n-dodecylthiol, which

increases crystallinity of P3HT due to the enhanced self-organization ability in the presence of n-dodecylthiol. However, the melting heat flow reflects the crystallinity of P3HT only, because previous research [49] showed that PCBM is not a crystalline material. Therefore, it is safe to assume that the addition of n-dodecylthiol only affects the crystallization of P3HT with little or no influence on the crystallization of PC70BM. Figure 20(b) shows that the highest crystallinity among the heat treated samples occurred with 2% n-dodecylthiol concentration. Increasing n-dodecylthiol content above 2% led to a decline in crystallinity due to uncontrolled phase separation, interruption in P3HT crystallization, and/or aggregation and insufficient dissolving of particles, as described by Soo et al [71].

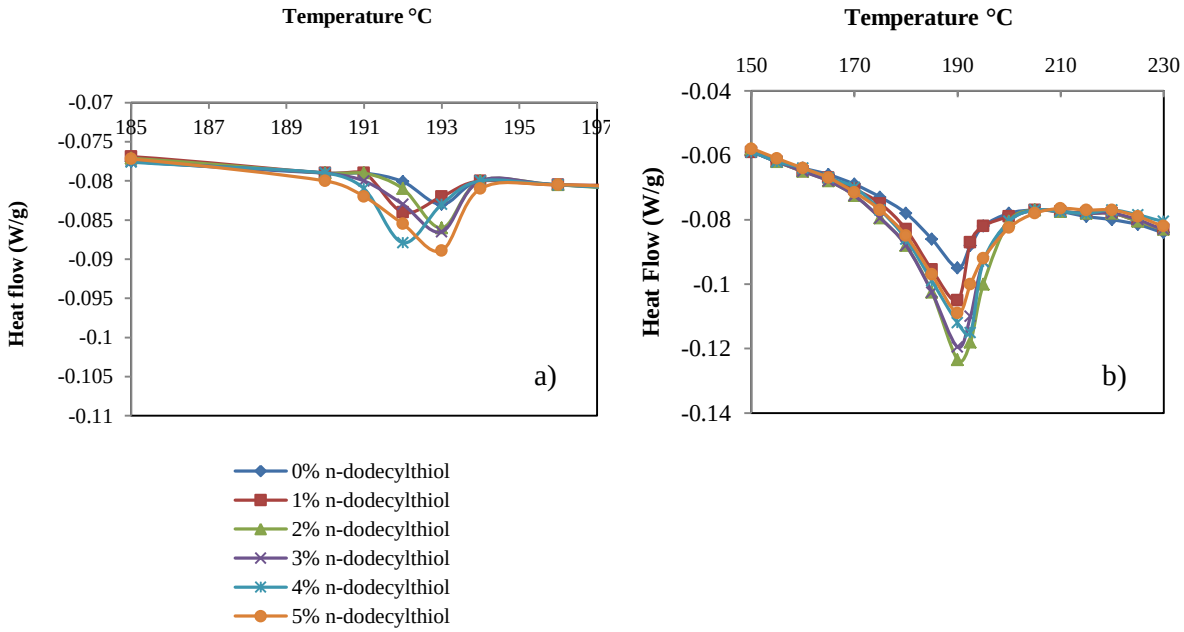

Figure 20: Differential Scanning Calorimetry (DSC) heat flow of P3HT:PC70BM :(0-5% vol.) n-dodecylthiol a) before annealing, b) after annealing.

The crystallinity (*X*c) of P3HT in a blend (P3HT:PC70BM:0-5% vol. n-dodecylthiol) was calculated using DSC at melting peak using the relation[55]:

% Crystallinity (X_c)= 100*ΔH /(ΔH_u*w_i).....(6)

Where:

Δ*H* is the enthalpy (in J/g of sample) of melting of semicrystalline polymer in a blend, Δ*Hu* is the enthalpy of melting of the theoretical 100% crystal (e.g., Δ*H*u,*P*3*HT=99 J/g*) [56] and w_i the weight fraction of component *i*.

Table 3: Calculation of percent crystallinity of samples prepared with 0:5% n-dodecylthiol.

n-dodecylthiol	ΔH(J/g) before annealing	ΔHu (J/g)	crystallinity X= ΔH/(Δhu*w) before annealing	Percent crystallinity X% before annealing	ΔH(J/g) after annealing	Percent crystallinity X% after annealing
0%	1.012	99	0.020	2.0	4.998	10.1
1%	1.258	99	0.025	2.5	6.933	14.0
2%	1.561	99	0.032	3.2	8.357	16.9
3%	1.693	99	0.034	3.4	8.149	16.5
4%	1.778	99	0.036	3.6	7.949	16.1
5%	1.845	99	0.037	3.7	7.831	15.8

Percent crystallinity calculations show an increase in crystallinity by adding n-dodecylthiol to P3HT:PC70BM polymer blends, before annealing, as shown in Figure 21(a) and Table 3. However, after annealing, crystallinity starts to decline when the content of n-dodecylthiol is higher than 2%. This is possibly due to the aggregation and/or polymer entanglement with excess amounts of n-dodecylthiol

during the annealing process, or due to uncontrolled phase separation and interruption in P3HT crystallization. Studies of aggregation using DLS showed an increase of aggregation of P3HT:PC70BM by adding n-dodecylthiol, as will be discussed in section (5.4).The aggregates can hinder crystallite formation and growth, which can result in reducing the crystallinity. DSC analysis showing the highest crystallinity occurring at 2% n-dodecylthiol is in line with our XRD analysis. Published literature [69] reported crystallinity values of pure P3HT between 40 and 60%, while mixing with PCBM hinders the crystallite growth, and hence reducing crystallinity.

In our research, n-dodecylthiol was added to P3HT:PC70BM to improve crystallinity, absorption, and power conversion efficiency. Pei Cheng et al. [78] added dimethylformamide (DMF) to P3HT:PC60BM to improve crystallinity and morphology. Higher crystallinity led to better charge transport, and hence improving in PCE. Results showed that adding DMF up to 10% improves crystallinity as shown. However above 10%, crystallinity starts to decline. P3HT:PC60BM:DMF maximum achieved PCE is 4.48% at 10%DMF additives. Effect of DMF additives on P3HT:PC60BM PSCs has a similar trend to our results, which show that n-dodecylthiol additive improve P3HT:PC70BM PSC crystallinity up to 2% then crystallinity drops. Their claim is correct, because it depends on their XRD measurements which show that DMF improves crystallinity of P3HT:PC60BM PSCs up to 10%, and above that crystallinity starts to decline. Our results show a similar trend to Pei Cheng et al. [78]. P3HT:PC70BM:n-dodecylthiol crystallinity greatly improved after annealing. However, crystallinity starts to slowly decline when the content of n-dodecylthiol is higher than 2%. This is possibly due to the polymer entanglement with excess amounts of n-dodecylthiol during the annealing process. In addition, excess amount of n-dodecylthiol can interrupt

P3HT crystals; i.e. leaving less space for crystals growth. This results in too fast crystallization with less ordered crystalline structure, i.e. less crystallinity [78].

Jiangang Liu et al [41] studied the effect of adding n-dodecylthiol to modify and improve properties of P3HT/PC60BM:n-dodecylhiol PSCs as shown in Figure 21(c). They claim that XRD results indicated higher crystallinity of P3HT after the addition of n-dodecylthiol as shown. Their results show improvement in crystallinity by adding n-dodecylhiol. Jiangang studies P3HT/PC60BM, and in our research PC70BM was used instead of PC60BM. Their claim is correct, but my observation that the difference in crystallinity between XRD for 2% and 4% additives was relatively small, and the authors should measure XRD for samples with 5 or 6% to see the changes in crystallinity behavior with the additives. Our results show that above 2% n-dodecylhiol, crystallinity of P3HT starts to decline.

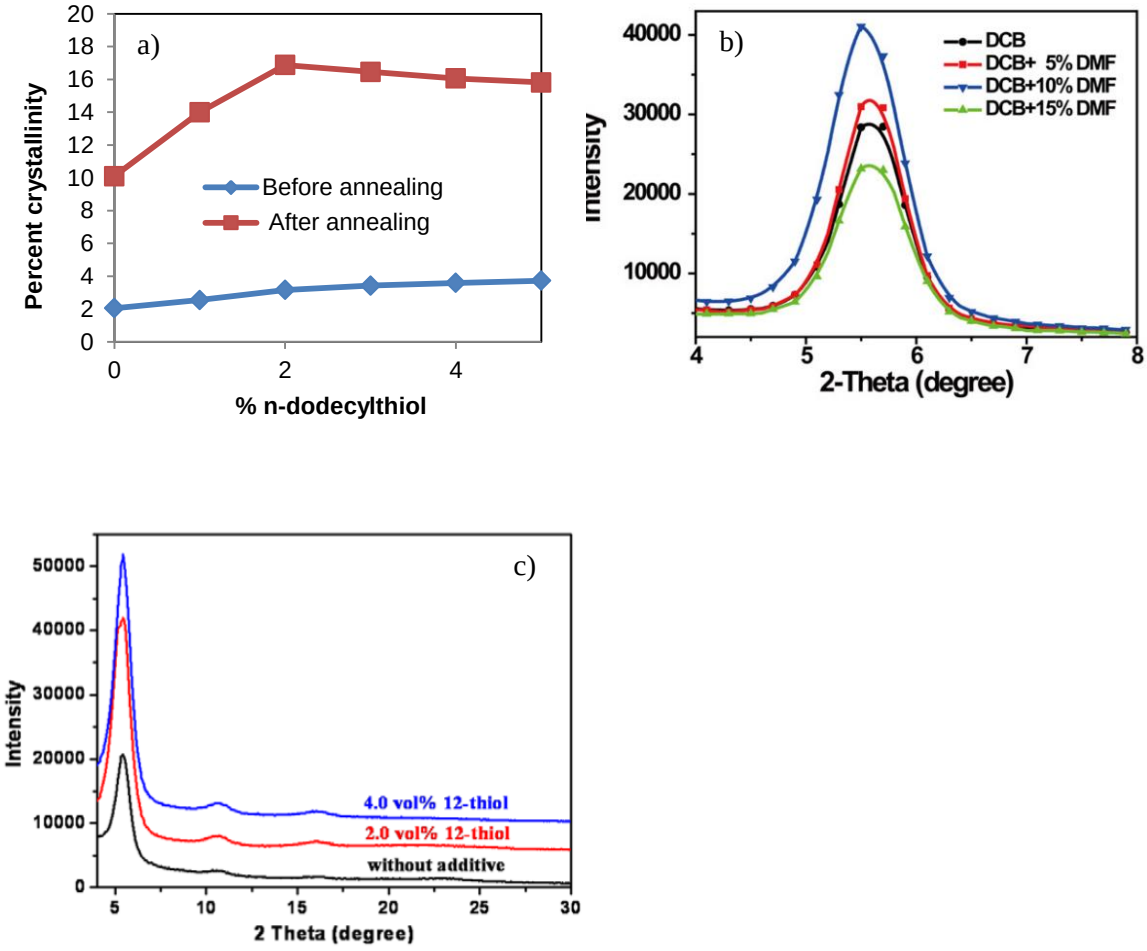

Figure 21:a) Percent crystallinity for P3HT:PC70BM:(0-5 vol.%)n-dodecylthiol before and after heat treatment, b) XRD patterns of P3HT:PC60BM blend films with different percentages of DMF [78], and c) XRD patterns of P3HT with different percentages of n-dodecylthiol [41].

4.1.1 Solar simulator measurements

Figure 22 shows the characterization of complete samples after depositing Al layer using physical vapor deposition (PVD) under ultralow pressure and without and with heat treatment. The results show that the maximum efficiency was 1.65% (2 volume % n-dodecylthiol) for the samples prepared without any heat treatment. The efficiency values were almost doubled after heat treatment.

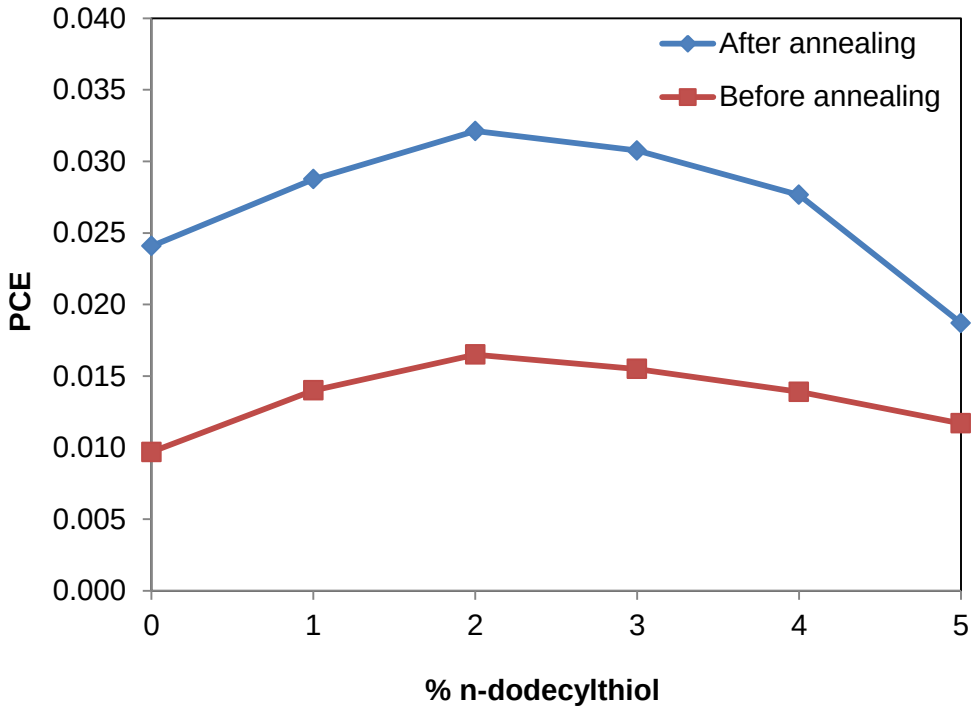

Figure 22: PSC of Glass/ITO/P3HT:PC70BM:0-5% volume n-dodecylthiol/Al before and after heat treatment.

EQE is also defined as the ratio of the number of charge carriers collected by the solar cell to the number of photons of a given energy shining on the solar cell from outside. Solar cell power conversion efficiency (PCE) is the ratio of the electrical output of a solar cell to the incident energy in the form of sunlight. Several factors affect PCE, including its reflectance and thermodynamic

efficiency, charge generation and separation efficiency, and conduction efficiency.

Although UV-Vis absorbance and EQE at 2% n-dodecylthiol is lower than at 5% n-dodecylthiol which means that devices with 5% n-dodecylthiol absorb more photons and generate more charge carriers than those with 2% n-dodecylthiol, PCE at 2% n-dodecylthiol before annealing (1.7%) is higher than those with 5% n-dodecylthiol (1.2%).

Our explanation of this behavior is that the excess amount of additives enhanced the absorption, and charge generation and this enhanced EQE. However for PCE, excess amount of additives contaminated the cell, which resulted in reducing Voc . Reducing Voc is not favorable because it results in reducing the power conversion efficiency (PCE = V_{oc}*J_{sc}*FF / Total incident power density). In addition, above 2% additives, Jsc continuously decreased, and this result in decreasing PCE too. Sung et al [82] approached 100% Quantum Efficiency, but with only 6.1% PCE. When measuring PCE, they reported that photo-generated excitons often recombine before reaching the interfaces in films cast leading to low PCE and cell performance.

J-V characteristics for the prepared PSC samples are summarized in Table 4. Figure 23shows J-V characteristics of the prepared devices. The open circuit voltage (V_{oc}) decreases with the addition of n-dodecylthiol (Figure 24) from 0.6615V to 0.6199V. It is well known that open circuit voltage (V_{oc}) of polymer solar cells depends on the difference in energy levels between the HOMO of the donor and the LUMO of the acceptor [57]. The addition of n-dodecylthiol results

in decreasing the value of V_{oc} for the polymer solar cell device, because adding n-dodecylthiol increases the active layer i.e., P3HT conjugation length. As a result, it decreases the HOMO energy level of P3HT.

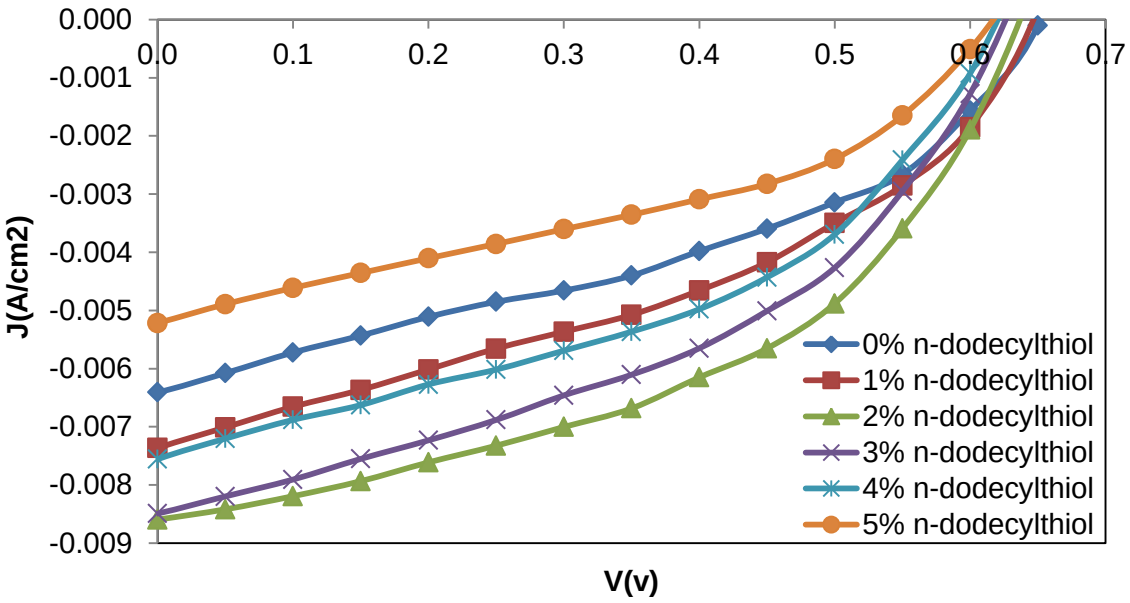

Figure 23: J-V characteristics of P3HT:PC70BM with (0-5)% n-dodecylthiol content under AM 1.5G illumination.

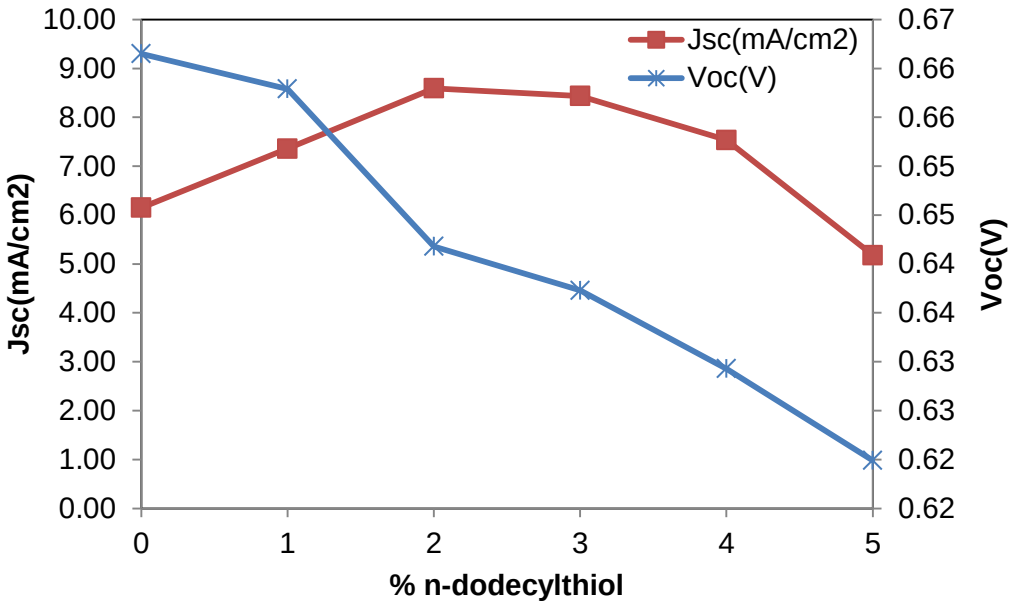

Figure 24: Short circuit current and open circuit voltage of P3HT:PC70BM with (0-5)% n-dodecylthiol content under AM 1.5G illumination.

Unlike V_{oc}, the short-circuit current density (J_{sc}) has a different trend when adding n-dodecylthiol as shown in Figure 24. The short circuit current increases by adding n-dodecylthiol up to 2%. This can be due to a smaller crystallite size; i.e. better electron mobility and higher crystallinity. After that the value of J_{sc} starts to drop down when increasing n-dodecylthiol more than 2%. Adding more than 2% n-dodecylthiol can contaminate the J_{sc} and affect phase separation which was not suited for the exciton dissociation, i.e. resulting in the reduction of J_{sc} and final power conversion efficiency [41,57-59].

The fill factor (FF) was almost constant, as illustrated in Figure 25. This indicates that adding n-dodecylthiol has a little effect on FF, but it has influence on both J_{sc} and V_{oc}. Based on the power conversion efficiency equation (PCE = V_{oc}*J_{sc}*FF / Total incident power density), V_{oc}, J_{sc} and FF play important roles in final power

conversion efficiency. Higher V_{oc}, J_{sc} and FF results in higher power conversion efficiency.

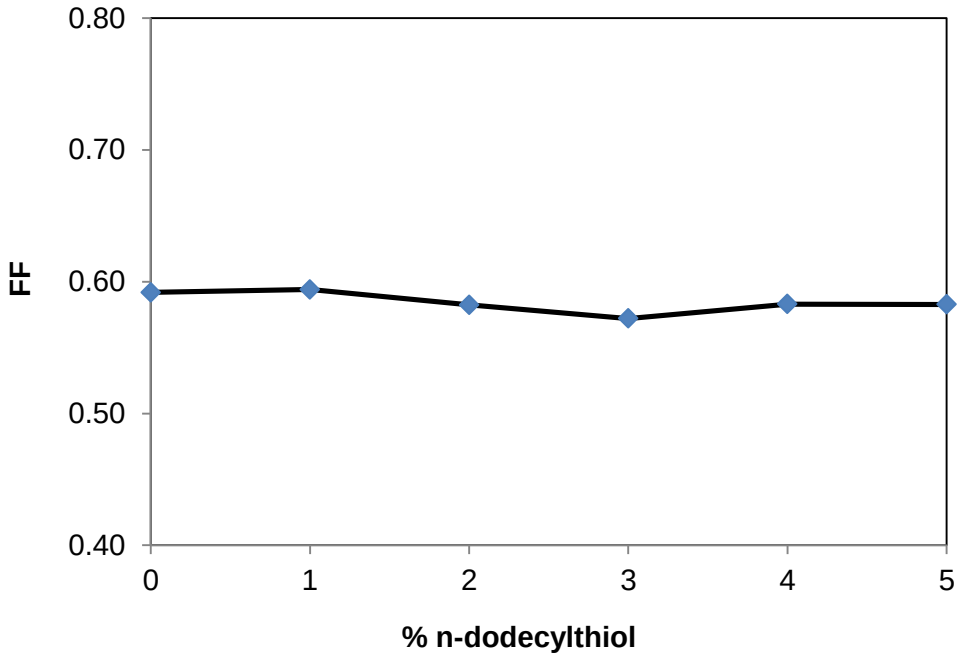

Figure 25: Fill factor of P3HT:PC70BM with (0-5)% n-dodecylthiol content under AM 1.5G illumination after annealing.

Finally, the power conversion efficiencies (PCE) of solar cells after depositing the Al layer using physical vapor deposition (PVD) process under ultralow pressure as shown earlier in Figure 22. The results show that the maximum efficiency obtained was at 1.65% (2 volume % n-dodecylthiol) for the samples prepared without any annealing. The efficiency values were almost doubled after annealing. At volume fractions of n-dodecylthiol up to 2%, PCE increased by adding n-dodecylthiol, which is a sign of lowering the number of recombine charges before reaching the electrode. At higher concentrations of n-dodecylthiol (> 2%), the efficiency starts to fall, which is a direct sign of recombining charges

and less charge phase separation. Results from DLS showed that more aggregation occurs by adding n-dodecylthiol to P3HT:PC70BM, which means less charge formation. The optimum balance between exciton dissociation and charge transport and/or collection at the electrodes was obtained at 2% n-dodecylthiol, resulting in a PCE maximum value of 3.2%, which was almost a 33.3% increase in device efficiencies compared to devices without any n-dodecylthiol in the photoactive layer. This phenomenon is consistent with the dynamical Monte Carlo modeling of organic solar cells [41, 60]. The maximum efficiency was 3.2% at 2% n-dodecylthiol, associated with the samples prepared and heat treated at 150°C for 30 min. Our results are in line with previous research, which shows that adding n-dodecylthiol up to 2 volume % enhances cells performance of P3HT/PCBM [41].PCE improved from 0.97% (at 0% n-dodecylthiol) to 1.65% (at 2% n-dodecylthiol) by additives only, i.e. 70.1% improvement. At 2% n-dodecylthiol, PCE improved from 1.65% (before annealing) to 3.21% (after annealing), i.e 94.7 % improvement. These results show that PCE improvement by annealing is higher than by additives. Our results are in line with Ma et al. [38] results, which show great improvement of polymer solar cells PCE after annealing, especially above 50°C, i.e. near P3HT glass transition temperature.

Table 4: J-V measurement for the P3HT/PC70BM/(0-5)% n-dodecylthiol after heat treatment at 150°C for 30 minutes.

% n-dodecylthiol	V_{oc}(V)	J_{sc}(mA/cm^2)	FF	PCE=Voc*Jsc*ff/Total incident power density
0	0.6615	6.152	0.5919	0.0241
1	0.6579	7.358	0.5941	0.0288
2	0.6418	8.594	0.5824	0.0321
3	0.6373	8.437	0.5721	0.0308
4	0.6293	7.537	0.5831	0.0277
5	0.6199	5.179	0.5828	0.0187

4.1.2 Additives effect on power conversion efficiency

Most researchers have PCE with up-down mode, where there is enhancement of PCE with additives up to a specific additives percentage, then PCE starts to decline as shown in figure 26.

4.1.2.1 Effect of n-dodecylthiol addiives on P3HT:PC60BM polymer solar cells

(1) Jiangang et al [41] studied the effect of n-dodecylthiol on P3HT:PC70BM polymer solar cells crystallinity, structure and electrical performance.

(2) Figure 26(a) shows effect of %n-dodecylthiol on P3HT:PC60BM [41], which show improvement in PCE with additives up to 2% n-dodecylthiol.

(3) In our study, PC70BM was used instead of PC60BM. Our results have a similar trend to Jinagang et al results.

(4) Authors [41] claim that PCE decline at high volume fraction of n-dodecylthiol (>2.0%), because adding excess amount of n-dodecylthiol contaminate the

phase separation, decrease exciton dissociation (charge separation), and this result in reducing Jsc which result in reducing PCE. When n-dodecylthiol was 2.0%, an optimum balance between exciton dissociation (charge separation) and charge transport and/or collection was obtained, resulting in a maximum PCE value of 2.61% [41]. Note that charge separation is important, because the separated charges transport toward the electrode. These collected charges at the electrode represent the current.

4.1.2.2 Effect of CN additives on DCV5T-Bu4:PC61BM polymer solar cells

(1) Gisela et al studied the effect of adding CN on DCV5T-Bu4:PC61BM polymer solar cells to improve structure, absorbance and electrical performance [79].

(2) Results show that maximum PCE is 3.0% at 0.375% additives as shown in Figure 26(b). Authors demonstrated that; the PCE increased from 2.1% to a maximum value of 3.0% by adding 0 to 0.375% CN. Upon further increase of CN% to 0.50%, the device efficiency decreased to 2.7% and then leveled off [79].

(3) Their results show that additives can improve polymer solar cell to specific limit, and excess amount of additives deteriorate the cell performance. These results are in line with our results trend.

(4) Jsc directly proportional to charge generation, transport and collection. The improvement in Jsc results in improving of PCE. Gisela et al claim that the main reason for the PCE trend was mainly due to the charge generation, transport and collection. This claim was supported by Jsc measurements, which has same trend as PCE. Above 0.375% CN, Jsc starts to decline. This indicated that excess additives contaminated the cell [79].

4.1.2.3 Effect of DIO additives on the performance of PBDTTT-C- T:PPDIDTT polymer solar cells

(1) Pei Cheng et al [80] studied the effect of adding DIO additives on the performance of PBDTTT-C- T:PPDIDTT polymer solar cells.

(2) Results show that adding up to 6% DIO increase the PCE of PBDTTT-C-T:PPDIDTT polymer solar cells as shown in Figure 26(c).

(3) Their results show that additives can improve polymer solar cell to specific limit, and excess amount of additives deteriorate the cell performance. These results are in line with our results trend.

(4) The author claims that PCE increases by adding up to 6%DIO, and this is because of increasing in Jsc i.e increasing in charge generation [80]. The author claim is correct because it is based on the I-J electrical performance of PBDTTT-C- T:PPDIDTT polymer solar cells, and above 6% additives Jsc starts to decline which results in reducing the PCE.

4.1.2.4 Effect of OT additives on P3HT:PC60BM polymer solar cells

(1) Hsiang et al [81] investigated the effect of OT on P3HT:PC60BM polymer solar cells.

(2) Figure 26(d) show that adding OT to P3HT:PC60BM, initially increases PCE until a peak value and then decreases.

(3) They used P3HT as an active polymer (P3HT) which is the same material that is used by our research. In addition, their results show that additives can improve polymer solar cell to specific limit, and excess amount of additives deteriorate the cell performance. These results are in line with our results trend.

(4) The author claims that PCE results initially increases until a peak value due to the increase in both Jsc and FF. Both Voc and FF starts to decline by adding more than 7.5µL, resulting in decreasing in PCE. The optimized concentration occurs when 7.5µL of OT added to 250µL of base solution. The PCE obtained by this concentration is~2.6% [81]. Their claim is correct, because it is based on I-J measurements.

Our work presented at figure 26(e). Our results are in line with other researcher's trend [41, 79-81], and it shows an improvement of PCE by adding up to 2% additives. The improvements was mainly due to increase in Jsc, which reflect that more charges were generated, transported and collected at the electrodes. Above 2% n-dodecylthiol, PCE start to decline. The main reason for this decline is believed to be the decrease in both Voc and Jsc. The lower Jsc(8.594 mA/cm2 at 2% additives Vs 0.5828 mA/cm2 at 5% additives) reflects the lower charge generation and collection at the electrodes [79]. Decrease in Voc reflect the decrease in the difference in energy levels between the HOMO of the donor and the LUMO of the acceptor, and this can be due to the increase in active layer which contribute in decrease of HOMO energy level. Decreasing of efficiency reflect reduction in charge generation and/or increase in charges recombination before reaching the electrode [80, 81]. Also, adding high volume fractions of additives contaminate Jsc and device performance as declared by Jiangang Liu [41].

Table 5: Effect of additives on polymer solar cells

P3HT:PC60BM: %n-dodecylthiol [41]		DCV5T-Bu4: PC61BM:%CN [79]		PBDTTT-C- T: PPDIDTT:%DIO [80]		P3HT:PC60BM:OT [81]	
%n-dodecylthiol	PCE	%CN	PCE	%DIO	PCE	OT (µL)	PCE
0	0.9	0	2.1	0	1.16	0	0.6
0.5	1.6	0.125	2.1	3	1.69	1	1.4
1	2.1	0.25	2.6	4	1.99	2	2.1
2	2.6	0.375	3.0	5	2.50	5	2.5
3	1.9	0.5	2.7	6	2.92	7.5	2.6
4	0.8	0.75%	2.7	7	2.36	15	2.2
						20	2.0

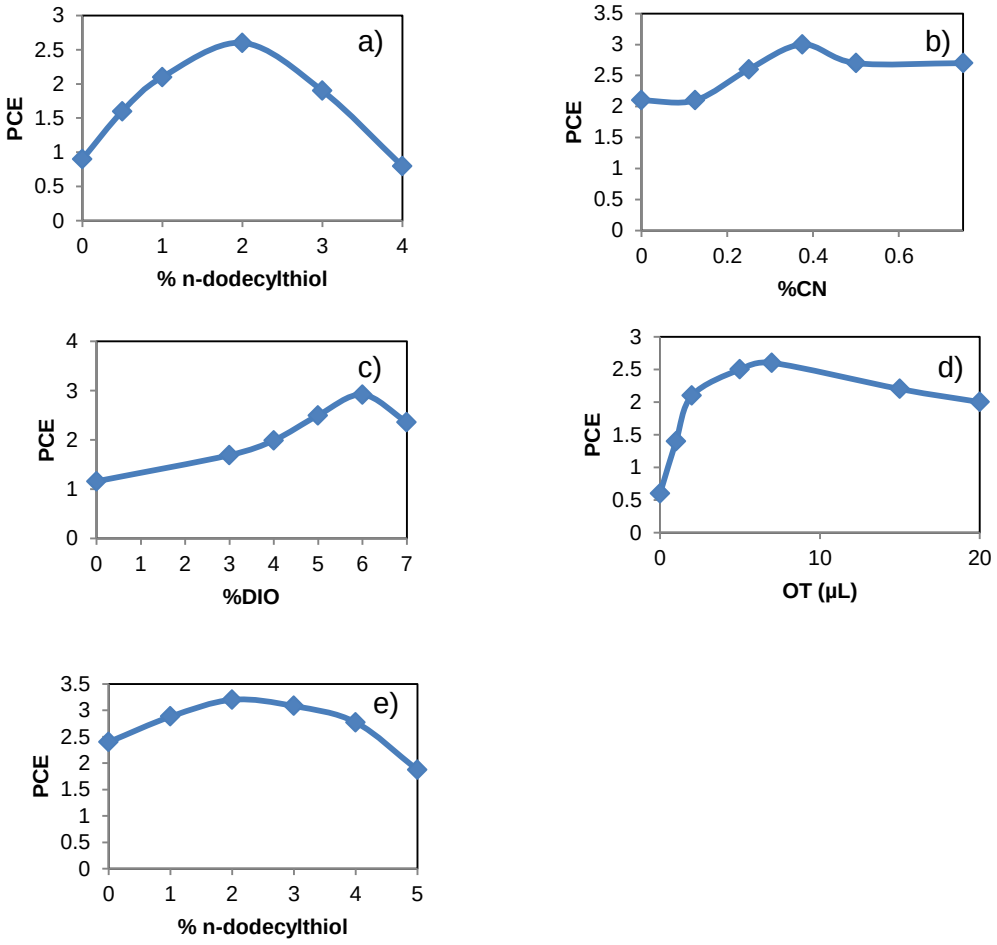

Figure 26: Effect of additives on polymer solar cells: a) P3HT:PC60BM:%n-dodecylthiol [41], b) DCV5T-Bu4:PC61BM:%CN [79], c) PBDTTT-C-T:PPDIDTT:%DIO [80], d) P3HT:PC60BM:OT [81], e) P3HT:PC70BM:%n-dodecylthiol.

4.2 Annealing of P3HT:PC70BM:n-dodecylthiol PSCs

Figure 27 (a-e) shows PCE curves (short-circuit current density (J_{sc}), open circuit voltage (V_{oc}), fill factor (FF), and power conversion efficiency (PCE)) for P3HT:PC70BM PSCs under white light illumination (100 mW/cm^2). The samples were prepared under various annealing temperatures (60°C, 90°C,120°C, 150°C and 180°C) and annealing times (0, 10, 20, 30 and 40 minutes). The photo-voltaic parameters (the short-circuit current density (J_{sc}), the open circuit voltage (V_{oc}), the fill factor (FF), and the power conversion efficiency (PCE)) are summarized in Appendix B. PSC devices without heat treatment showed a lower PCE between 1% and 1.5%. However, after heat-treatment, PCE values increased by increasing of annealing temperature up to 150°C. As a result, the photovoltaic cells prepared with heat treatment at 150 °C and 30 minutes showed the best device performance (J_{sc} = 8.59 mA/cm^2 , V_{oc} = 0.64V, FF = 0.58, and PCE = 3.21 %).

On the other hand, the cell performance started to deteriorate at temperatures higher than 150 °C, and the Al electrode reflection was not as strong as with lower temperature. This is attributed to partial melting of the polymer composite under the Al electrode. This was confirmed with the visibility of some cracks on the Al electrode and a change in the color of the polymer from purple to brown. Therefore, it is clear that there is an optimum annealing temperature and time combination to achieve optimum electrical and physical properties of the photoactive cells, which is shown to be 150 °C and 30 minutes. This is in line with previous published research [73-74], However, V_{oc} results show that there is

no big change of open circuit voltage by changing annealing temperature up to 150°C, whereas, V_{oc} starts to decline above 150°C due to partial melting of the P3HT which has a melting point in the range of 180-220°C [70].

Effect of annealing time has a different trend. Our results show that up to 150°C there is significant enhancement of electrical properties of the PSCs performance by increasing time.However, above 150°C the device performance will decline with increasing annealing time.

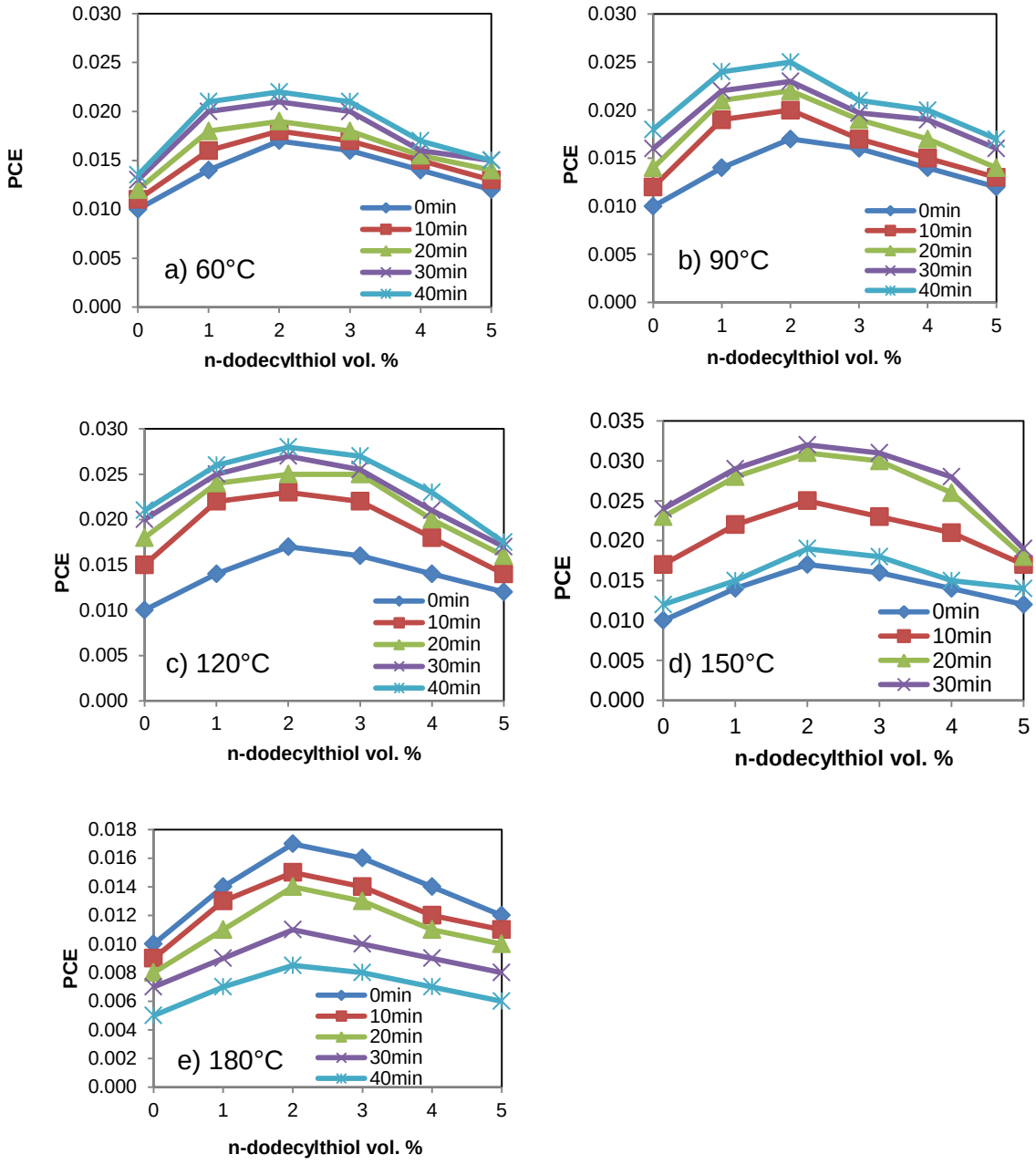

Figure 27: PCE curves of Glass/ITO/PEDOT:PSS/P3HT:PC70BM:n-dodecylthiol/Al at different annealing times and temperatures.

5 Morphology Analysis

5.1 Atomic Force Microscope (AFM)

Polymer solar cells (PSC) became an alternate energy source for the future because of their potential for inexpensive roll-to-roll printing technique, ease of processing, light weight and high flexibility. However, PSC current performance is still low for practical applications which require at least 10% efficiency for commercialization. We need a better understanding of the solar cell physics, such as nanoscale morphology of the photoactive layer. Photoconductive Atomic Force Microscopy (AFM) is often used to investigate the complex optoelectronic and morphological properties of organic solar cells at the nanoscale level. Surface topographical analysis was conducted using Agilent 5420 Atomic Force Microscope at the following settings: ACAFM non-contact mode, I-gain of 8, set point of 1.84, and scan size equal to 2µm x 2µm. Surface roughness parameters, as listed in Table 6, were measured using "PICO IMAGE BASICS" software.

AFM height images of P3HT:PC70BM films with different amounts of n-dodecylthiol are shown in Figure 28. The film spin casted from the solution containing n-dodecylthiol showed an increase in the peaks and a rougher surface. This result demonstrated that the reduced crystallite size and the increased number of P3HT single chains after the addition of n-dodecylthiol in the polymer solution could enhance the crystallinity of P3HT. In addition, increasing the surface roughness means more space for P3HT crystallite to form and increase percent crystallinity. The rougher surface and finer interpenetrating network of the polymer active layer for the polymer solar cells with n-dodecylthiol

should result from better nano-scaled phase separation between the crystalline P3HT donor and the PC70BM (fullerene) acceptor.

Surface parameters have been obtained using "PICO IMAGE BASICS" software at AAF.

The surface parameters that have been obtained are:

Table 6: Surface roughness Parameters.

Parameter	**Definition**	**Symbol**	**Equation**
Root Mean Square roughness	The root mean square average of the roughness profile ordinates.	S_q or R_q	$R_q=\sqrt{\frac{1}{n}*\sum_{i=1}^{n} y_i^2}$
Surface Skewness	The asymmetry of the height distribution histogram.	S_{sk} or R_{sk}	$R_{sk}=\frac{1}{nR_q^3}*\sum_{i=1}^{n} y_i^3$
Surface Kurtosis *	The “peakedness” of the surface topography.	S_{ku} or R_{ku}	$R_{ku}=\frac{1}{nR_q^4}*\sum_{i=1}^{n} y_i^4$
Roughness Average	The arithmetic average of the absolute values.	Sa or Ra	$R_a=\frac{1}{n}*\sum_{i=1}^{n}\lvert y_i\rvert$
Maximum Peak Height	The largest peak height value.	S_p	
Maximum Valley Depth	The largest valley depth value.	S_v	
The Peak-Vally Height	The height difference between the highest and lowest pixel in the image.	S_z	$S_z= S_p+ S_v$

* Kurtosis : The sharpness of the peak of a frequency-distribution curve.

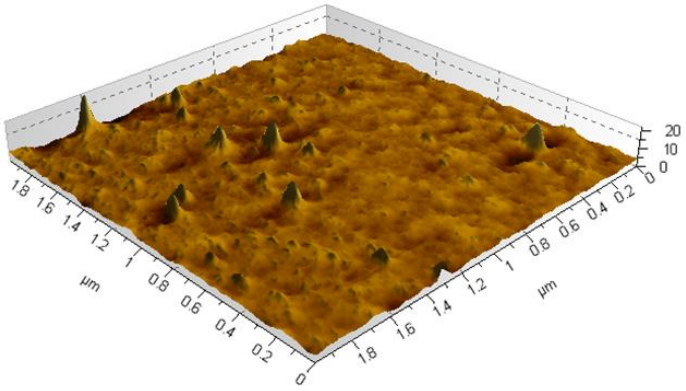

Figure 28A. AFM of P3HT:PC70BM:0% n-dodecylthiol before heat treatment.

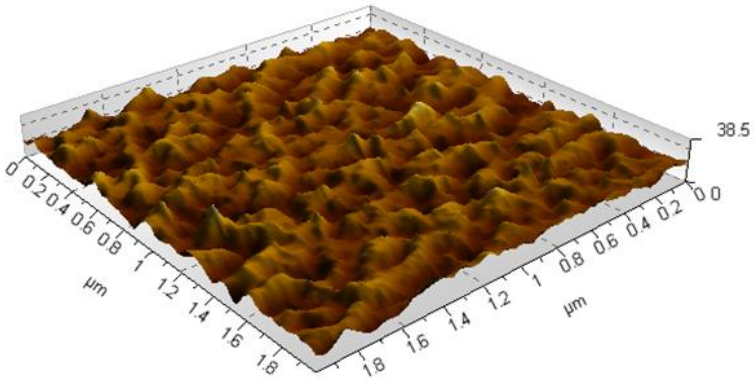

Figure 28B. AFM of P3HT:PC70BM:1% n-dodecylthiol before heat treatment.

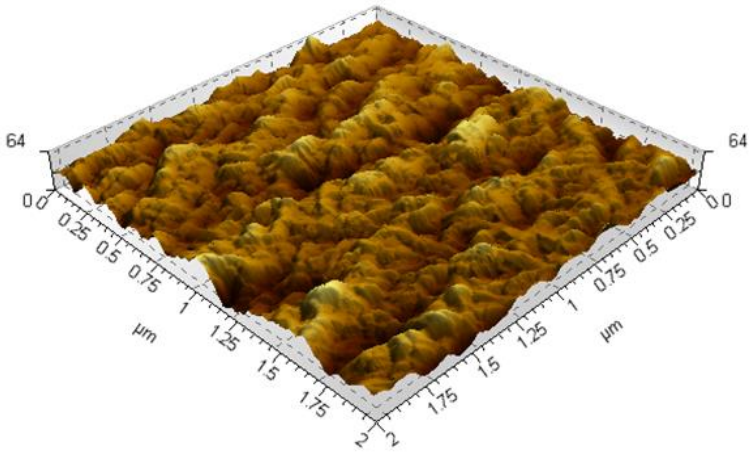

Figure 28C. AFM of P3HT:PC70BM:2% n-dodecylthiol before heat treatment.

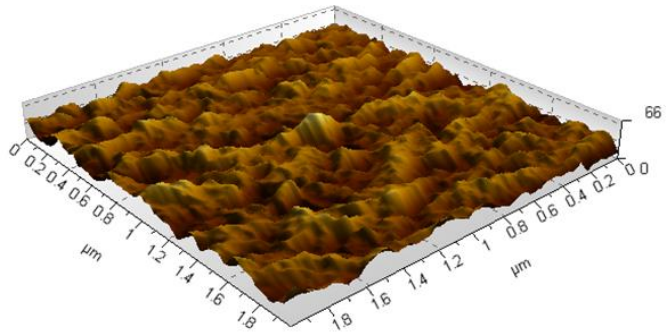

Figure 28D. AFM of P3HT:PC70BM:3% n-dodecylthiol before heat treatment.

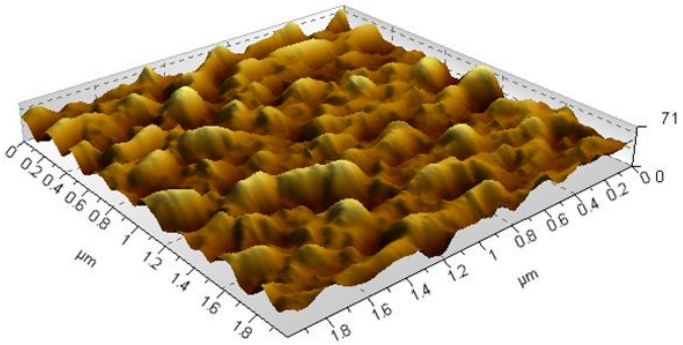

Figure 28E. AFM of P3HT:PC70BM:4% n-dodecylthiol before heat treatment.

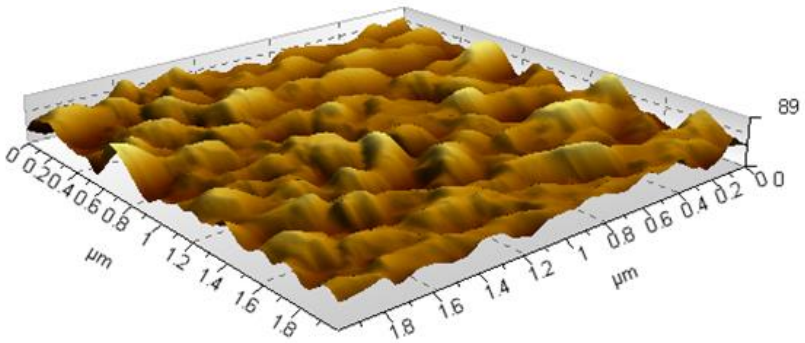

Figure 28F. AFM of P3HT:PC70BM:5% n-dodecylthiol before heat treatment.

The surface parameter shows that increasing percentage of n-dodecylthiol increases both roughness average and root mean square values, i.e. it increases the surface roughness. In contrast, the Surface Skewness (Ssk) and the Surface Kurtosis (Sku) sharply decline to a very low value compared to the surface without any additives, i.e. there is an increase in asymmetry and peakedness. Maximum Peak Height (Sp), Maximum Valley Depth (Sv) and The Peak-Peak Height (Sz) increase with an increase of n-dodecylthiol percentage.

These results demonstrate that adding n-dodecylthiol makes the surface rougher, and increasing the surface roughness means more space for P3HT crystallite to form and increases polymer percent crystallinity. The rougher surface and finer interpenetrating network of the polymer active layer for the polymer solar cells with the n-dodecylthiol should result from the better nano-scaled phase separation between the crystalline P3HT donor and the PC70BM (fullerene) acceptor. In conclusion, the AFM results show that adding n-dodecylthiol improves the morphology of the P3HT: PC70BM blend films, which increases the interfaces for exciton dissociation, and this leads to the improvement of J_{sc} and PCE of the polymer solar cells [35, 43-44].

Table 7.1: Parameters table of the sample with P3HT:PC70BM:(0-5)% of n-dodecylthiol before heat treatment.

% n-dodecylthiol	Sq	Ssk	Sku	Sp	Sv	Sz	Sa
0	1.15	5.56	60.4	20.7	3.46	24.16	0.637
1	5.24	0.086	2.87	23.5	17.4	40.9	4.21
2	10.7	0.018	2.99	34.7	30.2	64.9	6.59
3	11	0.0156	3.02	43	32.5	75.5	8.76
4	13.1	0.548	3.05	48.2	34.8	83	10.6
5	16.3	0.343	2.53	50.2	37	87.2	13.4

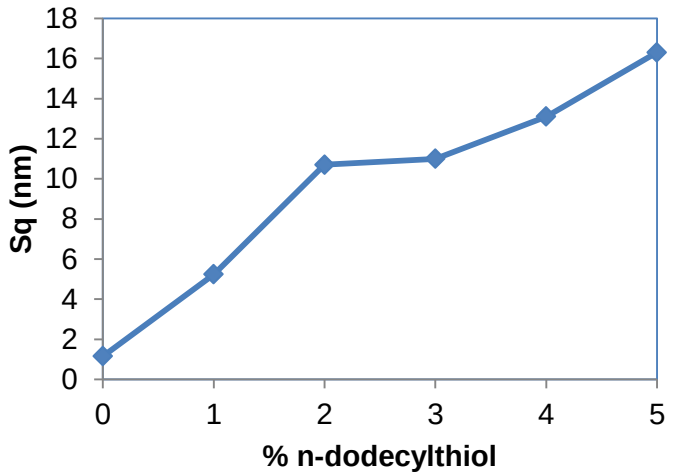

Figure 29A: Sqof P3HT:PC70BM:(0-5)**%**n-dodecylthiol.

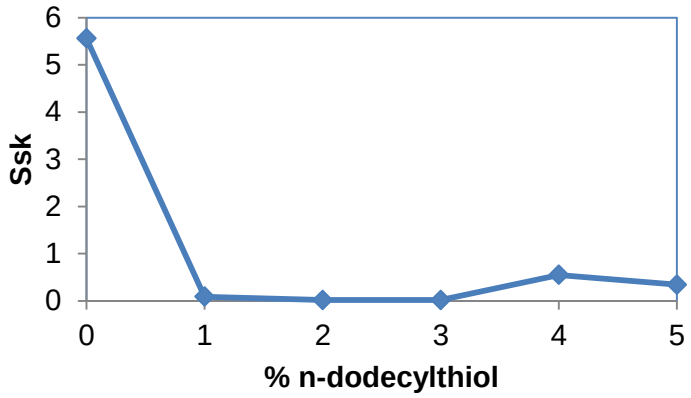

Figure 29B: Ssk of P3HT:PC70BM:(0-5)**%**n-dodecylthiol.

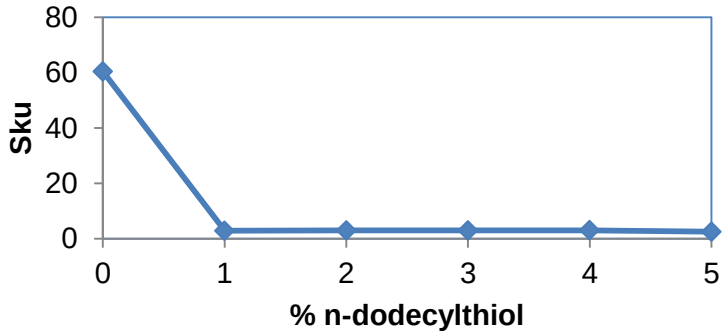

Figure 29C: Sku of P3HT:PC70BM:(0-5)**%**n-dodecylthiol.

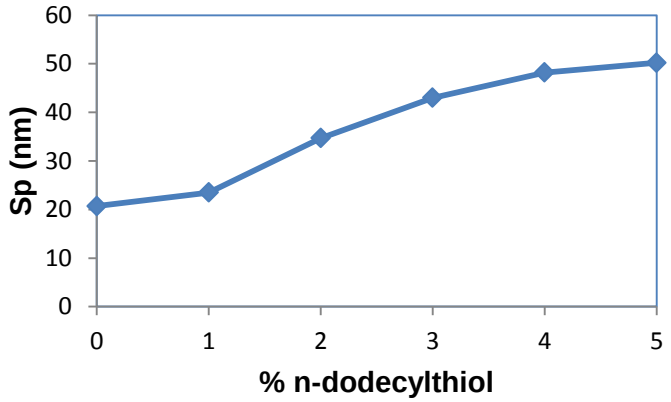

Figure 29D: Sp of P3HT:PC70BM:(0-5)**%**n-dodecylthiol.

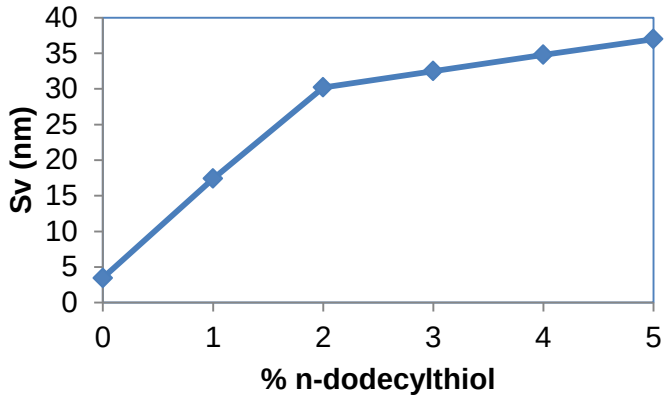

Figure 29E: Sv of P3HT:PC70BM:(0-5)**%**n-dodecylthiol.

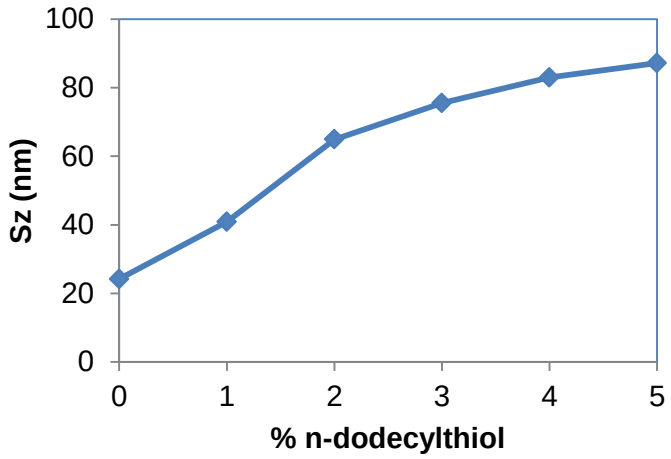

Figure 29F: Sz of P3HT:PC70BM:(0-5)**%**n-dodecylthiol.

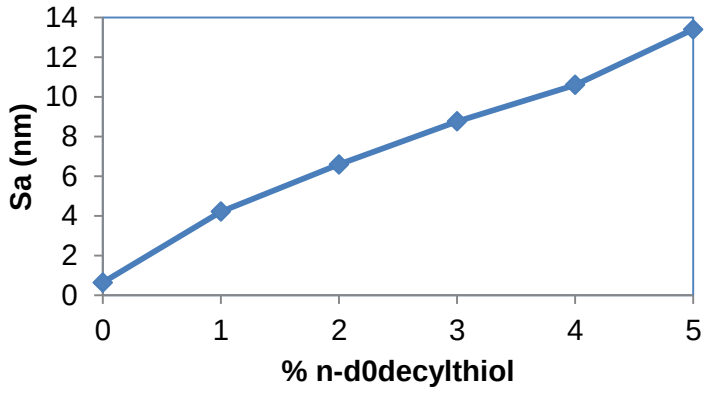

Figure 29G: Sa of P3HT:PC70BM:(0-5)**%**n-dodecylthiol.

AFM surface parameters for samples prepared with annealing are summarized in Table 7.2 and the surface images are shown in Figure 30 (a-f). Up to date, there is no research about the effect of annealing on P3HT:PC70BM:n-dodecylthiol.Surface roughness of the samples after annealing is relatively higher than those without annealing. Sq and Sa values start to decline above 2% n-dodecylthiol, which indicates reduction in surface roughness due to aggregation and uncontrolled phase separation in P3HT crystallization with higher additives, thus blocking the crystallite growth. In conclusion, AFM results show that adding n-dodecylthiol enhances the morphology of P3HT: PC70BM blend films, which increases the interfaces for exciton dissociation. This ultimately leads to improvements in short-circuit current (Jsc) and PCE of the polymer solar cells as will be demonstrated later by our tests and in line with findings reported by other researchers [35, 43, 44].

Table 7.2: Surface parameters of the P3HT:PC70BM:0-5**%** of n-dodecylthiol after heat treatment at 150 C for 30 min.

% n-dodecylthiol	Sq	Ssk	Sku	Sp	Sv	Sz	Sa
0	1.4	0.27	2.54	3.21	4.81	8.02	1.16
1	8.96	0.0749	3.54	28.8	28	56.8	6.71
2	28	0.385	2.8	84.9	99.2	184	22.3
3	14.7	0.09	2.44	65.1	60.7	126	12.1
4	13.3	0.109	3.14	42.1	52.8	94.9	10.3
5	10.8	0.104	2.65	42.7	61.8	104.5	8.84

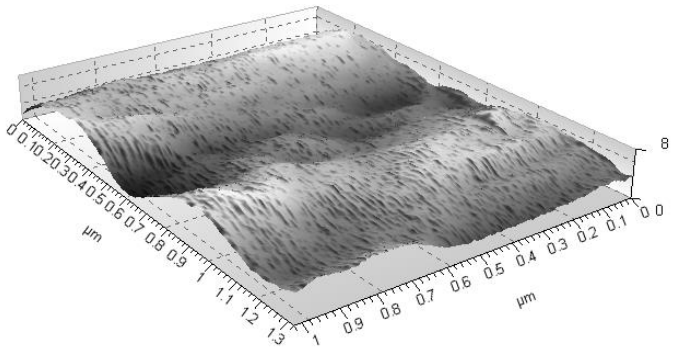

Figure 30A: AFM of P3HT:PC70BM:0%n-dodecylthiol after heat treatment.

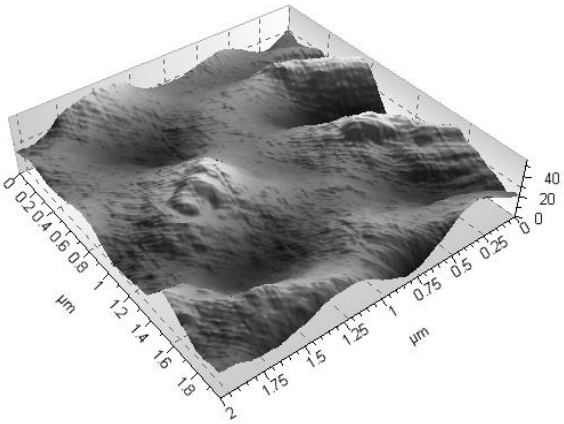

Figure 30B: AFM of P3HT:PC70BM:1%n-dodecylthiol after heat treatment.

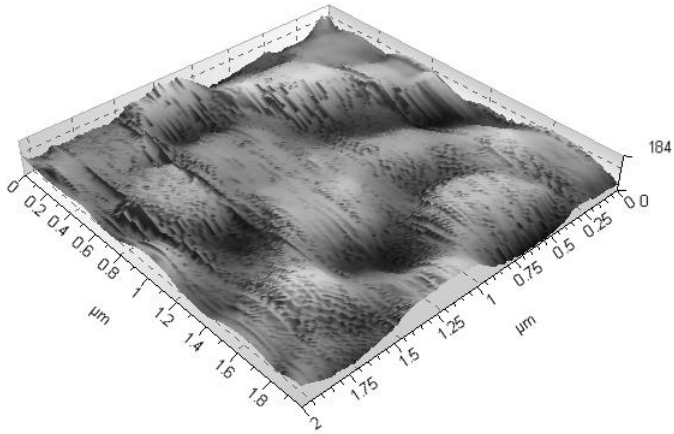

Figure 30C: AFM of P3HT:PC70BM:2%n-dodecylthiol after heat treatment.

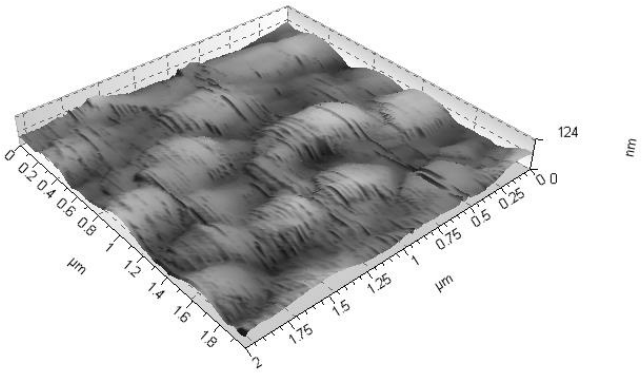

Figure 30D: AFM of P3HT:PC70BM:3%n-dodecylthiol after heat treatment.

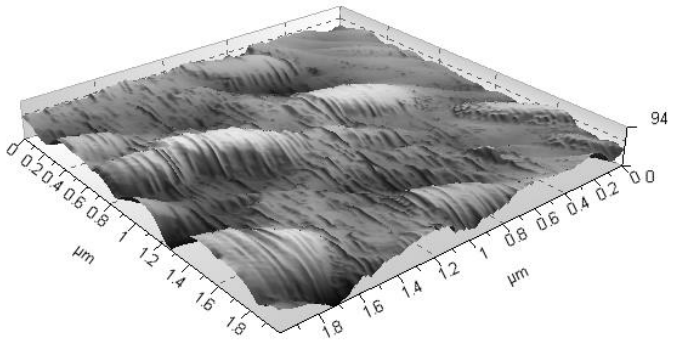

Figure 30E: AFM of P3HT:PC70BM:4%n-dodecylthiol after heat treatment.

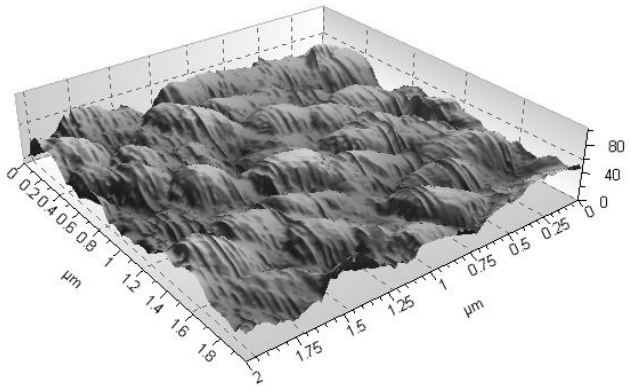

Figure 30F: AFM of P3HT:PC70BM:5%n-dodecylthiol after heat treatment.

5.2 Transmission Optical Microscope:

Aggregation and undissolved particles block charge mobility. This can reduce electrical properties of the polymer solar cells sharply. The Transmission Optical Microscope is used to determine if there is any aggregation or undissolved particles in the polymer solution. Figure 31 shows transmission optical microscope images of P3HT dissolved in cholrobenzene solution and spin coated on a glass slide. This figure shows that there is either aggregation or undissloved particles. This image was taken before the usage of the sonicator. The sonicator was used later to improve dissolving of the polymer and fullerene in chlorobenzene. Figure 31 shows an image of P3HT (without PC70BM) spin coated on a glass slide, and it shows incomplete dissolving of P3HT, since it shows some black dots or aggregates, which we improve later with use of the sonicator.

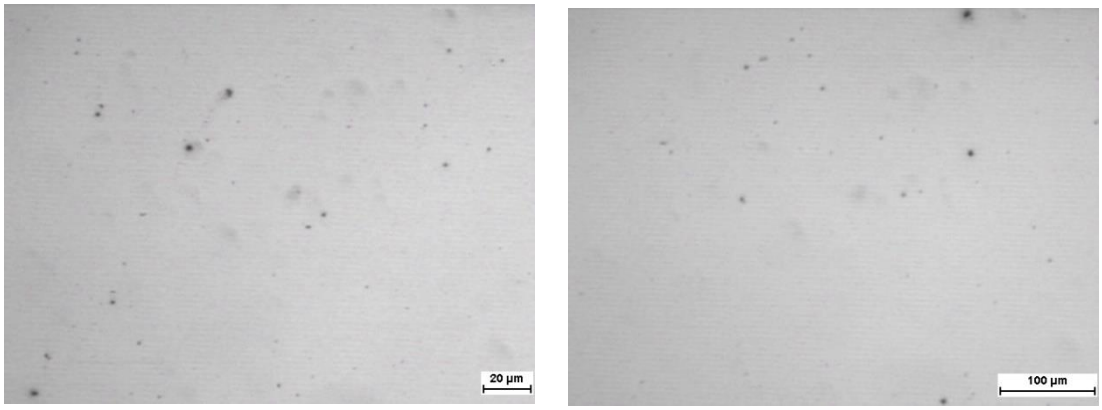

a) b)

Figure 31: a) P3HT spin coated on a glass slide (spin coater 800RPM for 1MIN) at 500X.

b) P3HT spin coated on a glass slide (spin coater 800RPM for 1MIN) at 100X.

Figures 32 shows undissolved PC70BM particles (without P3HT). These samples are also made without the sonicator. This figure shows undissolved particles in the center, and the surrounding of the particles is only partially dissolved.

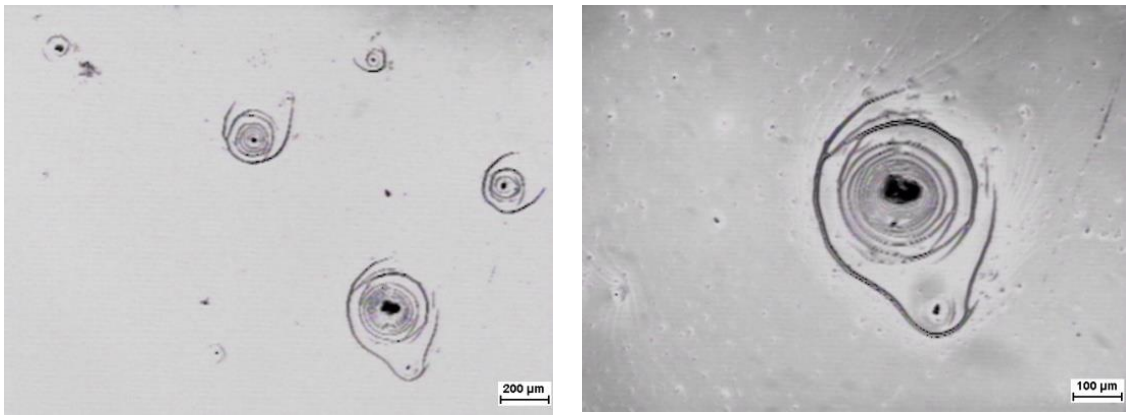

a) b)

Figure 32: a) PC70BM spin coated on a glass slide (800RPM 1min 50X).
b) PC70BM spin coated on a glass slide (800RPM 1min 100X).

Comparing Figure 31 and Figure 32 shows that PC70BM undissolved particles are much bigger than P3HT. This indicates that PC70BM needs more mixing/dissolving time than P3HT. So PC70BM is more difficult to dissolve than P3HT. Later we used the sonicator, which accelerated the mixing and dissolving process.

Figure 33 shows glass/P3HT/PC70BM slides. These samples are prepared at 200 RPM for 2 minutes with the usage of the HIELESCHER UP200H sonicator for 1 minute. This Figure shows that the sonicator enhances the dissolving of the particles in the solution. The sonicator parameters were set at 0.2 cycle, 60% amplitude, 100 Volt, 4 Ampere and frequency of 50/60.

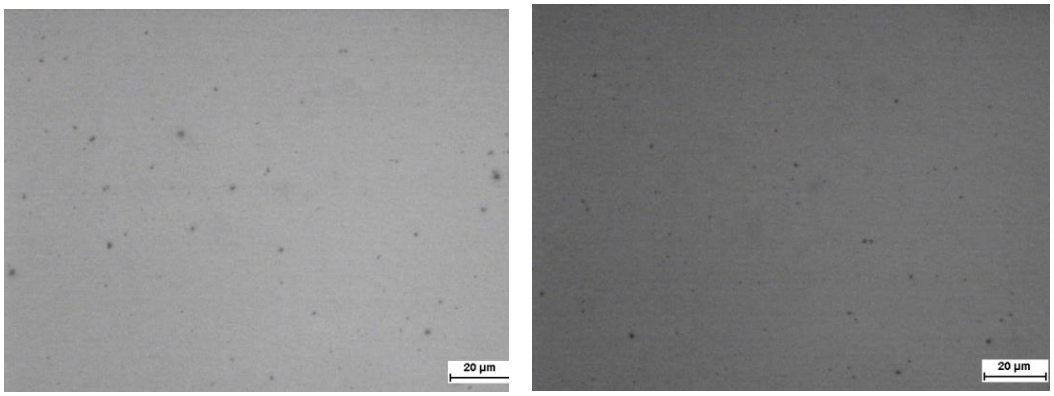

a) b)

Figure 33: a) P3HT spin coated on a glass slide glass 200X,

b) PC70BM spin coated on a glass slide glass 200X.

5.3 Scanning Electron Microscopy (SEM)

Figure 34 shows a SEM of Glass/ITO(30nm)/ PEDOT:PSS (>1µm). The PEDOT:PSS layer is very thick compared to that in other researchers' work. They mentioned that the PEDOT:PSS layer should be around 40-60 nm. This was my first experiment during my research and it shows that the solution needs to be diluted or spun at a higher speed in order to get a thinner layer. If the PEDOT:PSS layer is thicker than 40-60 nm, charge recombination occurs. Charge recombination lowers the cell electrical properties because the charges will combine instead of moving toward the electrodes.

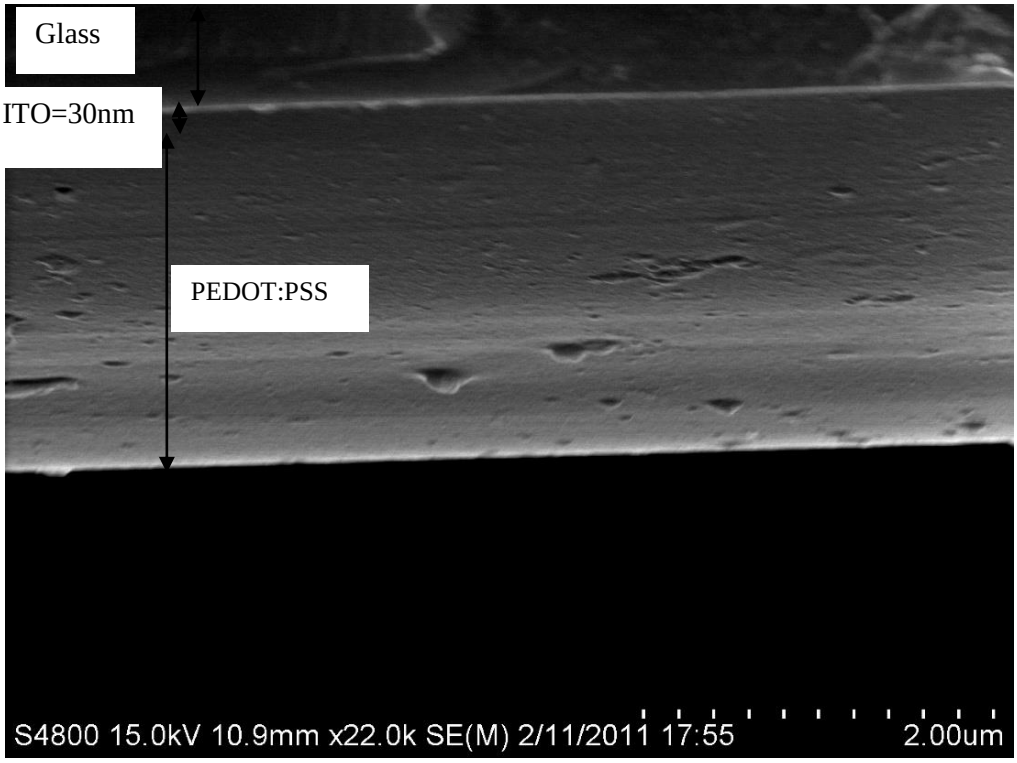

Figure 34: SEM of undiluted PEDOT:PSS spin coated on ITO-Glass slide.

Figures 35 shows a SEM of Glass/ITO(30nm)/PEDOT:PSS (40nm). The PEDOT:PSS layer thickness is acceptable now compared to that in other researchers' work. This thickness has been achieved by diluting PEDOT:PSS with distilled water (PEDOT:PSS to water ratio is 1:1). As noted earlier, the thinner the PEDOT:PSS layer, the faster the charges will reach the electrodes, so there is no time for the charges to recombine again. If the charges recombine, this will result in reducing the electrical efficiency and power conversion efficiency.

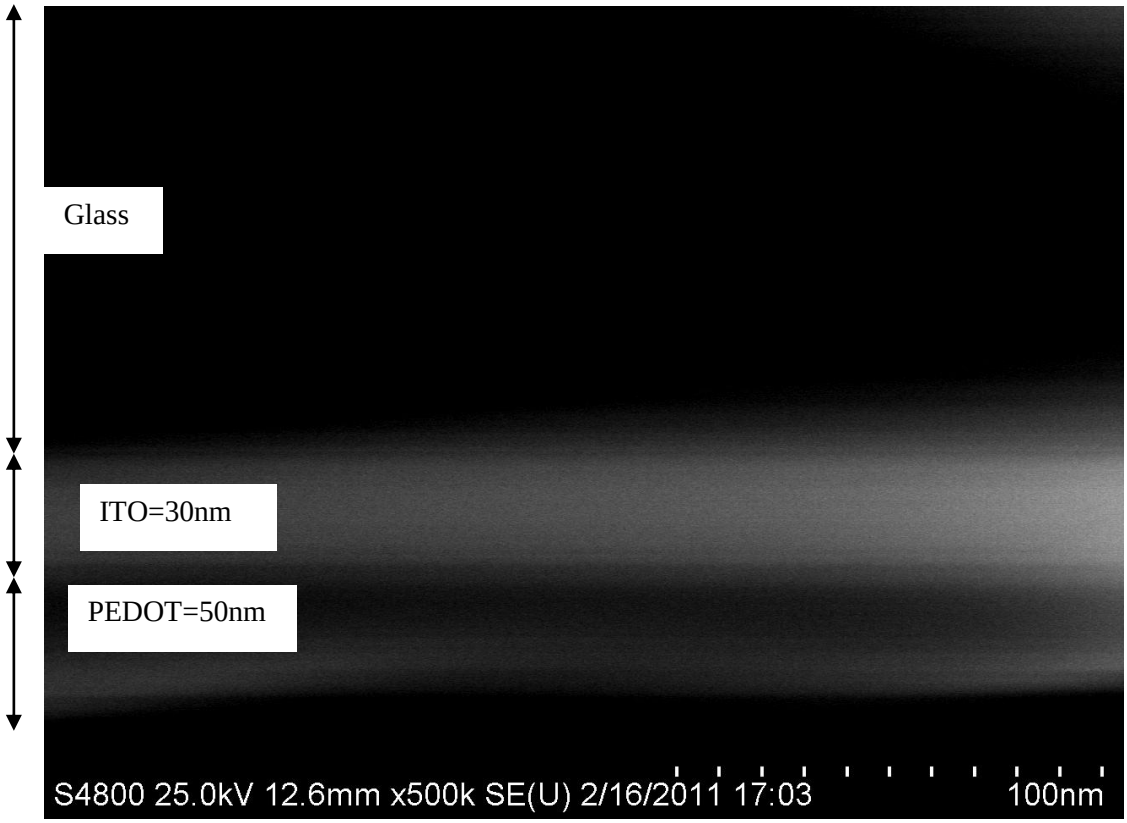

Figure 35: SEM of diluted PEDOT:PSS spin coated on ITO-Glass slide and with controlled cross section.

Figure 36 shows a cross section area of the polymer solar cell with different coating layers. ITO (25nm) coated glass slides were purchased from Nanocs Corporation. Two layers have been applied using a spin coater. The first layer is PEDOT:PSS (50nm) and the second layer is P3HT:PCBM:n-dodecylthiol (100-150nm). The last layer was applied using a metal evaporator to apply 50-100 nm of aluminum. The aluminum layer was applied using the Edward Coating System (see Figure 37) and the layer was prepared as follows: 150 mm of aluminum was wrapped tightly around the middle of a 3 stranded Tungsten filament. The filament was tightened between the 2 anchors with the aluminum at the bottom (2 points of the V facing up). I made sure that the V was perfectly up and down, not tilted. This is necessary to get even Al deposition on the solar cell. I clipped the solar cells to the top mounting area and closed the cage. Previous researchers have used a 1×10^{-6} mbar, but ours can only reach 2×10^{-4} mbar. Finally, I slowly increased the power control over a period of five minutes, and increased the current to about 80 m amps. The filament and aluminum layer will heat up and visibly turn red, depositing a thin layer of Al on the sample.

Figure 38 shows the SEM of P3HT/PC70BM/0-5% n-dodecylthiol. (0 and 1) % n-dodecylthiol are similar, but the figure shows that by increasing n-dodecylthiol over 1 % the polymer will start to aggregate. 5% n-dodecylthiol shows the highest aggregation between the 6 different compositions. This aggregation will hinder the charge dissociation and transportation, resulting in higher resistance and lower current density. This lower current and high resistance will reduce the overall efficiency of the polymer solar cell.

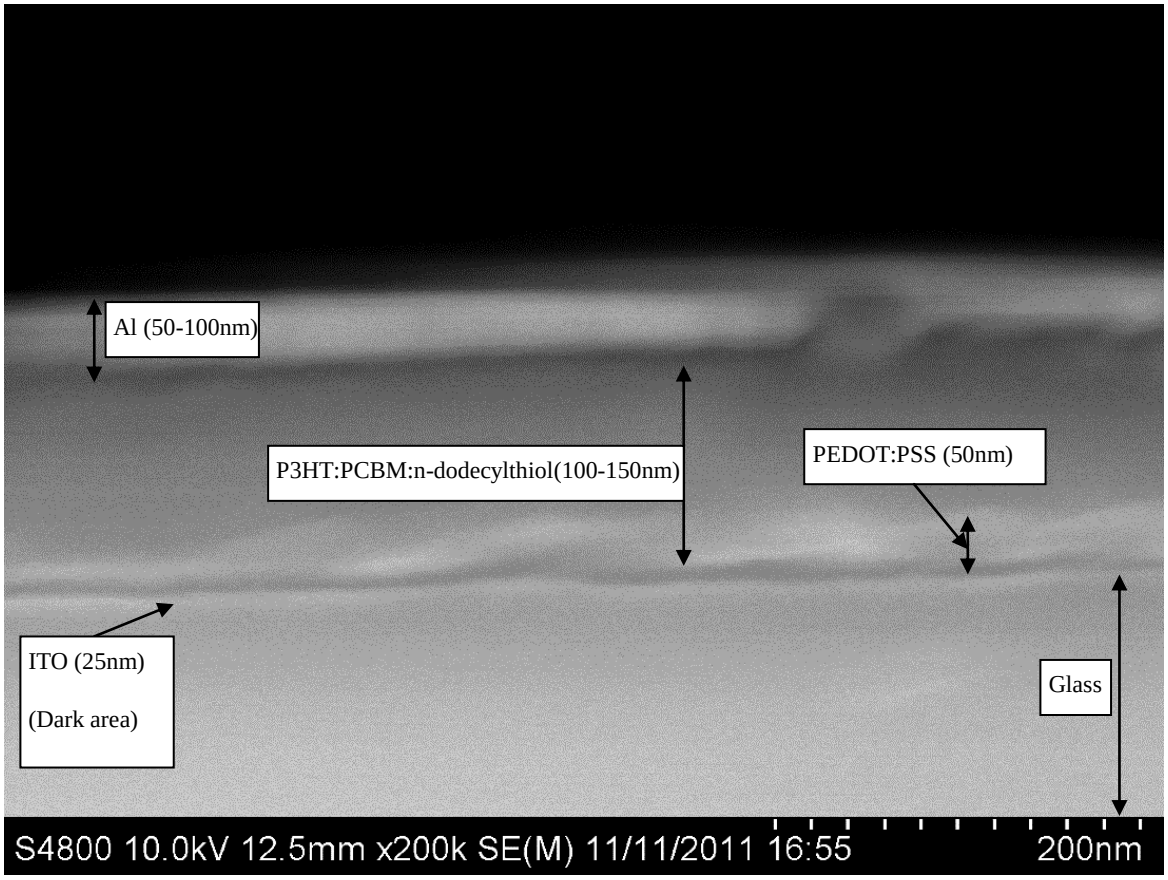

Figure 36: SEM cross-section of Glass/ITO/PEDOT:PSS/P3HT:PC70BM/Al.

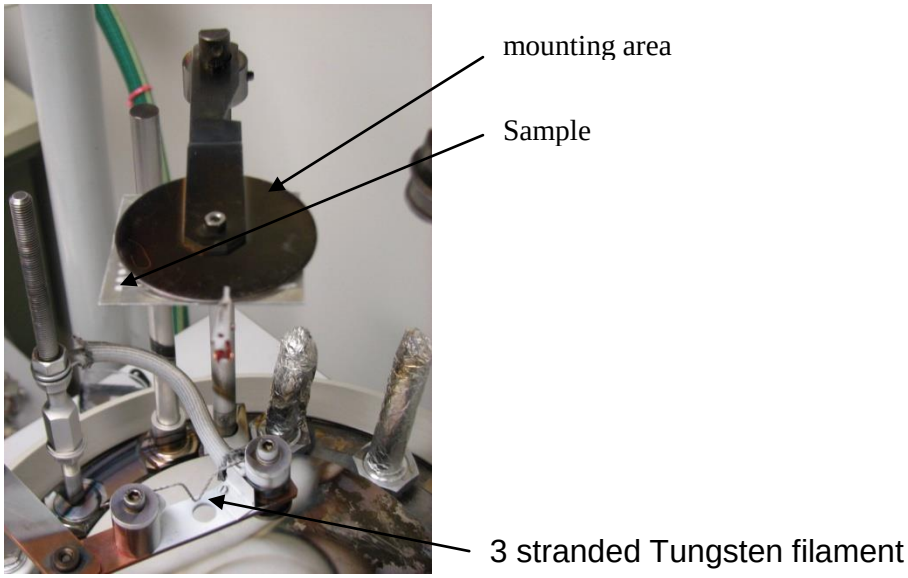

Figure 37: Sample setup for coating inside theEdward Coating System.

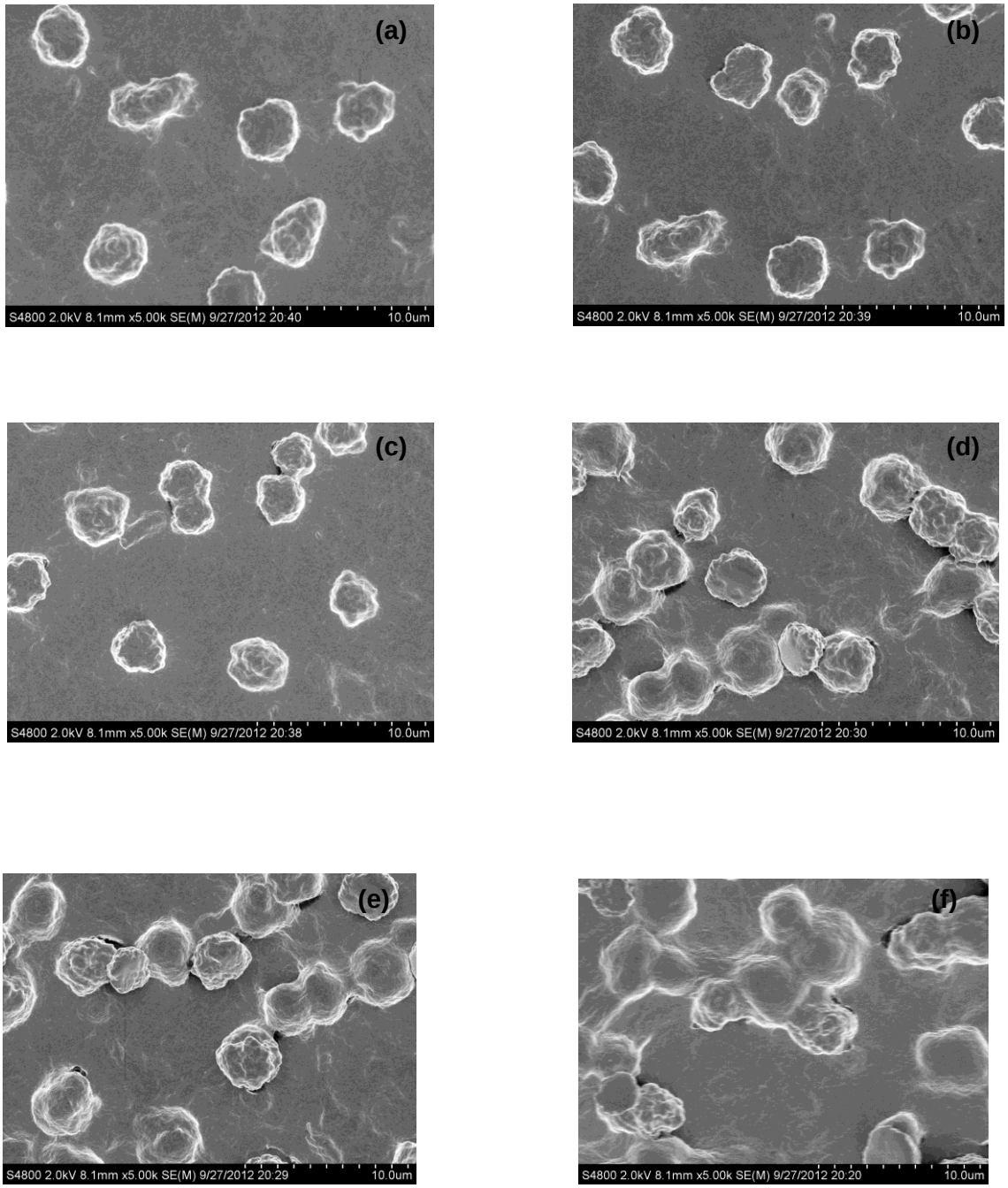

Figure 38(a-f): SEM of P3HT/PC70BM/0,1,2,3,4, and5%n-dodecylthiol respectively.

5.4 Aggregation measurement

Dynamic Light Scattering (DLS) is a technique that can be used to determine the size distribution of small particles or aggregates in a solution. In this research, DLS (Brookhaven instruments-Plas Zeta potential analyzer) was used at the following operating parameters: temperature = 23°C, cycle = 5, runs = 5, Reference index = 1.331, and liquid = Benzene. In order to study the aggregation and/or particle entanglement, DLSwas used to measure the average aggregate size of P3HT:PC70BM:n-dodecylthiol dissolved in chlorobenzene solution. The solution was mixed for 12, 24 and 36 hours.Three sets of samples were prepared as the following:

Set number	1	2	3
Prepared solution	10 mg of P3HT in 1 ml of chlorobenzene, then add 0-5% n-dodecylthiol by volume.	10 mg of PC70BM in 1 ml of chlorobenzene, then add 0-5% n-dodecylthiol by volume.	P3HT:PC70BM:0-5%vol. n-dodecylthiol (Regioregular P3HT was blended with PC70BM at a ratio of 10:10 mg with 0-5% volume n-dodecylthiol and then dissolved in a chlorobenzene (CB) 1 ml chlorobenzene.

DLS results show that adding n-dodecylthiol slightlyimproves the dispersion of P3HT in chlorobenzene.Figure 39 shows the average aggregate size of P3HT:PC70BM dissolved in chlorobenzene, and the error in measurement was

less than 5%. As shown in Figure 40 (a), the size of P3HT aggregatesreduced from 113 nm to 80 nm after adding 5% n-dodecylthiol to P3HT in chlorobenzene solution.P3HT:PC70BM:n-dodecylthiol dissolved in chlorobenzene solution showed an increase in average size by adding n-dodecylthiol; this result confirms the SEM result. However, DLS values are smaller than SEM values, because DLS values represent the average value and SEM shows aggregates. The results show that n-dodecylthiol does not enhance the dispersion of P3HT:BC70BM in the chlorobenzene solution. Also, it shows that the more n-dodecylthiol is added, the more aggregation will be formed. In addition, aggregation is low at lower n-dodecylthiol percentages up to 2%, and above that the composite dissolving becomes less, i.e. there are more aggregates in the P3HT:PCBM composites. The aggregation of the particles will leave less contact area between P3HT and PC70BM. This results in a smaller number of generated charges between fullerene and the polymer interface. This will result in reducing the electrical properties of PSCs. To overcome this problem, most of researchers mix the polymer composite in the solvent for a long period e.g. over 24 hours [75], and others apply heat (50 °C) and 24hours of mixing to achieve a better dispersion of polymer composite in the solvent [76]. Even after mixing, it is preferable to use a syringe with submicron filter [77] to separate undesired or aggregated particles from the solution.

Figure 40 (b-d) shows the aggregate size in nm for solution prepared ofP3HT:PC70BM:(0-5%)n-dodecylthiol dissolved in chlorobenzene solution prepared at room temperature (21°C), 35°C and 50°C, respectively. Solution

prepared at 21°C shows that aggregates getting smaller in size by increasing of mixing time as shown in figure 40(b). Figure 40(c) shows that the aggregates getting smaller than the solution prepared at room temperatureand after 36 hours of mixing the aggregate was nearly constant at 75nm. The solution prepared at 50 °C show the smallest aggregate size, and the effect of mixing time is insignificant, and the lowest value of aggregates was 51nm. Figure 40(e) shows enhancement of PCE by stir mixing at 50°C compared to mixing at room temperature. Note that mixing temperature cannot be more than solvent evaporation temperature.

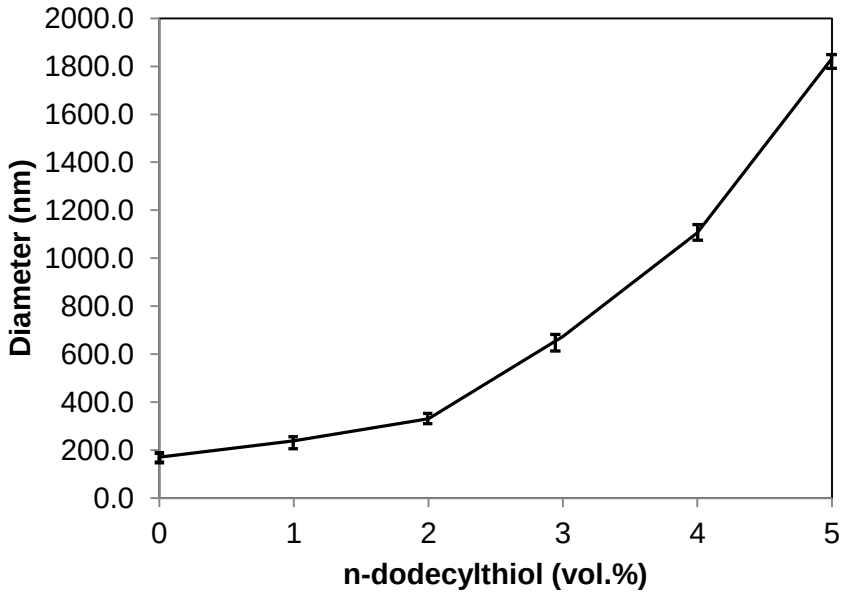

Figure 39: Aggregate size of P3HT:PC70BM:(0-5%)n-dodecylthiol dissolved in chlorobenzene solution.

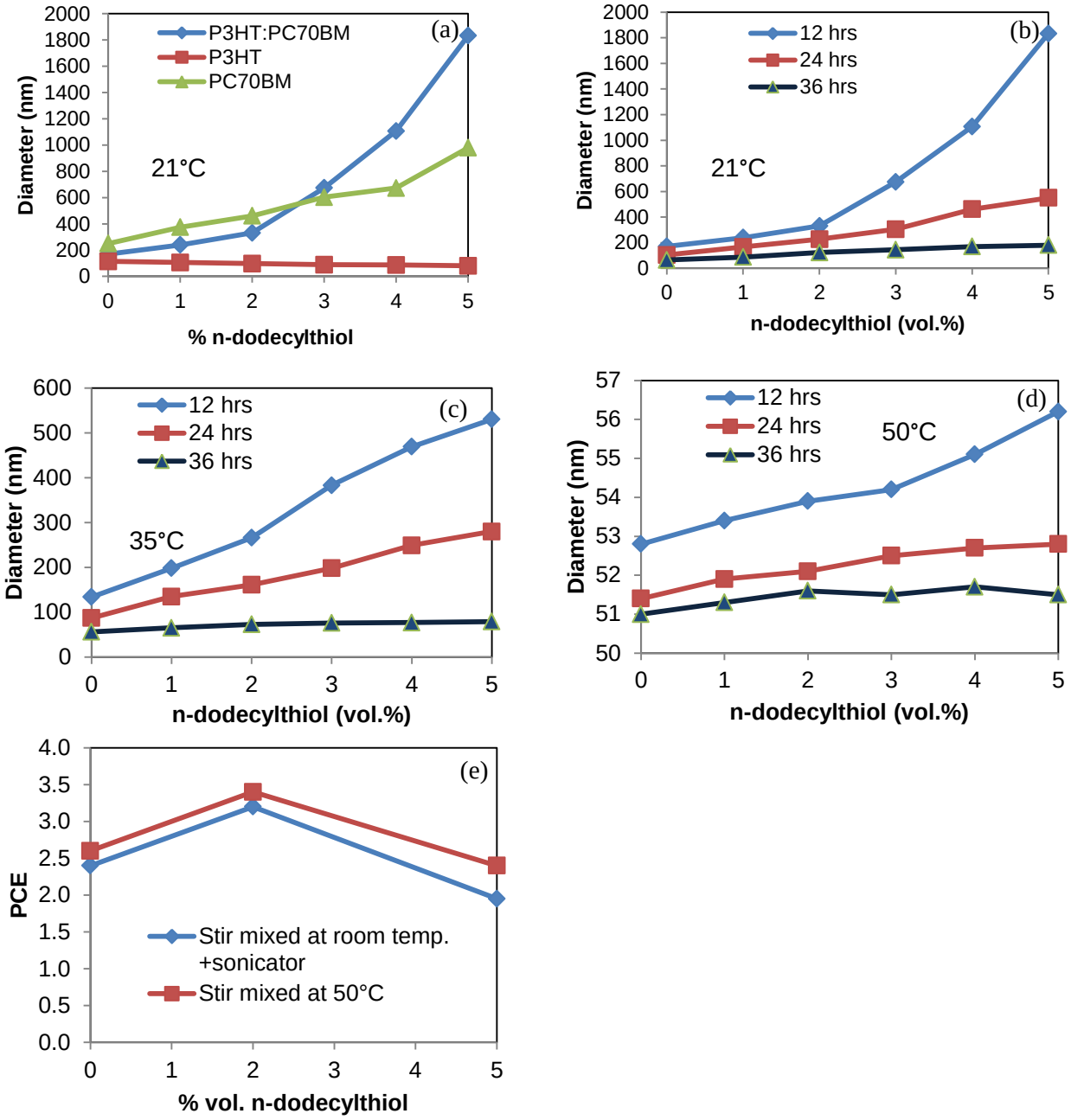

Figure 40: a) Aggregate size of P3HT, PC70BM and P3HT:PC70BM:(0-5%) n-dodecylthiol dissolved in chlorobenzene solution.
b)Aggregate size of P3HT:PC70BM:(0-5%) n-dodecylthiol dissolved in chlorobenzene solution prepared at room temp. (21°C).
c) Aggregate size of P3HT:PC70BM:(0-5%) n-dodecylthiol dissolved in chlorobenzene solution prepared at 35°C.
d) Aggregate size of P3HT:PC70BM:(0-5%) n-dodecylthiol dissolved in chlorobenzene solution prepared at 50°C.
e) PCE at different mixing conditions

5.5 Kinetics of the polymer solar cell

There is little research associated with the kinetics of transformation of polymer solar cells during the heat treatment process. The most popular model which describes transformation kinetics is the Avrami model: [62-64]

The Avrami equation is given as:

$$\mathbf{X(t) = 1 - \exp(-Kt^n)} \quad \text{.....(7)}$$

$$\mathbf{\log [-\ln(1-X(t)] = n.\log(t) + \log(K)} \quad \text{.....(8)}$$

Where:

X(t): is the relative crystallinity at time t,

K : is the crystallization rate constant depending on nucleation and growth rate.

n: a constant that depends on the nature of nucleation and growth geometry of the crystals, it usually range between 1 and 4. [64, 66, 67]

For polymer crystallization, if n has a value of 2 or 3, it indicates two or three dimensional nucleation of the crystal nucleus. However, a fractional value of n can be an indication of secondary crystallization or crystal perfection [65].

Isothermal crystallization kinetics of P3HT:PC70BM:0%n-dodecylthiol blends were investigated by XRD (see Figure 42A-D appendix C). Figure 41A shows the area under the peak of XRD curves Each point represents the area under an XRD curve for one sample at 2θ = 5.4°. At 60 °C the area under the curve increases very slowly and the final area is only 60% more than the initial area. This indicates that there is little increase in crystallinity by annealing at low temperatures, e.g. 60 °C compared to higher temperatures 120-150 °C.

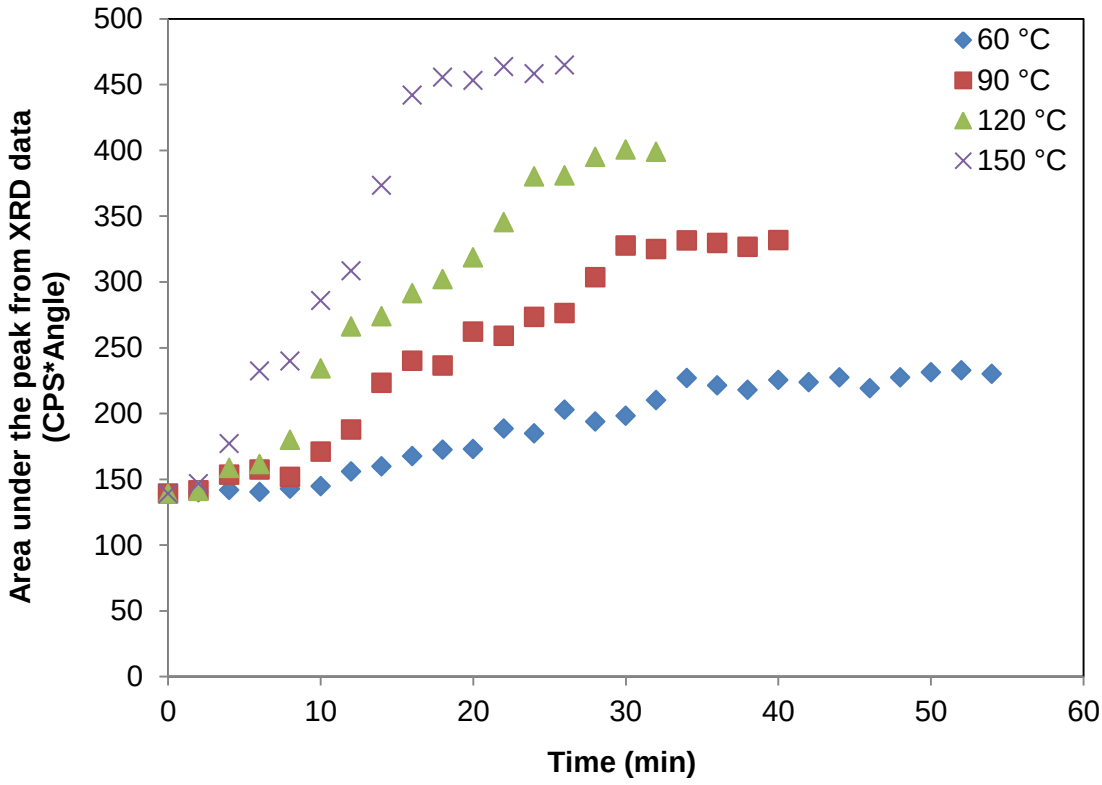

Figure41A: Area under XRD peaks at various annealing temperatures of P3HT:PC70BM.

Figure 41B shows the variation of relative crystallinity X(t) with the change of crystallization time for a P3HT:PC70BM:0%n-dodecylthiol blend. The crystallization isotherms display an "S" shape or sigmoidal shape. Additionally, the crystallization time decreases with the increase in the annealing temperature, i.e. samples heat treated at 150 °C need less time to develop full cold crystallinity compared to those heat treated at 60 °C. The Avrami equation is usually used to analyze the isothermal crystallization kinetics of crystalline materials, which describes the development of relative degree of crystallinity X(t) with crystallization time (t).

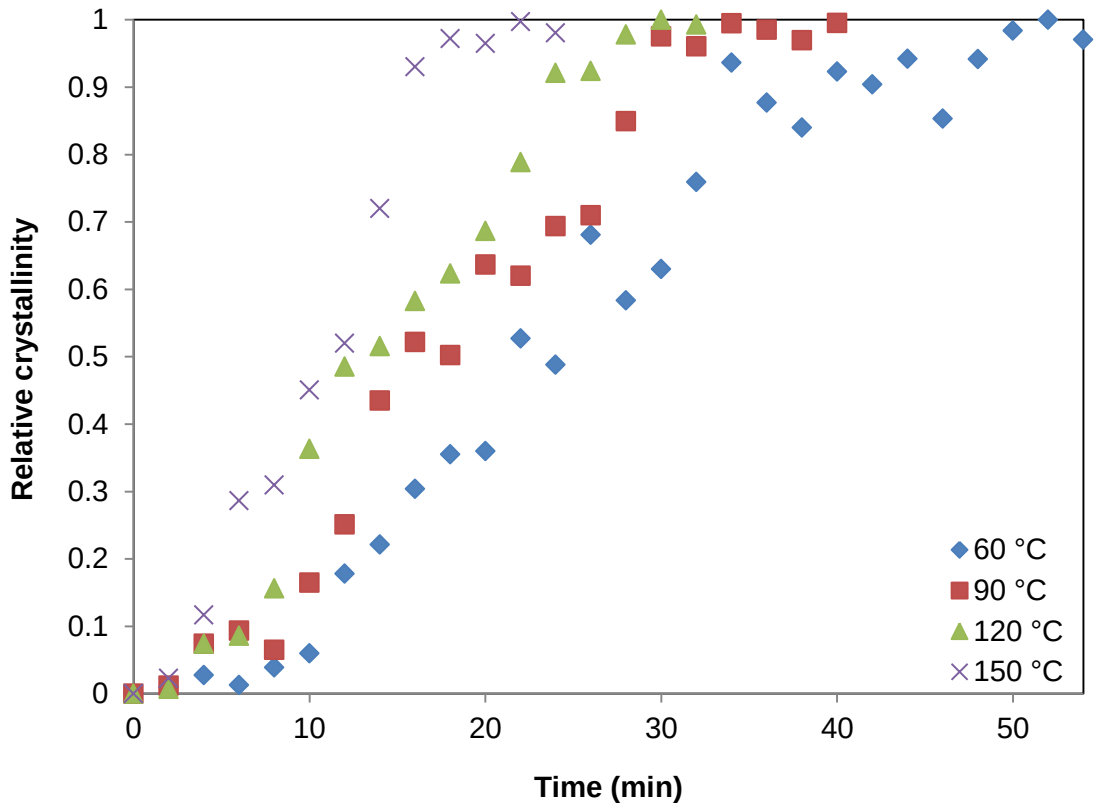

Figure 41B: Relative crystallinity X(t) versus crystallization time of P3HT:PC70BM.

Figure 41C shows the Avrami plots for P3HT:PC70BM:0%n-dodecylthiol blends. A series of straight lines represent the Avrami model at 60, 90, 120 and 150 °C, which indicate that the Avrami method can describe the development of the relative degree of crystallinity X(t) as a function of crystallization time (t). Using Figure 41C, the Avrami parameters n and K can be obtained from the slopes (n) and intercepts (log K); respectively. The values of n and K are summarized in Table 2. The values of n are between 2 and 3, suggesting that the crystallization of P3HT:PC70BM may correspond to three-dimensional truncated spherulitic growth with a thermal nucleation [68].

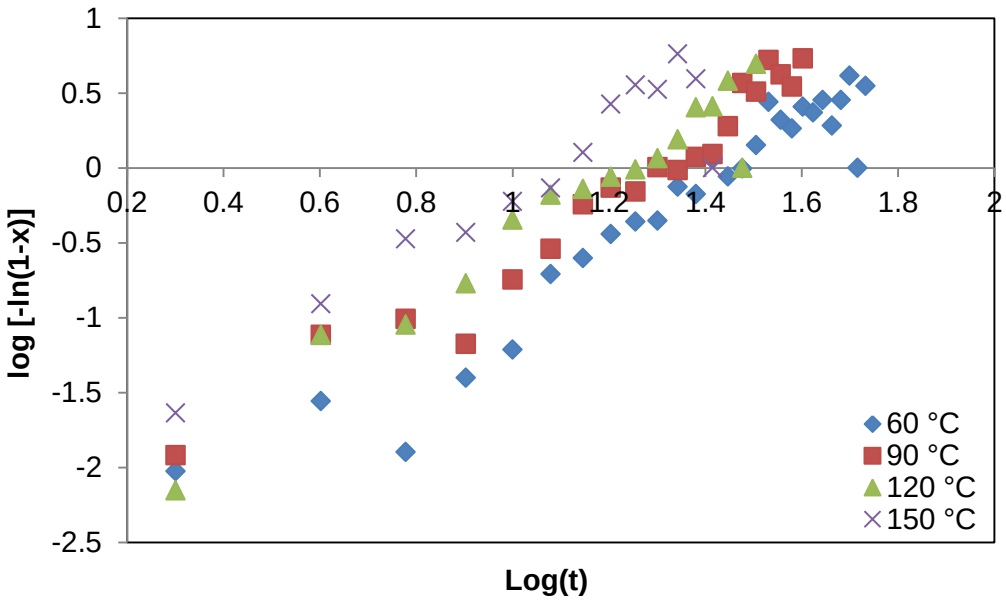

Figure41C: Avrami log equation for the P3HT:PC70BM samples prepared at 60, 90, 120 and 150 °C.

The half-time of crystallization ($t_{0.5}$), defined as the time required to complete half of the final crystallinity, can be obtained by:

$$t_{0.5}=[(\ln 2)/K]^{(1/n)} \quad \text{.....(9)}$$

The overall crystallization rate can be simply represented by the reciprocal of the half-time of crystallization ($1/t_{0.5}$). Using equation 5, the values of $t_{0.5}$ and $1/t_{0.5}$ were calculated and are shown in Figure 41D. Appendix B, Table 7 summarizes the values of $t_{0.5}$ for P3HT:PC70BM:n-dodecylthiol blend. It is evident that the values of $1/t_{0.5}$ increase with the increase in annealing temperature, indicating a faster crystallization rate.

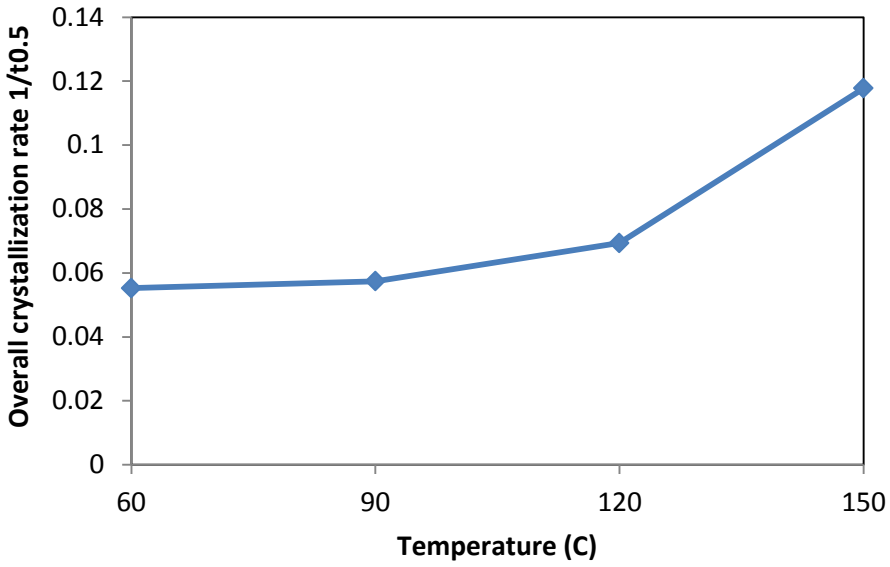

Figure41D: Overall crystallization rate at annealing temperature of 60, 90, 120 and 150 °C.

Chapter V

Summary and Conclusions

6.1 Summary

* 0-5 volume % n-dodecylthiol was added to P3HT/ PC70BM solution to improve the P3HT crystallinity and to improve the P3HT/ PC70BM phase separation.

* UV-Vis results show enhancement of the self-organization ability of the polymer which results in improvement of P3HT crystallinity and increase of phase separation extent of P3HT/PC70BM in films.

* n-dodecylthiol played an important role during the formation process of the polymer film, and the UV-Vis absorbance increases by adding n-dodecylthiol.

* AFM images of the samples prepared before heat treatment show that adding n-dodecylthiol to P3HT:PC70BM results in higher peak values, and increases the surface roughness. This indicates more space for P3HT crystallites to form, and hence an increase of crystallinity.

* After heat treatment, AFM analysis shows that above 2% n-dodecylthiol there is a decline in surface roughness and the fibered structure of the polymer becomes clearer on the AFM image surface.

* SEM images show that adding more than 2% n-dodecylthiol can result in an aggregation of the polymers, which has a negative effect on both crystallinity and electric properties. Also, SEM cross-sectional images show that the thicknesses of ITO/PEDOT/P3HT:PC70BM/Al are 25, 50, 100-150 and 50-100 nm,respectively.

* DLS analysis of P3HT:PC70BM:n-dodecylthiol dissolved in chlorobenzene solution showed an increase of aggregate size by adding n-dodecylthiol; which confirms the SEM images. This also shows that n-dodecylthiol does not enhance

the dispersion of P3HT:BC70BM in the chlorobenzene solution. Also, it shows that the more n-dodecylthiol is added, the more aggregation will be formed. In addition, increasing mixing time and temperature improves the mixing process and results in smaller aggregates.

* During the film-forming process, due to the addition of n-dodecylthiol, the polymer crystallinity was improved from 10.1% to 16.9% as measured using DSC. Increased P3HT crystallinity leads to phase separation balancing for exciton dissociation and charge transport and/or collection.

* 2% n-dodecylthiol, resulted in an increase of power conversion efficiency from 2.41% to 3.21%.

* There is an increase of crystallinity with the addition of n-dodecylthiol, due to the presence of n-dodecylthiol in a polymer blend. Both XRD and DSC were used for characterization, and both methods show an increase in crystallinity which led to a 33% improvement of polymer solar cell power conversion efficiency. Also, XRD for the samples heat treated at 150 °C for 30 minutes showed an increase of crystallinity of the composite with the addition of n-dodecylthiol up to 2 vol.%. Above 2 % n-dodecylthiol, the crystallinity declines, which indicate that 2% n-dodecylthiol represents the highest crystallinity after heat treatment, reflecting the highest efficiency of 3.21%.

* The PSC devices without heat treatment have a low PCE of nearly 1%. However, after the heat-treatment the PCEs values increased by increasing of temperature up to 150°C. Up to 150°C, the photovoltaic parameters were remarkably improved. On the contrary, the cell performance deteriorated abruptly

at a temperature higher than 150 °C. This may be due to a partial melting of the polymer composite under the Al electrode; also, some cracks were observed on the Al electrode. Besides, the polymer color changed from purple to brown.

* Effect of annealing time has a different trend, and our results show that up to 150°C there is significant enhancement of electrical properties of the PSCs performance by increasing time. Above 150°C the device performance will decline when increasing annealing time.

* 2% n-dodecylthiol shows the smallest polymer crystallites size L, which was nearly 11.2 nm after heat treatment at 150°C for 30 min in a vacuum atmosphere. The smaller crystallite size suggests a shorter path of the charge carriers between P3HT backbones, which could be beneficial to get a higher J_{sc} (short circuit current) in the devices with the additive.

* Isothermal cold crystallization kinetics of P3HT:PC70BM blend was investigated using the Avrami model. The results show that the variation of relative crystallinity X(t) with crystallization time for a P3HT:PC70BM:0 %n-dodecylthiol blend displays an "S" shape or sigmoidal shape. The crystallization time decreases with the increase of crystallization temperature.

* The Avrami plots for a P3HT:PC70BM:0 %n-dodecylthiol blend show a series of straight lines representing the Avrami model at 60, 90, 120 and 150 °C. The Avrami parameters n and K are obtained from the slopes (n) and intercepts (logK), respectively. The values of n are between 2 and 3, suggesting that the crystallization of P3HT:PC70BM:n-dodecylthiol may correspond to three-

dimensional truncated spherulitic growth with athermal nucleation as described by Wunderlich *et al* [68].

* The half-time of crystallization ($t_{0.5}$), is the time required to complete half of the final crystallinity. The results show that the values of $t_{0.5}$ decrease with the increase of temperature, indicating a faster rate with increased temperature. The faster rate can be an indication of enhancement of crystallinity by adding n-dodecylthiol to the P3HT:PC70BM blend.

6.2 Conclusions

In this work n-dodecylthiol was added to P3HT/ PC70BM to improve crystallinity of P3HT and reduce the crystallite size of the bulk heterojunction active polymer. Higher crystallinity improves charge mobility due to increase in intermolecular interactions between polymer chains and smaller crystallite size associated with large PCBM clusters. Both EQE and absorbance increased by adding n-dodecylthiol due to enhancement of polymer crystallinity. 2% n-dodecylthiol was the most balanced additive quantity which resulted in increased P3HT crystallinity, smaller crystallite size, and higher surface roughness.Adding 2% n-dodecylthiol to P3HT:PC70BM led to a better exciton dissociation and charge transport, which resulted in an increase of 33% in the PSC efficiencies compared to PSCs without any additives in the photoactive layer. Isothermal cold crystallization kinetics showed that the crystallization time decreases with the increase of crystallization temperature. The half-time of crystallization ($t_{0.5}$) decreased with the increase of temperature, indicating a faster rate with increased temperature. The faster rate can be an indication of enhancement of crystallinity by adding n-dodecylthiol to the P3HT:PC70BM blend.

References

[1] Frederik C. Krebs, “Polymer photovoltaics: Apractical approach” SPIE Press, edition 2008.

[2] Wanzhu Cai, Xiong Gong, Yong Cao “Polymer solar cells: Recent development and possible routes for improvement in the performance” Solar Energy Materials and Solar Cells, 94(2), (2010), pp. 114-127.

[3] YU, G., Gao, l, Hummelen, J.e., Wudl, F, and Heeger, A.J., "Polymer photovoltaic cells-Enhanced efficiencies via a network of internal donoracceptor heterojunctions," Science, 270, (1995), pp. 1789-1791.

[4] H. Hoppe, N.S. Sariciftci, "Morphology of polymer/fullerene bulk hetero-junction solar cells ", J. Mater. Chem., 16, (2006), pp. 45-61.

[5] Seok-In Na, Seok-Soon Kim, Jang Jo, Ki-Sung Lee, Seong-Ju Park, Dong-Yu Kim “Modified electrode architecture for efficient and air-stable polymer solar cells based on P3HT:PCBM” Journal of Photochemistry and Photobiology A: Chemistry, 194(23), (2008), pp. 161-166 .

[6] Jianyong Ouyang, Yijie Xia “High-performance polymer photovoltaic cells with thick P3HT:PCBM films prepared by a quick drying process” J.Energy Materials and Solar Cells, 93(9), (2009), pp. 1592-1597.

[7] Seok-Soon Kim, Seok-In Na, Seok-Ju Kang, Dong-Yu Kim , “Annealing-free fabrication of P3HT:PCBM solar cells via simple brush painting” Solar Energy Materials and Solar Cells, 94(2), (2010), pp. 171-175.

[8] Quentin Bricaud, Antonio Cravino, Philippe Leriche, Jean Roncali, “Terthiophene-cyanovinylene π-conjugated polymers as donor material for organic solar cells” J. Synthetic Metals, 159, (2009), pp. 2534–2538.

[9] S. Millefiorini, E. Kozma, M. Catellani, S. Luzzati, “Dithienothiophene based polymer as electron donor in plastic solar cells” Thin Solid Films, 516, (2008), pp. 7205–7208.

[10] Jan C. Hummelen, Brian W. Knight, F. LePeq, Fred Wudl, Jie Yao, Charles L. Wilkins “Preparation and Characterization of Fulleroid and Methanofullerene Derivatives” J. Org. Chem. , 60 (3), (1995), pp.532–538.

[11] Wienk, M.M., Kroon, J.M., Yerhees, W.J.H., Knol, J., Hummelen, le., van Hal, PA., and Janssen, R.A.J., "Efficient methano[70]fullerene/MDMO-PPY bulk heterojunction photovoltaic cells," Angew. Chem., Int. Ed., 42, (2003), pp. 3371-3375.

[12] Padinger, F, Rittberger, R.S., and Sariciftci, N .S., "Effects of postproduction treatment on plastic solar cells," Adv. Funct. Mater., 13, (2003), pp. 85-109,

[13] E. Cohen, E. Gutoff , "Modern Coating and Drying Technology", Wiley-VCH,(1992).

[14] A.A. Tracton, E.D. "Coatings Technology Handbook". 3rd Ed., CRC Press, Boca Raton, FL, (2006).

[15] E.B. Gutoff, E.D. Cohen, "Coating and Drying Defects. Troubleshooting Operating Problems", 2nd Ed., Wiley, New Jersey, (2006).

[16] Arthur A. Tracton,“Coatings Technology: Fundamentals, Testing, and Processing Techniques” CRC Press; 1st Ed. , (2006).

[17] Artur Goldschmidt and Hans-Joachim Streitbeger, “BASF Handbook on Basics of Coating Technology”, Vincentz press, (2003).

[18] Frederik C. Krebs, “Fabrication and processing of polymer solar cells: A review of printing and coating techniques”, Solar Energy Materials & Solar Cells, 93, (2009), pp. 394–412.

[19] Norrman, A. Ghanbari-Siahkali, N.B. Larsen, "Studies of spin-coated polymer films". Physical Chemistry Annual Reports(C), 101, (2005), pp. 174-201

[20] G. Li, V. Shrotriya, J. Huang, Y. Yao, T. Moriarty, K. Emety, Y. Yang, "Highefficiency solution processable polymer photovoltaic cells by self-organization of polymer blends", Nat. Mater. 4 (2005), pp. 864-868.

[21] W. Ma, e. Yang, X. Gong, K. Lee, A.j. Heeger, "Thermally stable, efficient polymer solar cells with nanoscale control of the interpenetrating network morphology", Adv. Funct. Mater. 15, (2005), pp. 1617-1622.

[22] R. Mens, P. Adriaensens, L. Lutsen, A. Swinnen, S. Bertho, B. Ruttens, J. D'Haen, j. Manca. T. Cleij. D. Vanderzande, J. Gelan, "NMR Study of the nanomorphology in thin films of polymer blends used in organic PV devices: MDMO-PPV/PCBM", J. Pol. Sci. A Pol. Chem. 46, (2008), pp. 138-145.

[23] P. Schilinsky, e. Waldauf, q. Brabec, "Performance analysis of printed bulk heterojunction solar cells", Adv. Funct. Mater. 16, (2006), pp. 1669-1672.

[24] F.C. Krebs, M.Jergensen, K. Norrman, O. Hagemann,j. Alstrup, T.D. Nielsen,J. Fyenbo, K. Larsen,J. Kristensen, "A complete process for production of flexible large area polymer solar cells entirely using screen

printing-first public demonstration", Solar Energy Materials& Solar Cells, 93, (2009), pp. 422-441.

[25] S.E. Shaheen, R. Radspinner, N. Peyghambarian, G.E. Jabbour, “Fabrication of bulk heterojunction plastic solar cells by screen printing”, Appl. Phys. Lett., 79, (2001), pp.2996-2998.

[26] F.e. Krebs, J. Alstrup, H. Spanggaard, K. Larsen, E. Kold, “Production of large area polymer solar cells by industrial silk screen printing, lifetime considerations and lamination with polyethyleneterephthalate”, Solar Energy Materials& Solar Cells, 83, (2004), pp.293-300.

[27] F.e. Krebs. H. Spanggaard, T. Kjaer, M. Biancardo,J. Alstrup, “Large area plastic solar cell modules”, Mater. Sci. Eng. B, 138, (2007), pp. 106-111.

[28] T. Aernouts. P. Vanlaeke. J. Poortmans, P. Heremans, “Polymer solar cells: screen printing as a novel deposition technique”, Proc. SPIE 5464, (2004), p. 252.

[29] M.Jergensen, O. Hagemann,j. Alstrup, Fe. Krebs, “Thermo-cleavable solvents for printing conjugated polymers: application in polymer solar cells”, Solar Energy Materials & Solar Cells, 93, (2009), pp.413-421.

[30] Minas M. Stylianakis , John A. Mikroyannidis, Emmanuel Kymakis, “A facile, covalent modification of single-wall carbon nanotubes by thiophene for use in organic photovoltaic cells”, Solar Energy Materials & Solar Cells, 94, (2010), pp. 267–274.

[31] Zhihui Feng, Yanbing Hou, Desheng Lei, “The influence of electrode buffer layers on the performance of polymer photovoltaic devices”, Renewable Energy, 35, (2010), pp.1175–1178.

[32] T.M.W.J. Bandara, M.A.K.L. Dissanayake, I. Albinsson, B. Mellander, “Dye-sensitized, nano-porous TiO2 solar cell with poly (acrylonitrile): MgI2plasticized electrolyte”, Journal of Power Sources, 195, (2010), pp. 3730–3734.

[33] Peter Harrop and Raghu Das, “Organic Electronics Forecasts, Players & Opportunities“, IDTechEx, (2006).

[34] Mi Sun Ryu , Hyuk Jin Cha , Jin Jang, “Effects of thermal annealing of polymer:fullerene photovoltaic solar cells for high efficiency”, Current Applied Physics, 10(2), (2010) pp. S206-S209.

[35] John J. Bozzola , Lonnie Dee Russell, ” Electron Microscopy“, Jones & Bartlett Publishers, 2nd Ed. , (1998).

[36] Claudio Girotto, Barry P. Rand, Soeren Steudel , Jan Genoe , Paul Heremans, “Nanoparticle-based, spray-coated silver top contacts for efficient polymer solar cells”, Organic Electronics, 10, (2009), pp.735–740.

[37] Lars Blankenburg, Karin Schultheis, Hannes Schache, Steffi Sensfuss, Mario Schrödner ”Reel-to-reel wet coating as an efficient up-scaling technique for the production of bulk-heterojunction polymer solar cells”, Solar Energy Materials & Solar Cells, 93, (2009), pp.476–483.

[38] W. Ma, C. Yang, X. Gong, K. Lee, A. J. Heeger, “Thermally Stable, Efficient Polymer Solar Cells with Nanoscale Control of the Interpenetrating Network Morphology”, Advanced Functional Materials, 15(10), (2005), pp. 1617-1622.

[39] Xuan-Dung Dang and Thuc-Quyen Nguyen, ”Photoconductive Atomic Force Microscopy for Understanding Nanostructures and Device Physics of Organic Solar Cells”,http://www.nanowerk.com/spotlight/spotid=18038.php, September 15, (2010).

[40] The University of Toledo, “Fundamental properties of solar cells”,http://astro1.panet.utoledo.edu/~relling2/teach/archives/6980.4400.2012/20120131_PHYS_6980_4400_FundamentalProperties.pdf, (2011).

[41] Jiangang Liu, Shuyan Shao, Hanfu Wang, Kui Zhao, Longjian Xue, Xiang Gao, Zhiyuan Xie, Yanchun Han, “The mechanisms for introduction of n-dodecylthiol to modify the P3HT/PCBM morphology”, Organic Electronics, 11, (2010), pp. 775–783.

[42] Yongbo Yuan, Timothy J. Reece, Pankaj Sharma, Shashi Poddar, Stephen Ducharme, Alexei Gruverman, Yang Yang, Jinsong Huang, “Efficiency enhancement in organic solar cells with ferroelectric polymers“, Nature Materials, 10, (2011), pp. 2296–3002.

[43] Patrick Boland, Sri Sabarinadh Sunkavalli, Sampath Chennuri, Kurniawan Foe, Tarek Abdel-Fattah and Gon Namkoong, “Investigation of structural, optical, and electrical properties of regioregular poly(3-hexylthiophene) /fullerene blend nanocomposites for organic solar cells”, Thin Solid Films, 518(6), (2010), pp. 1728-1731.

[44] S. Rughooputh, S. Hotta, A.J. Heeger, F. Wudl, "Chromism of soluble polythienylenes", Journal of Polymer Science Part B-Polymer Physics, 25(5), (1987), p. 1071.

[45] N. Kiriy, E. Jahne, H.J. Adler, M. Schneider, A. Kiriy, G. Gorodyska, S. Minko, D. Jehnichen, P. Simon, A.A. Fokin, M. Stamm, "One-Dimensional Aggregation of Regioregular Polyalkylthiophenes", Nano Letters, 3, (2003), pp. 707-712.

[46] H. Sirringhaus, P.J. Brown, R.H. Friend, M.M. Nielsen, K. Bechgaard, B.M.W. Langeveld-Voss, A.J.H. Spiering, R.A.J. Janssen, E.W. Meijer, P. Herwig, D.M. de Leeuw, "Two-dimensional charge transport in self-organized, high-mobility conjugated polymers", Nature, 401, (1999), pp. 685-688.

[47] P.J. Brown, D.S. Thomas, A. Kohler, J.S. Wilson, J.S. Kim, C.M. Ramsdale, H. Sirringhaus, R.H. Friend,"Effect of interchain interactions on the absorption and emission of poly(3-hexylthiophene)", Physical Review B, 67(6), (2003), p. 64203.

[48]- Y. Kim, S. Cook, S.M. Tuladhar, S.A. Choulis, J. Nelson, J.R. Durrant, D.D.C. Bradley, M. Giles, I. McCulloch, C.S. Ha, M. Ree, "A strong regioregularity effect in self-organizing conjugated polymer films and high-efficiency polythiophene:fullerene solar cells", Nature Materials, 5(3), (2006), pp. 197-203.

[49] T. Erb, U. Zhokhavets, G. Gobsch, S. Raleva, B. Stuhn, P. Schilinsky, C. Waldauf, C.J. Brabec, "Correlation Between Structural and Optical

Properties of Composite Polymer/Fullerene Films for Organic Solar Cells", Advanced Functional Materials, 15(7), (2005), p.1193.

[50] Gang Li, Vishal Shrotriya, Yan Yao, Jinsong Huang and Yang Yang “Manipulating regioregular poly(3-hexylthiophene) : [6,6]-phenyl-C61-butyric acid methyl ester blends—route towards high efficiency polymer solar cells” J. Mater. Chem., 17, (2007), pp. 3126–3140.

[51] Chang Y.M., L. Wang, "Efficient Poly(3-hexylthiophene)-Based Bulk Heterojunction Solar Cells Fabricated by an Annealing-Free Approach", Journal of Physical Chemistry C, 112, (2008), pp.17716-17720.

[52] Jung-Hsun Tsai, Yi-Cang Lai, Tomoya Higashihara, Chih-Jung Lin, Mitsuru Ueda and Wen-Chang Chen “Enhancement of P3HT/PCBM Photovoltaic Efficiency Using the Surfactant of Triblock Copolymer Containing Poly (3-hexylthiophene) and Poly(4-vinyltriphenylamine) Segments”, Macromolecules , 43 (14), (2010), pp. 6085–6091.

[53] Shimomura M., M. Kaga, N. Nakayama, S. Miyauchi, “Thermal and electrical properties of poly(3-alkylthiophene)s prepared by the oxidative polymer-ization”,Synthetic Metals, 69(1), (1995), pp. 313–314.

[54] Yue Zhao, Guoxiong Yuan and Philippe Roche, “A calorimetric study of the phase transitions in poly(3-hexylthiophene)”, Polymer, 36 (11), (1995) pp. 2211-2214.

[55] van Krevelen D. W. "Properties of polymers", 3rd Ed, Elsevier Science Publishers, Amsterdam, Oxford, New York, 1990.

[56] Yeping Sun, Chaohua Cui, Haiqiao Wang,Yongfang Li “Efficiency Enhancement of Polymer Solar Cells Based on Poly(3-hexylthiophene)/Indene-C 70 Bisadduct via Methylthiophene Additive”,Advanced Energy Materials,1(6), (2011), pp. 1058–1061.

[57] G. Li, Y. Yao, H. Yang, V. Shrotriya, G. Yang, Y. Yang," Solvent Annealing” Effect in Polymer Solar Cells Based on Poly(3-hexylthiophene) and Methanofullerenes", Advanced Functional Materials, 17, (2007), p. 1636.

[58] A.L. Ayzner, D.D. Wanger, C.J. Tassone, S.H. Tolbert, B.J. Schwartz," Room to Improve Conjugated Polymer-Based Solar Cells: Understanding How Thermal Annealing Affects the Fullerene Component of a Bulk Heterojunction Photovoltaic Device", Journal of Physical Chemistry C, 112, (2008), p. 18711.

[59] A.R. Campbell, J.M. Hodgkiss, S. Westenhoff, I.A. Howard, R.A. Marsh, C.R. McNeill, R.H. Friend, N.C. Greenham, "Low-Temperature Control of Nanoscale Morphology for High Performance Polymer Photovoltaics", Nano Letters, 8(11), (2008), p. 3942.

[60] P.K. Watkins, A.B. Walker, G.L.B. Verschoor, " Dynamical Monte Carlo Modelling of Organic Solar Cells: The Dependence of Internal Quantum Efficiency on Morphology", Nano Letters, 5(9), (2005), p. 1814.

[61] Christoph Brabec, Ullrich Scherf and Vladimir Dyakonov “Organic Photovoltaics” , Wiley-VCH, 1st Ed, (August 26, 2008)

[62] Mandelkern, L. "Crystallization of Polymers", 1st Ed, McGraw-Hill, New York, (1964).

[63] Dierk Raabe , "A texture-component Avrami model for predicting recrystallization textures, kinetics and grain size", Modelling Simul. Mater.Sci. Eng. 15(39), 2007.

[64] Avrami, M., "Kinetics of Phase Change. I General Theory", J. Chem. Phys. 1939, 7(12), (1939), p. 1103.

[65] Cheng SZD, "Kinetics of mesophase transitions in thermotropic copolyesters. 1. Calorimetric study", Macromolecules, 21, (1988), p. 2475.

[66] Avrami M., "Kinetics of Phase Change. II Transformation-Time Relations for Random Distribution of Nuclei", J Chem Phys, 8(2), (1940), p. 212.

[67] Avrami M., " Granulation, Phase Change, and Microstructure Kinetics of Phase Change", J Chem Phys, 9(2), (1941), p.177.

[68] Wunderlich, B., Macromolecular Physics, Vol. 2, "Crystal Nucleation, Growth,Annealing", Academic Press, 1st Ed, New York, (1976).

[69] Brian A. Collins , John R. Tumbleston , and Harald Ade, "Miscibility, Crystallinity, and Phase Development in P3HT/PCBM Solar Cells: Toward an Enlightened Understanding of Device Morphology and Stability" , J. Phys. Chem. Lett., 2 (24), 2011, pp. 3135–3145.

[70] Yi-Cang Lai, Tomoya Higashihara, Jung-Ching Hsud, Mitsuru Uedab, Wen-Chang Chen “Enhancement of power conversion efficiency and long-term stability of P3HT/PCBM solar cells using C60 derivatives with thiophene units as surfactants”, Solar Energy Materials & Solar Cells,97, (2012), pp. 164–170.

[71] Soo Won Heo, Kwan Wook Song, Min Hee Choi , Hwan Sool Oh, Doo Kyung Moon, "Influence of alkanediol series as processing additives in photo-active layer on the power conversion efficiency of polymer solar cells", Solar Energy Materials and Solar Cells, 114, (2013), pp. 82–88.

[72] Cullity, B. D, “Elements Of X-Ray Diffraction”, Prentice Hall, 3rd Ed, (2001), p. 113.

[73] Heejoo Kim, Won-Wook So and Sang-Jin Moon, "Effect of Thermal Annealing on the Performance of P3HT/PCBM Polymer Photovoltaic Cells", Journal of the Korean Physical Society, 48(3), (2006), pp. 441-445.

[74] O. Oklobia, T.S. Shafai, "A quantitative study of the formation of PCBM clusters upon thermal annealing of P3HT/PCBM bulk heterojunction solar cell", Solar Energy Materials and Solar Cells, 117, (2013), pp. 1–8.

[75] Liqiang Ren, Shiren Wang, Mark Holtz, Jingjing Qiu, "The synergistic effect of nanocrystal integration and process optimization on solar cell efficiency", Nanotechnology, 23(7), (2012, p. 075401.

[76] Alexandre M. Nardes, Alexander L. Ayzner, Scott R. Hammond, Andrew J. Ferguson,Benjamin J. Schwartz, Nikos Kopidakis, "Photoinduced Charge Carrier Generation and Decay in Sequentially Deposited Polymer/Fullerene Layers: Bulk Heterojunction vs Planar Interface", Journal of Physical Chemistry, C,116, (2012), pp. 7293−7305.

[77] Jin Hyuck Heo, Sang Hyuk Im, Jun Hong Noh, Tarak N. Mandal,Choong-Sun Lim, Jeong Ah Chang, Yong Hui Lee, Hi-jung Kim, Arpita Sarkar, Md. K. Nazeeruddin, Michael Grätzel, Sang Seok, "Efficient inorganic–organic

hybrid heterojunction solar cells containing perovskite compound and polymeric hole conductors", Nature Photonics, 7, (2013), pp.486–491.

[78] Pei Cheng, Yongfang Li, Xiaowei Zhan, “A DMF-assisted solution process boosts the efficiency in P3HT:PCBM solar cells up to 5.31%”, Nanotechnology, 24, (2013), pp.1-7.

[79] Gisela L. Schulz , Marta Urdanpilleta, Roland Fitzner, Eduard Brier, Elena Mena-Osteritz, Egon Reinold, Peter Bäuerle, “Optimization of solution-processed oligothiophene:fullerene based organic solar cells by using solvent additives”, J. Nanotechnology, 4, (2013), pp.680–689.

[80] Pei Cheng, Long Ye, Xingang Zhao, Jianhui Hou, Yongfang Li, Xiaowei Zhan, “Binary additives synergistically boost the efficiency of all-polymer solar cells up to 3.45%”, Energy Environ. Sci., (2014), Advance Article.

[81] Hsiang-Yu Chen, Hoichang Yang, Guanwen Yang, Srinivas Sista, Ruben Zadoyan, Gang Li, Yang Yang, “Fast-Grown Interpenetrating Network in Poly(3-hexylthiophene): Methanofullerenes Solar Cells Processed with Additive”. Journal of Physical Chemistry,113, (2009), pp.7946–7953.

[82] Sung Heum Park, Anshuman Roy, Serge Beaupre, Shinuk Cho, Nelson Coates, Ji Sun Moon,Daniel Moses, Mario Leclerc, Kwanghee Lee1, Alan J. Heeger, “Bulk heterojunction solar cells with internalquantum efficiency approaching 100%”, Nature Photonics, 3, (2009), pp. 297–303.

[83] P.G. Karagiannidis, S. Kassavetis, C. Pitsalidis, S. Logothetidis, “Thermal annealing effect on the nanomechanical properties and structure of P3HT:PCBM thin films”, Thin Solid Films 519 (2011),pp.4105–4109.

[84] Mao-Yuan Chiu, U-Ser Jeng, Chiu-Hun Su, Keng S. Liang, and Kung-Hwa Wei, “Simultaneous Use of Small- and Wide-Angle X-ray Techniques to Analyze Nanometerscale Phase Separation in Polymer Heterojunction Solar Cells”, Adv. Mater.20, (2008), pp.2573–2578.

Appendix A: Sample preparation

* Sample preparation for AFM

1- Cut a glass slide to 1”x1” with a glass cutter (do not forget to use cutting oil to get a good cut).

2- Clean the slide with detergent followed by washing under tap water. Then, clean it using the ultrasonic cleaner.

2- Dry the slides using hot air stream.

3- Weigh 10mg of P3HT + 10mg of PCBM.

4- Add 2ml of chlorobenzene to the mixture of P3HT and PCBM.

5- Leave the mixture at 50^{o}C for a minimum of 12 hours to get a suitable dissolving of the materials in the solvent. Then sonicate the solution 2 minutes.

6- Prepare the spin coater to use, making sure to open the Ni tube and set the pressure to 40 to 60 psi. Open the vacuum pump, because we use the vacuum pump to hold the sample on the spin coater.

7- Put one slide over the spin coater, then press "VACUUM" (to apply vacuum to hold the sample). The spin coater should read vacuum of about 20. If the reading is low, then the spin coater will not work, and we need to check the valves and connections.

8- Press “RUN” button to start spinning, and then add the solution by using a syringe.

9- Wait about 2 minutes to let the solution dry during spinning.

10- Press “RUN” button again to stop spinning, then open the spin machine cover and remove the sample by using a clamp. Do not touch the sample surface.

11- After finishing all samples, go to AAF to characterize the surface using the Atomic Force Microscope.

Morphology area = 2μmx2μm

* Sample preparation for optical microscope

1- Cut a glass slide to 1”x1” with a glass cutter (do not forget to use cutting oil to get a good cut).

2- Clean the slide with detergent followed by washing under tap water. Then clean it using the ultrasonic cleaner.

3- Dry the slides using hot air stream.

4- Weigh 10mg of P3HT + 10mg of PCBM.

5- Add 2ml of chlorobenzene to the mixture of P3HT and PCBM.

6- Leave the mixture at 50 °C for minimum of 12 hours to get a suitable dissolving of the materials in the solvent.

7- Some samples were prepared without using the sonicator; other samples after using the sonicator.

8- Prepare the spin coater to use making sure to open the Ni tube and set the pressure to 40 to 60 psi. Open the vacuum pump, because we use vacuum pump to hold the sample on the spin coater.

9- Put one slide over the spin coater, then press "VACUUM" (to apply vacuum to hold the sample). The spin coater should read vacuum of about 20. If the reading is low, then the spin coater will not work, and we need to check the valves and connections.

10- Press “RUN” button to start spinning, and then add the solution by using a syringe.

11- Wait about 2 minutes to let the solution dry during spinning.

12- Press “RUN” button again to stop spinning, then open the spin machine cover and remove the sample by using a clamp, and do not touch the sample surface.

13- After finishing all samples, then go to the AAF to characterize the surface using the Atomic Force Microscope.

14- The samples had a glass/ITO/PEDOT:PSS/P3HT:PC70BM:n-dodecylthiol/Al structure. The glass ITO substrates were cleaned in an ultrasonic bath with acetone and isopropanol, and then rinsed in deionised water. They were dried in an oven. A 30-50 nm thick PEDOT:PSS film was then spin-coated and dried under air for 30min at 110-160 °C. The P3HT:PCBM:n-dodecylthiol active layer was deposited next by spin-coating in a glove box. The P3HTand PCBM concentration was 10 mg/ml dissolved in a chlorobenzene solution (o-dichlorobenzene). Active layer thickness was 100-150 nm. The samples were finally annealed at 150 °C for 10 min inside a vacuum furnace immediately after spin-coating. The solution for spin-coating was prepared as follows: P3HT was first dissolved in chlorobenzene to make 10 mg/ml

solution, followed by blending with n-dodecylthiol after 12 h, then PC70BM (10 mg/ml) was added into the solution. The solution was stirred for 12 h prior to use.

*** Sample preparation for UV-Vis**

Regioregular P3HT was blended with PC70BM at a ratio of 1:1 (w/w) with 0-5%vol. n-dodecylthiol and then dissolved in a chlorobenzene (CB) solvent. A P3HT:PC70BM solution was prepared at the concentration ratio of 10:10 mg, in 1 ml of solvent. The polymer solutions P3HT:PC70BM:n-dodecylthiol were spin-coated at 1000 rpm on clean glass substrates to produce a nearly 100 nm thick layer.

*** Sample preparation for DLS.**

Three sets of samples were prepared to study aggregation of P3HT:PC70BM:n-dodecylthiol. First set is 10 mg of P3HT in 10 ml of chlorobenzene, then add 0-5% n-dodecylthiol by volume, second set is PC70BM:0-5% n-dodecylthiol same concentration as first set, and last set is P3HT: PC70BM:0-5%vol. n-dodecylthiol (Regioregular P3HT was blended with PC70BM at a ratio of 10:10 mg with 0-5% volume n-dodecylthiol and then dissolved in a chlorobenzene (CB) 1 ml chlorobenzene. The solutions were magnetic stirred for 12, 24 and 36 hours.

*** Sample preparation for DSC**

Regioregular P3HT was blended with PC70BM at a ratio of 1:1 (w/w) with 0-5%vol. n-dodecylthiol and then dissolved in a chlorobenzene (CB) solvent. A P3HT:PC70BM solution was prepared at the concentration ratio of 10:10 mg, in 1 ml of solvent. The polymer solutions P3HT:PC70BM:n-dodecylthiol were poured into a DSC lid. For the sample without heat treatment, samples were dried slowly at room temperature. Other samples were heat treated at 150 °C for 10, 20 and 30 minutes.

*** Sample preparation for I-J characteristics**

1- Wear a safety goggles to protect your eyes from any faying broken glass parts.

2- Mark the area that will be cut by pencil and stainless steel ruler.

3- Prepare the glass cutter and lubricate the glass cutter with oil to have a smooth good cut.

4- Score the glass with the cutter using a light pressure. Note that any extra pressure can fragment the glass into pieces.

5- Break the glass by applying a pressure opposite to the score direction.

6- Clean the slide with detergent.

7- Wash the slides under tap water.

8- Clean the slides using the ultrasonic cleaner.

9- Dry the slides using hot air stream.

10- Prepare an etching solution

Etchant solution (Aqueous solution of 20% HCL and 5% HNO3 by volume,

Other researchers use (etch mixture is 300mL deionized water, 225mL hydrochloric acid (HCl), and 75mL nitric acid (HNO3)).

11- Add a drop of liquid detergent to enhance wet-ability between ITO and the etching solution.

12- Heat the etchant solution to 55°C to increase etching rate, which should be about 15 minutes to remove the 100 nm ITO layer.

13- Cover the slide area that will not be etched with a tape.

14- The tape is carefully rubbed so it adheres firmly against the ITO side of the glass slide. If the is any cavity between the tape and the slide, then this will be a channel for the etchant to go and after etching you will find that this area etched intentionally.

15- After 10 min measure the resistance of the ITO with simple ohmmeter, resistance before etching it is about 20-30Ω and after etching this number should be very high, which prove that the ITO conducting electrode was etched and the ITO layer is totally removed from the designated area.

16- If the ITO layer was not removed yet, then continue etching until ITO layer completely removed.

17- Once the ITO-glass slides was etched the, remove the mask (tape).

18- Now check the etched and non-etched area with ohmmeter.

19- researchers can distinguish between the etched and non-etched area by reflection.

20- After etching, wash the slide with water immediately.

21- Wash the slide in ethanol.

22- Place the slides in chloroform in an ultrasonic bath for 5-15 min this to remove the tape residues and other soluble organic materials.

23- Slides can be stores after drying.

24- Submerge the slides in ultrasonic bath of 2-propanol (known as isopropanol) then rinse it in pure water. Or clean the substrate in cyclohexane, chloroform, acetone and ending with 2-propanol or water.

25- Apply PEDOT:PSS at 2000-4000 rpm to improve surface roughness and electrical contact between ITO and active layer. Continue spinning for few minutes until drying

26- Remove PEDOT:PSS on the ITO side electrode by wetted cotton bud.

27- Heat the slides to 120-200 C for 10-60 min to dry the film prior to applying of active layer.

28- Move the sample inside the glove box under nitrogen atmosphere.

29- Weigh 10mg of P3HT + 10mg of PC70BM.

30- Add 2ml of chlorobenzene to the mixture of P3HT and PCBM.

31- Leave the mixture at 23-60 °C for a minimum of 12 hours to get a suitable dissolving of the materials in the solvent. Do not increase the temperature above evaporation point of solvent. Sonicator can be used to enhance mixing process.

32- Prepare the spin coater to use, making sure to open the Ni tube and set the pressure to 40 to 60 psi. Open the vacuum pump, because we use the vacuum pump to hold the sample on the spin coater.

33- Put one slide over the spin coater, then press "VACUUM" (to apply vacuum to hold the sample). The spin coater should read vacuum of about 20. If the reading is low, then the spin coater will not work, and we need to check the valves and connections.

34- Press “RUN” button to start spinning, and then add the solution by using a syringe with 450nm PTFE membrane or 0.2 micron Teflon. This will remove any dust or particles.

35- Wait about 2 minutes to let the solution dry during spinning at 800rpm.

36- Press “RUN” button again to stop spinning, and then open the spin machine cover and remove the sample by using a clamp. Do not touch the sample surface.

37- Remove the active layer from the top of the ITO electrode.

38- Evaporation of the Al electrode.

39- Cells should be annealed at 100-150°C for 5-30 minutes in vacuum furnace or hot plate under nitrogen atmosphere.

Note: if annealing at atmosphere, then annealing should be for a short time (less than 5 min).

40- Measure electrical performance using solar simulator.

Appendix B: Photovoltaic properties of P3HT:PC70BM:n-dodecylthiol at different annealing times and temperatures.

At 60 °C

	0min				10min			
n-dodecylthiol %	V_{oc}(V)	J_{sc}(mA/cm^2)	FF	PCE	V_{oc}(V)	J_{sc}(mA/cm^2)	FF	PCE
0	0.59	3.31	0.53	0.010	0.60	3.41	0.54	0.011
1	0.60	4.36	0.54	0.014	0.60	5.00	0.52	0.016
2	0.58	5.52	0.54	0.017	0.59	5.62	0.55	0.018
3	0.59	5.33	0.52	0.016	0.61	5.53	0.52	0.017
4	0.58	4.41	0.53	0.014	0.60	4.51	0.54	0.015
5	0.58	4.00	0.53	0.012	0.59	4.10	0.54	0.013

20min				30min			
V_{oc}(V)	J_{sc}(mA/cm^2)	FF	PCE	V_{oc}(V)	J_{sc}(mA/cm^2)	FF	PCE
0.60	3.51	0.55	0.012	0.61	3.71	0.55	0.013
0.61	5.50	0.55	0.018	0.62	5.70	0.56	0.020
0.60	5.80	0.55	0.019	0.61	6.00	0.56	0.021
0.60	5.70	0.54	0.018	0.61	5.90	0.56	0.020
0.60	4.71	0.55	0.0157	0.60	4.80	0.56	0.016
0.60	4.30	0.54	0.014	0.61	4.40	0.55	0.015

40min			
V_{oc}(V)	J_{sc}(mA/cm^2)	FF	PCE
0.61	4.10	0.56	0.0140
0.63	5.90	0.56	0.021
0.62	6.20	0.57	0.022
0.62	6.00	0.57	0.021
0.61	4.90	0.57	0.017
0.61	4.50	0.56	0.015

At 90 °C

	0min				10min			
n-dodecylthiol %	V_{oc}(V)	J_{sc}(mA/cm^2)	FF	PCE	V_{oc}(V)	J_{sc}(mA/cm^2)	FF	PCE
0	0.59	3.31	0.53	0.010	0.60	3.81	0.54	0.012
1	0.60	4.36	0.54	0.014	0.61	5.80	0.55	0.020
2	0.58	5.52	0.54	0.017	0.60	5.90	0.55	0.020
3	0.59	5.33	0.53	0.017	0.59	5.47	0.54	0.017
4	0.58	4.41	0.53	0.014	0.60	4.61	0.54	0.015
5	0.58	4.00	0.53	0.012	0.59	4.10	0.54	0.013

20min				30min			
V_{oc}(V)	J_{sc}(mA/cm^2)	FF	PCE	V_{oc}(V)	J_{sc}(mA/cm^2)	FF	PCE
0.60	4.35	0.55	0.014	0.61	4.72	0.56	0.016
0.61	6.30	0.56	0.022	0.62	6.60	0.56	0.023
0.61	6.30	0.56	0.022	0.62	6.60	0.57	0.023
0.61	5.40	0.57	0.019	0.61	5.70	0.56	0.0195
0.60	5.00	0.56	0.017	0.61	5.30	0.57	0.019
0.59	4.31	0.55	0.014	0.60	4.61	0.56	0.016

40min			
V_{oc}(V)	J_{sc}(mA/cm^2)	FF	PCE
0.62	5.05	0.57	0.018
0.63	6.90	0.57	0.025
0.63	6.80	0.57	0.025
0.62	5.90	0.56	0.0204
0.62	5.60	0.56	0.020
0.62	4.90	0.56	0.017

At 120 °C

	0min				10min			
n-dodecylthiol %	V_{oc}(V)	J_{sc}(mA/cm^2)	FF	PCE	V_{oc}(V)	J_{sc}(mA/cm^2)	FF	PCE
0	0.59	3.31	0.53	0.010	0.60	4.51	0.54	0.015
1	0.60	4.36	0.54	0.014	0.61	6.60	0.54	0.022
2	0.58	5.52	0.54	0.017	0.59	6.92	0.55	0.0226
3	0.59	5.33	0.52	0.016	0.60	6.63	0.54	0.022
4	0.58	4.41	0.53	0.014	0.59	5.51	0.54	0.018
5	0.58	4.00	0.53	0.012	0.59	4.50	0.54	0.014

20min				30min			
V_{oc}(V)	J_{sc}(mA/cm^2)	FF	PCE	V_{oc}(V)	J_{sc}(mA/cm^2)	FF	PCE
0.61	5.15	0.56	0.018	0.62	5.65	0.57	0.020
0.62	6.90	0.56	0.024	0.63	7.10	0.57	0.026
0.60	7.30	0.56	0.025	0.62	7.70	0.57	0.027
0.61	7.15	0.56	0.025	0.63	7.20	0.57	0.0260
0.60	5.91	0.56	0.020	0.61	6.21	0.56	0.021
0.60	4.71	0.55	0.016	0.61	4.91	0.56	0.017

40min			
V_{oc}(V)	J_{sc}(mA/cm^2)	FF	PCE
0.63	5.75	0.57	0.021
0.64	7.20	0.57	0.026
0.63	7.80	0.57	0.028
0.64	7.30	0.57	0.027
0.62	6.31	0.57	0.023
0.62	5.01	0.56	0.0175

At 150 °C

	0min				10min			
n-dodecylthiol %	V_{oc}(V)	J_{sc}(mA/cm^2)	FF	PCE	V_{oc}(V)	J_{sc}(mA/cm^2)	FF	PCE
0	0.59	3.31	0.53	0.010	0.61	5.15	0.55	0.017
1	0.60	4.36	0.54	0.014	0.61	6.36	0.57	0.022
2	0.58	5.52	0.54	0.017	0.59	7.59	0.56	0.025
3	0.59	5.33	0.52	0.016	0.60	7.14	0.55	0.023
4	0.58	4.41	0.53	0.014	0.59	6.42	0.56	0.021
5	0.58	4.00	0.53	0.012	0.59	5.01	0.56	0.017

20min				30min			
V_{oc}(V)	J_{sc}(mA/cm^2)	FF	PCE	V_{oc}(V)	J_{sc}(mA/cm^2)	FF	PCE
0.65	6.25	0.56	0.023	0.66	6.15	0.59	0.024
0.65	7.46	0.58	0.028	0.66	7.36	0.59	0.029
0.63	8.74	0.57	0.031	0.64	8.59	0.58	0.032
0.63	8.52	0.57	0.030	0.64	8.44	0.57	0.031
0.62	7.52	0.56	0.026	0.63	7.54	0.58	0.028
0.61	5.21	0.56	0.018	0.62	5.18	0.58	0.019

40min			
V_{oc}(V)	J_{sc}(mA/cm^2)	FF	PCE
0.66	3.15	0.55	0.012
0.65	4.36	0.54	0.015
0.64	5.59	0.53	0.019
0.64	5.44	0.51	0.018
0.63	4.42	0.53	0.015
0.62	3.61	0.53	0.012

At 180 °C

	0min				10min			
n-dodecylthiol %	V_{oc}(V)	J_{sc}(mA/cm^2)	FF	PCE	V_{oc}(V)	J_{sc}(mA/cm^2)	FF	PCE
0	0.59	3.31	0.53	0.010	0.55	3.23	0.51	0.009
1	0.60	4.36	0.54	0.014	0.58	4.12	0.55	0.013
2	0.58	5.52	0.54	0.017	0.54	5.21	0.53	0.015
3	0.59	5.33	0.52	0.016	0.53	5.01	0.52	0.014
4	0.58	4.41	0.53	0.014	0.50	4.22	0.55	0.012
5	0.58	4.00	0.53	0.012	0.51	3.82	0.55	0.011

20min				30min			
V_{oc}(V)	J_{sc}(mA/cm^2)	FF	PCE	V_{oc}(V)	J_{sc}(mA/cm^2)	FF	PCE
0.49	3.13	0.49	0.008	0.46	3.01	0.47	0.007
0.49	4.00	0.50	0.010	0.46	4.28	0.46	0.009
0.50	5.20	0.52	0.014	0.44	5.00	0.51	0.011
0.51	4.95	0.50	0.013	0.50	4.91	0.42	0.010
0.53	4.15	0.49	0.011	0.51	4.24	0.41	0.009
0.52	3.70	0.50	0.010	0.51	3.68	0.41	0.008

40min			
V_{oc}(V)	J_{sc}(mA/cm^2)	FF	PCE
0.46	2.81	0.41	0.005
0.45	3.93	0.40	0.007
0.43	4.89	0.41	0.0085
0.44	4.82	0.39	0.008
0.50	3.90	0.36	0.007
0.50	3.01	0.38	0.006

Appendix C: Avrami model calculations

Table 8: Relative crystallinity calculations.

Time (min)	Area under the XRD peak at				Relative crystallinity $X(t)=(X_i-X_0)/(X_f-X_0)$			
	60 °C	90 °C	120 °C	150 °C	60 °C	90 °C	120 °C	150 °C
0	139.12	139.12	139.12	139.12	0	0	0	0
2	140	141.44	140.95	146.57	0.009367	0.011996	0.00699	0.02289
4	141.69	153.4	158.51	177.06	0.027446	0.073837	0.07415	0.11691
6	140.3	157.23	161.58	232.23	0.012600	0.09364	0.08587	0.28613
8	142.77	151.65	179.92	239.85	0.038974	0.064788	0.15599	0.30954
10	144.7	171.01	234.16	285.74	0.059583	0.164891	0.36337	0.45057
12	155.8	187.71	266.07	308.3	0.17811	0.251241	0.48537	0.51989
14	159.85	223.26	273.95	373.34	0.221356	0.435057	0.51550	0.71976
16	167.57	240.06	291.48	441.88	0.303790	0.521923	0.58252	0.93039
18	172.39	236.28	302.14	455.47	0.355258	0.502378	0.62328	0.97215
20	172.82	262.26	318.7	453.06	0.359850	0.636711	0.68659	0.96475
22	188.46	259.07	345.39	463.53	0.526855	0.620217	0.78864	0.99692
24	184.85	273.3	380.08	458.22	0.488307	0.693795	0.92127	0.98060
26	202.89	276.39	380.79	464.83	0.680939	0.709772	0.92399	1.00092

28	193.75	303.45	394.95		0.583342	0.84969	0.97813	
30	198.13	327.71	400.67		0.630112	0.975129	1	
32	210.23	324.9	398.82		0.759316	0.9606	0.99292	
34	226.83	331.52			0.936572	0.994829		
36	221.24	329.65			0.876882	0.98516		
38	217.78	326.61			0.839935	0.969442		
40	225.56	331.63			0.923011	0.995398		
42	223.79				0.904111			
44	227.35				0.942124			
46	219.01				0.853069			
48	227.28				0.941377			
50	231.26				0.983876			
52	232.77				0.97413			
54	230.01				0.970528			

Table 9: log [-ln(1-x)] calculations for samples heat treated at T=60°C.

log(t)	ln(1-x)	-ln(1-x)	log [-ln(1-x)]
0.30103	-0.00944	0.009441	-2.02497661
0.60206	-0.02783	0.027826	-1.55554629
0.778151	-0.01268	0.01268	-1.89687522
0.90309	-0.03975	0.039755	-1.40061088
1	-0.06143	0.061432	-1.21160198
1.079181	-0.19615	0.196149	-0.70741458
1.146128	-0.2502	0.250201	-0.60171013
1.20412	-0.3621	0.362105	-0.44116553
1.255273	-0.43891	0.438907	-0.35762798

Table 10: log [-ln(1-x)] calculations for samples heat treated at T=90°C.

log(t)	ln(1-x)	-ln(1-x)	log [-ln(1-x)]
0.30103	-0.01207	0.012068	-1.91835
0.60206	-0.0767	0.076705	-1.11518
0.778151	-0.09832	0.098319	-1.00736
0.90309	-0.06698	0.066982	-1.17404
1	-0.18019	0.180194	-0.74426
1.079181	-0.28934	0.289338	-0.53859
1.146128	-0.57103	0.57103	-0.24334
1.20412	-0.73798	0.737984	-0.13195
1.255273	-0.69792	0.697916	-0.1562
1.30103	-1.01256	1.012558	0.00542
1.342423	-0.96816	0.968156	-0.01405

Table 11: log [-ln(1-x)] calculations for samples heat treated at T=120°C.

log(t)	ln(1-x)	-ln(1-x)	log [-ln(1-x)]
0.30103	-0.00702	0.007021	-2.15358
0.60206	-0.07703	0.077027	-1.11336
0.778151	-0.08979	0.089785	-1.04679
0.90309	-0.16959	0.169595	-0.77059
1	-0.45157	0.45157	-0.34527
1.079181	-0.66432	0.664318	-0.17762
1.146128	-0.72465	0.724646	-0.13987
1.20412	-0.87354	0.873536	-0.05872
1.255273	-0.97626	0.976264	-0.01043
1.30103	-1.16027	1.160272	0.06456
1.342423	-1.55421	1.554214	0.191511
1.380211	-2.54182	2.54182	0.405145
1.414973	-2.57691	2.576911	0.411099
1.447158	-3.82266	3.822657	0.582365

Table 12: log [-ln(1-x)] calculations for samples heat treated at T=150°C.

log(t)	ln(1-x)	-ln(1-x)	log [-ln(1-x)]
0.30103	-0.02316	0.02316	-1.63526
0.60206	-0.12397	0.123967	-0.90669
0.778151	-0.33706	0.337056	-0.4723
0.90309	-0.37041	0.370409	-0.43132
1	-0.59887	0.598874	-0.22266
1.079181	-0.73376	0.733757	-0.13445
1.146128	-1.27214	1.272141	0.104535
1.20412	-2.66493	2.664926	0.425685
1.255273	-3.58122	3.581217	0.554031
1.30103	-3.34535	3.345351	0.524442
1.342423	-5.78509	5.785086	0.76231
1.380211	-3.94295	3.94295	0.595821

Table 13: Avrami constants calculations.

% n-dodecylthiol	T (°C)	n	log (K)	K	$t_{0.5}$=[(ln2)/K]^(1/n)	$1/t_{0.5}$
0	60	2.1	-2.8	0.001585	18.09405616	0.055267
0	90	2.45	-3.2	0.000631	17.42421613	0.057391
0	120	2.46	-3.01	0.000977	14.41690838	0.069363
0	150	2.52	-2.5	0.003162	8.48982997	0.117788

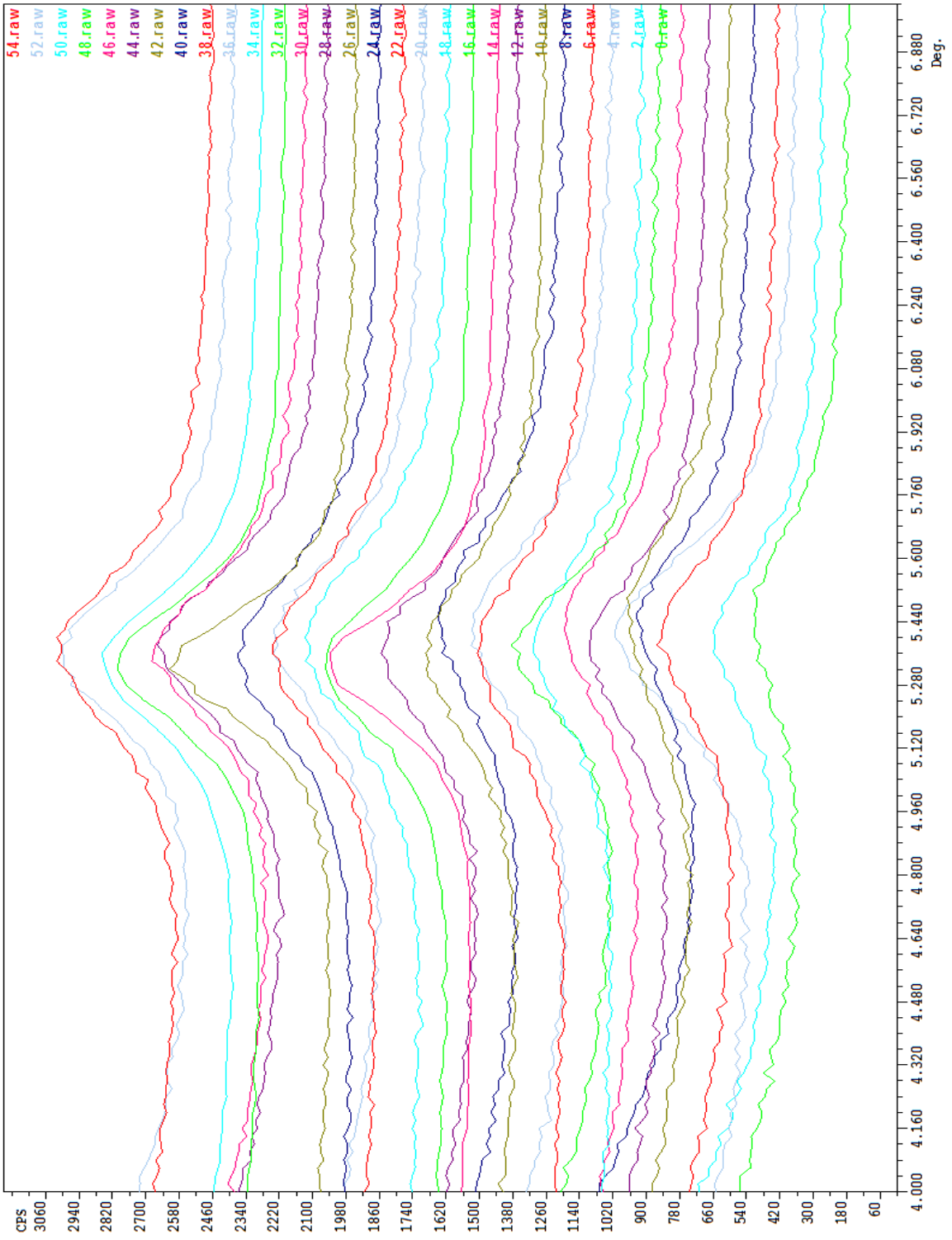

Figure42A: XRD data at 60 °C.

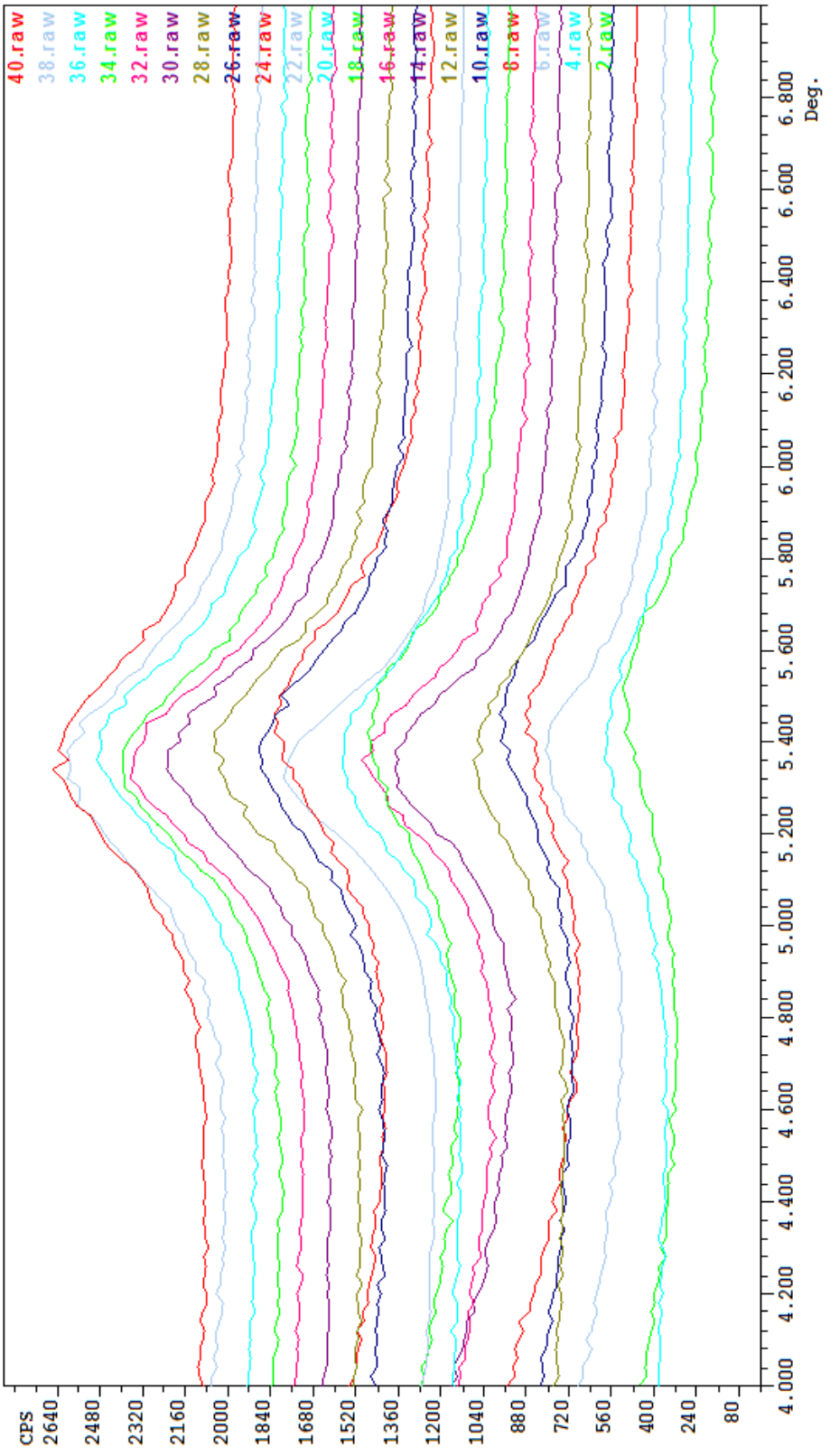

Figure42B: XRD data at 90 °C.

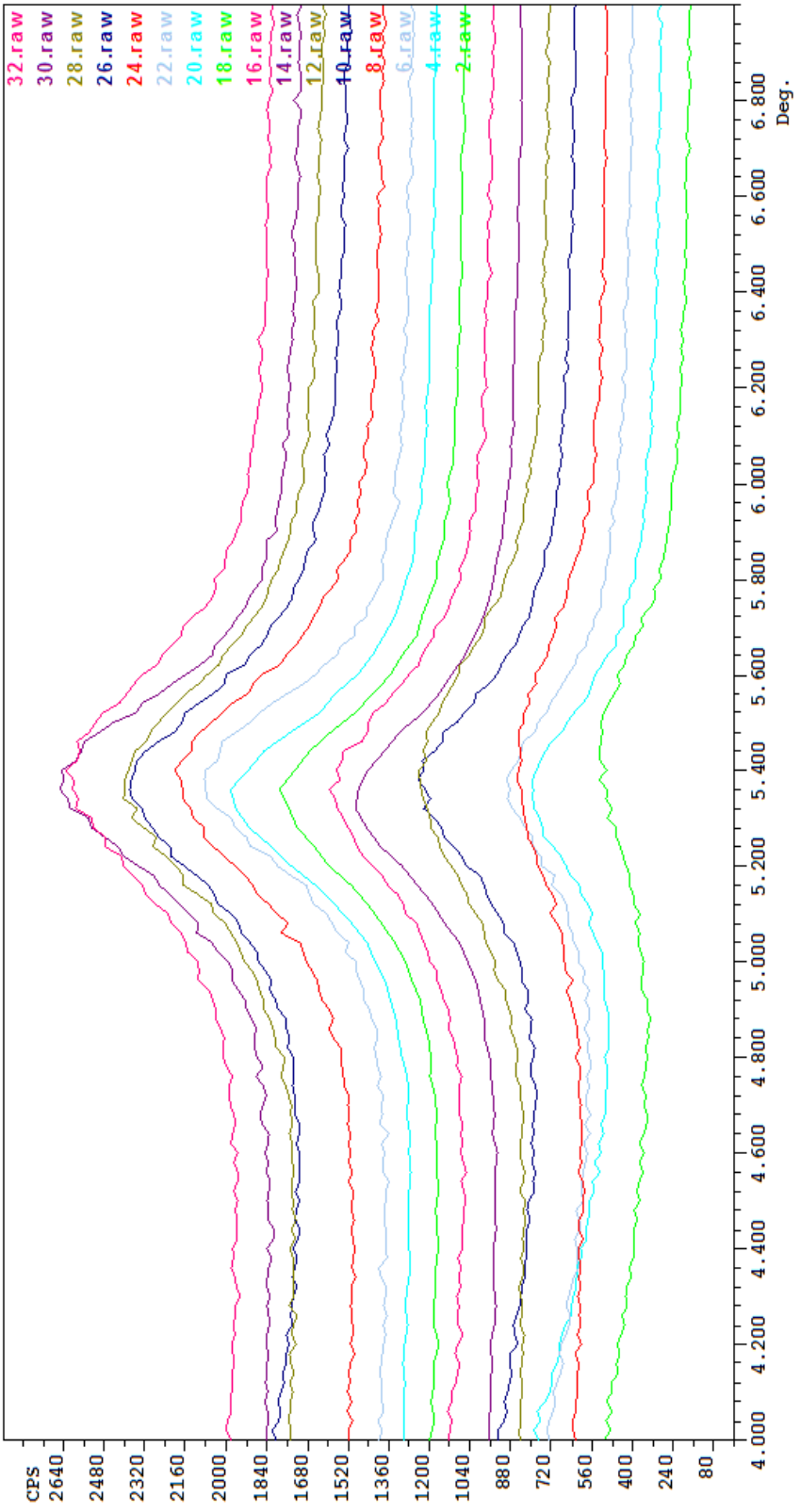

Figure42C: XRD data at 120 °C.

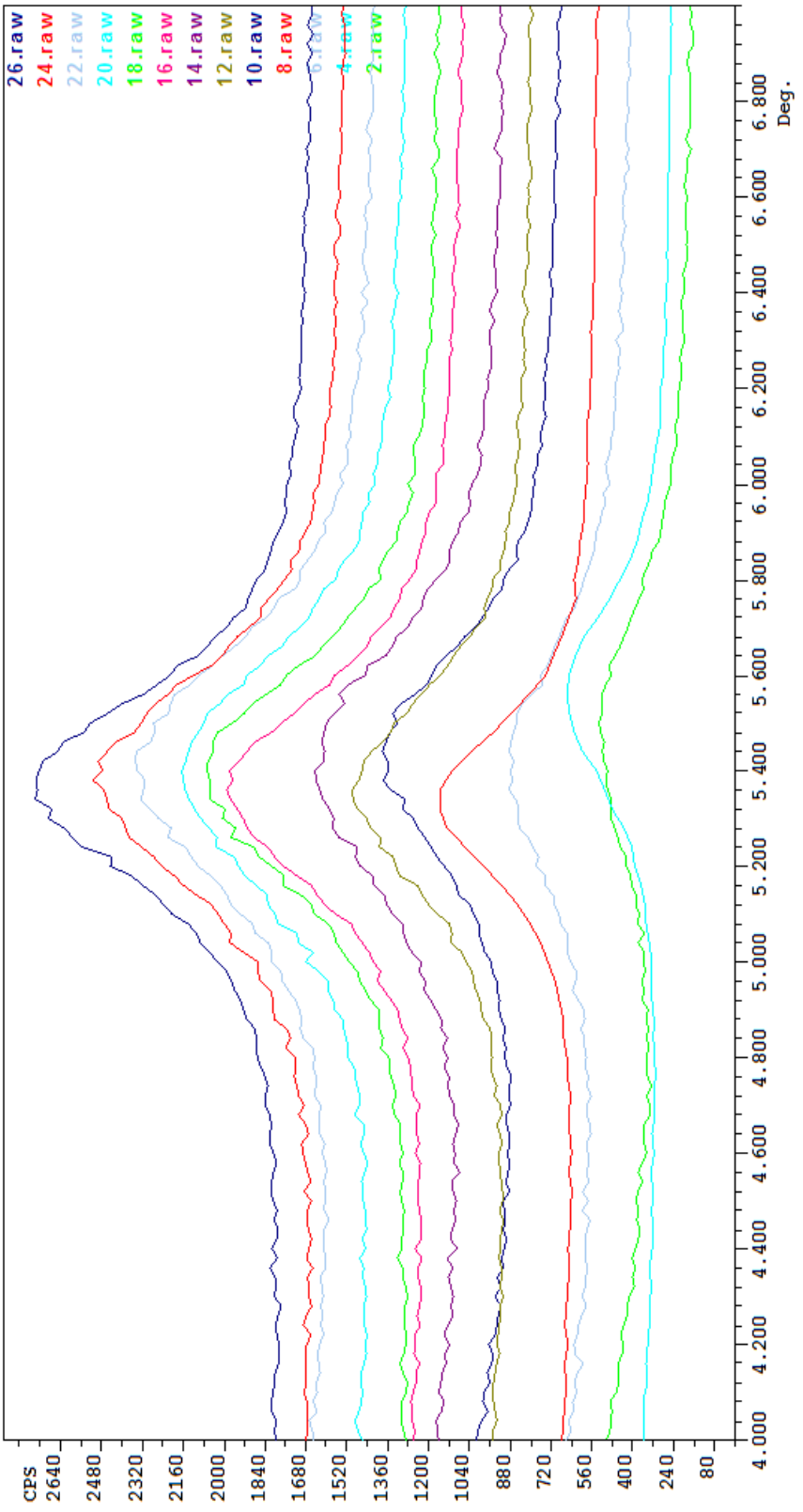

Figure42D: XRD data at 150 °C.

CURRICULUM VITAE

Mahmoud I. Algazzar

Place of birth: Qaliob, Egypt

Education:

B.Sc., Benha University, May 2000

Major: Mechanical Engineering

M.Sc., Benha University, June 2006

Major: Mechanical Engineering

Dissertation Title: ADDING N-DODECYLTHIOL TO MODIFY THE P3HT/PC70BM POLYMER SOLAR CELL